

FILTERING N.M.R. SPECTRA

Thesis by

George A. Petersson

In Partial Fulfillment of the Requirements

For the Degree of

Doctor of Philosophy

California Institute of Technology

Pasadena, California

January 22, 1970

To Smiley – Who has shown me the deeper truth which is beauty.

ACKNOWLEDGMENTS

I am deeply indebted to Professor Andrew D. McLachlan, Professor Vincent McKoy, and Professor John D. Roberts for the patience each has shown while he was my research advisor.

I am also grateful to my friends--both students and faculty--for providing an intellectually stimulating and thoroughly enjoyable environment during the past several years. I am particularly grateful to Dr. Robert L. Lichter and Professor John D. Roberts for their help in clarifying some of the more obscure passages in this thesis.

Finally, I am indebted to the National Institutes of Health, the National Science Foundation, and the California Institute of Technology for providing financial support for myself and for the research described in this thesis.

ABSTRACT

Methods of filtering an n. m. r. spectrum which can improve the resolution by as much as a factor of ten are examined. They include linear filters based upon an information theory approach and non-linear filters based upon a statistical approach. The appropriate filter is determined by the nature of the problem. Once programmed on a digital computer they are both simple to use.

These filters are applied to some examples from ^{13}C and ^{15}N n. m. r. spectra.

TABLE OF CONTENTS

	<u>Page</u>
1. INTRODUCTION	2
1.1 Matched Filters	3
2. THE THEORY OF LINEAR FILTERS	7
2.1 Line Width	8
2.2 Convolution Integrals and Fourier Transforms	15
2.3 Generalized Harmonic Analysis	18
2.4 Optimum Resolution Enhancement Filters	27
2.5 Numerical Fourier Transforms	32
2.6 RC Filters	43
2.7 Sequences of Filters	46
2.8 The Determination of Signal-to-Noise Ratios	49
3. RESULTS OBTAINED WITH LINEAR FILTERS	53
3.1 Optimum Line Widths of Weighting Functions	54
3.2 Resolution Enhancement	57
3.3 Line Shapes Resulting from Resolution Enhancement	74
3.4 Signal-to-Noise Ratios	79
3.5 The Effects of Sweep Rate	87
4. NON-LINEAR FILTERS	104
4.1 The Principle of Maximum Likelihood	104
4.2 Least-Squares Filters	111
4.3 Comparison of Linear and Non-Linear Filters	120

	<u>Page</u>
5. RESOLUTION OF SATELLITE PEAKS	131
5.1 The Least-Squares Approach	132
5.2 Least-Squares Fitting with Non-Linear Parameters	135
5.3 Filtering the Satellite Peak	141
5.4 The Pseudo-Linear Approach	149
5.5 Spectral Analysis Using Satellites	166
6. ERROR ESTIMATES	170
7. APPLICATIONS	173
7.1 Signal-to-Noise Enhancement	173
7.2 Resolution Enhancement	175
7.3 Filtering Satellite Peaks	178
8. EXPERIMENTAL	188
APPENDIX A: Using the Program SNARE	190
APPENDIX B: A Listing of the Program SNARE	204
APPENDIX C: A Semiempirical Calculation of Spin-Spin Coupling Constants	217
REFERENCES	226
PROPOSITIONS	231

Copyright © by

GEORGE ARTHUR PETERSSON

1970

FILTERING N. M. R. SPECTRA

1. INTRODUCTION

A nuclear magnetic resonance spectrum is a plot of the intensity of out-of-phase absorbed radiation as a function of the frequency, ν . We wish to find one or more signals (resonance lines) in a background of noise (random fluctuations in intensity). A signal is a set of intensities which vary in a well-defined manner given by $g(\nu)$, the line-shape function.¹ Noise is essentially all other variations of the intensity with frequency.

Since the sweep rate is held constant, the frequency is proportional to the time:

$$\nu = \alpha t, \quad (1.1)$$

where α is the sweep rate. We shall find it convenient to consider the signal a function of time $s(t)$.

A filtered or transformed spectrum is obtained from the unfiltered spectrum by a process which can be described by an operator \underline{H} :

$$f_0(t) = \underline{H} [f_1(t)], \quad (1.2)$$

where $f_1(t)$ is the input spectrum and $f_0(t)$ is the output spectrum. Filters may be divided into two general types; linear and non-linear. A linear filter satisfies the condition:

$$f_0(t)_1 + f_0(t)_2 = \underline{H} [f_1(t)_1 + f_1(t)_2], \quad (1.3)$$

while a non-linear filter does not. We shall show applications for both types. Linear transformations are more convenient to use since it is not necessary to know the multiplicity of overlapping peaks in advance.

Ernst has written an excellent article² on filters. We shall partly follow his development of linear filters, but obtain a result for a general line shape instead of restricting ourselves to even functions.

First, we shall derive a matched filter from a simple statistical approach. This will give us a feeling for the nature of a filtering process. Later, we shall show that this filter is a special case of a linear resolution enhancement filter.

1.1 Matched Filters

We shall calculate the most probable intensity of absorption at the time t , given the input spectrum, $f_i(t)$. The line-shape function, $s(t)$, will typically have the form shown in Figure 1.1. We shall define the zero of time as the time when $s(t)$ is a maximum. Consider an absorption $f(t)$ with a maximum at the time t_0 , and intensity $f(t_0)$. The simplest method of measuring $f(t_0)$ is to simply observe the intensity at t_0 :

$$f(t_0) \doteq f_i(t_0). \quad (1.1.1)$$

In fact, however when we record an n. m. r. spectrum we measure $f(t_0)$ each time we measure $f_i(t_1)$ at any time t_1 :

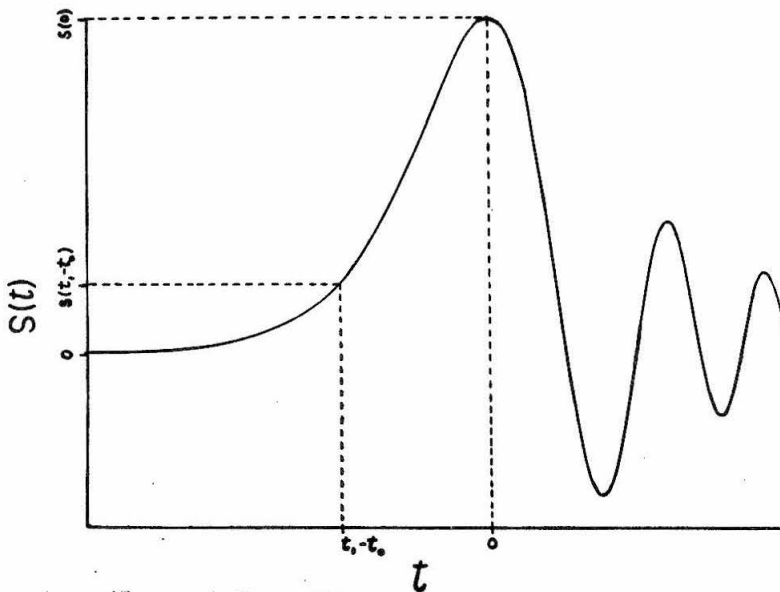


Figure 1.1. A typical n. m. r. signal $s(t)$.

$$f(t_0) \doteq f_i(t_1) \frac{s(0)}{s(t_1 - t_0)}, \quad (1.1.2)$$

where $s(t_1 - t_0)$ is the value of s at $t_1 - t_0$. This is displaced from the maximum, $s(0)$, by the displacement of $f_i(t_1)$ from $f_i(t_0)$. Since these measurements are not all of the same accuracy, the most probable value of $f(t_0)$ is a weighted average of the values obtained from each of these measurements:

$$f_0(t_0) = \int_{-\infty}^{\infty} f_i(t_1) \frac{s_i(0)}{s_i(t_1 - t_0)} W(t_1) dt_1 / \int_{-\infty}^{\infty} W(t_1) dt_1, \quad (1.1.3)$$

where the $W(t_1)$ are the statical weights. If the noise is random (i. e., it has a Gaussian distribution of errors), then the proper weights are:

$$W(t_1) = 1/\sigma^2(t_1), \quad (1.1.4)$$

where $\sigma(t_1)$ is the standard deviation of $f_i(t_1)$.³ The standard deviation of $f_i(t_1)$ is simply the inverse of the signal to noise ratio:

$$\sigma(t_1) = n_{\text{rms}}/s_i(t_1 - t_0), \quad (1.1.5)$$

where this ratio is calculated at $f_i(t_1)$. Substitution of Eqs. (1.1.4) and 1.1.5) in Eq. (1.1.3) gives:

$$f_0(t_0) = s_i(0) \left[\int_{-\infty}^{\infty} s_i^2(t_1 - t_0) dt_1 \right]^{-1} \int_{-\infty}^{\infty} s_i(t_1 - t_0) f_i(t_1) dt_1, \quad (1.1.6)$$

for the most probable value of the intensity of a line with a maximum at t_0 . If we compute this integral, $f_0(t_0)$ for all t_0 , then the output spectrum $f_0(t)$ is a linear transformation of the input spectrum $f_i(t)$. This transformation can be carried out if we know the line shape $s_i(t)$ of an unfiltered line. Finally, we make the substitution $\tau = t_0 - t_1$ in Eq. (1.1.6) and obtain:

$$f_0(t) = s_i(0) \left[\int_{-\infty}^{\infty} s_i^2(\tau) d\tau \right]^{-1} \int_{-\infty}^{\infty} s_i(-\tau) f_i(t - \tau) d\tau, \quad (1.1.7)$$

where we have changed the variable of integration in the first integral. This is the standard form of a matched filter.⁴

This particular filter is normalized to be height preserving. A matched filter is the filter which gives the maximum signal-to-noise ratio in $f_0(t)$.⁴ It is also the optimum filter for the determination of line positions.⁵ The output spectrum at a given time $f_0(t')$ depends upon the input spectrum at all times $f_1(t' - \tau)$. Thus, it is known much more accurately. Measuring a property from an unfiltered spectrum assumes that we have no knowledge of the correlation between $f_1(t)$ and $f_1(t')$. This is not generally true.

Both analog and digital filters can easily be constructed. Digital filters can represent any filter arbitrarily accurately and are more easily varied than analog devices. If a filter operates on the spectrum while the spectrometer is in operation, it must be selected in advance and can only use the points measured at an earlier time — not those measured at a later time. The most powerful filter is therefore a digital one which is used after the complete spectrum has been determined.

2. THE THEORY OF LINEAR FILTERS

The intuitive concept of the resolution of a spectrum involves the question of whether adjacent lines appear as one peak with distorted line shape or are resolved into two discrete peaks. If the signal is a rectangular pulse, the width of the pulse is a quantitative measure of the resolution. Two rectangular peaks more than one line width apart appear as separate lines (Fig. 2.1a). Two rectangular signals less than one line width apart appear as a single peak of more complex shape (Fig. 2.1b). This simple situation gives our

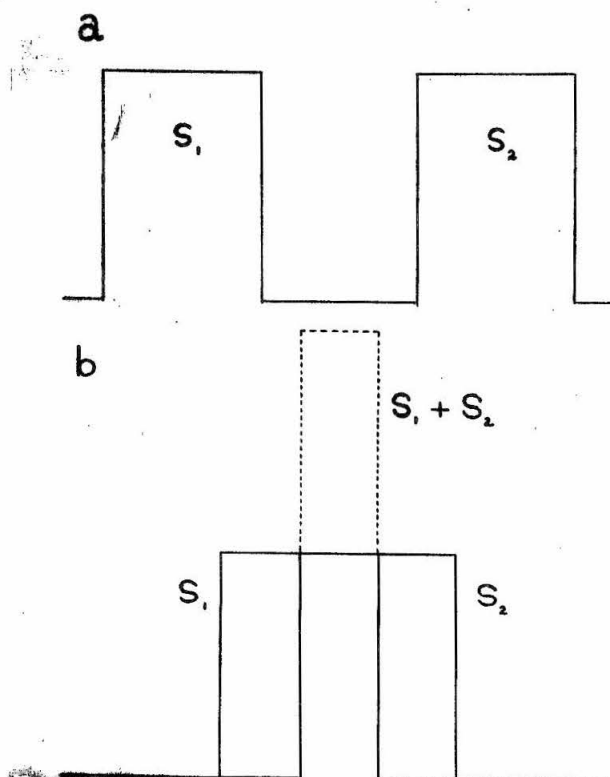


Figure 2.1. The resolution of rectangular peaks.

conceptual framework for the discussion of resolution enhancement. We shall now seek to find a suitable definition of the line width of a general line shape. That is, we seek a suitable rectangular model, so that we can derive a linear transformation to improve resolution.

Although Fig. 2.1b shows only one peak, it is obvious what the separation between the two peaks is. This is because of the discontinuity in the first derivative of a rectangular pulse. The derivative of the spectrum is two Dirac delta functions separated by the line width. Unfortunately, the noise is greatly increased due to the inherent instability of numerical differentiation.⁶ Since both differentiation and integration are linear processes, the optimum amount of either is automatically included in the filter we shall derive below.

2.1 Line Width

We define the resolution line width of two peaks as the minimum separation between them which permits their detection as discrete signals. Figure 2.1.1 shows two peaks of the same line shape with different amplitudes. If s_2 is less than s_1 the peaks are not resolved. If s_2 is greater than s_1 the peaks are resolved. The resolution line width of s_1 is thus a function of the size and line shape of both peaks. The optimum process for improving resolution is therefore non-linear. This is a serious drawback since we frequently will not know the multiplicity of overlapping peaks. We therefore seek a property related to the resolution line width which will lead to a linear process. This property must be a function of the line shape of a single peak.

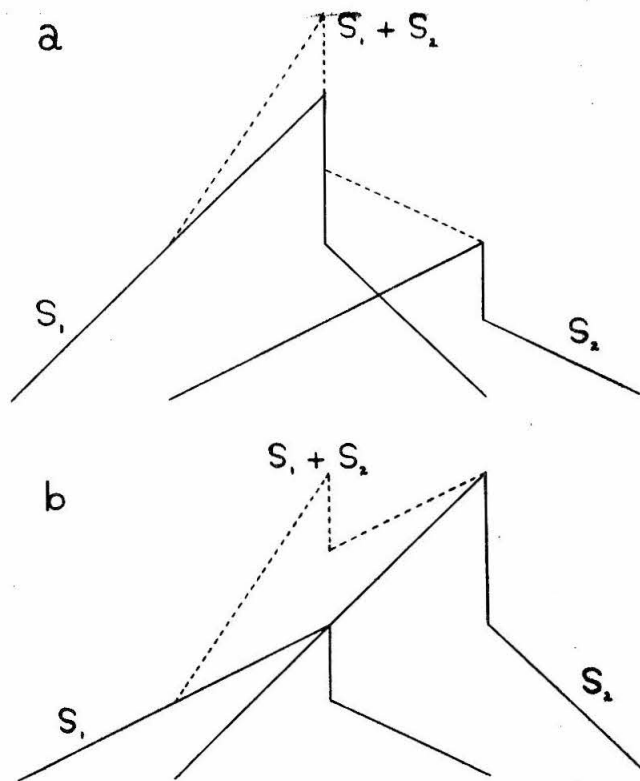


Figure 2.1.1. The resolution line width can be a function of relative peak height.

So far we have only considered whether or not two overlapping peaks have two discrete maxima. We have not discussed where the maxima occur. In the case of two overlapping Lorentzians (Fig. 2.1.2) the maxima will not correspond to the original peak positions. Although they are resolved, their maxima are shifted and a coupling constant measured by the separation of the maxima will be too small. This will occur at any separation for line shapes which do not go to

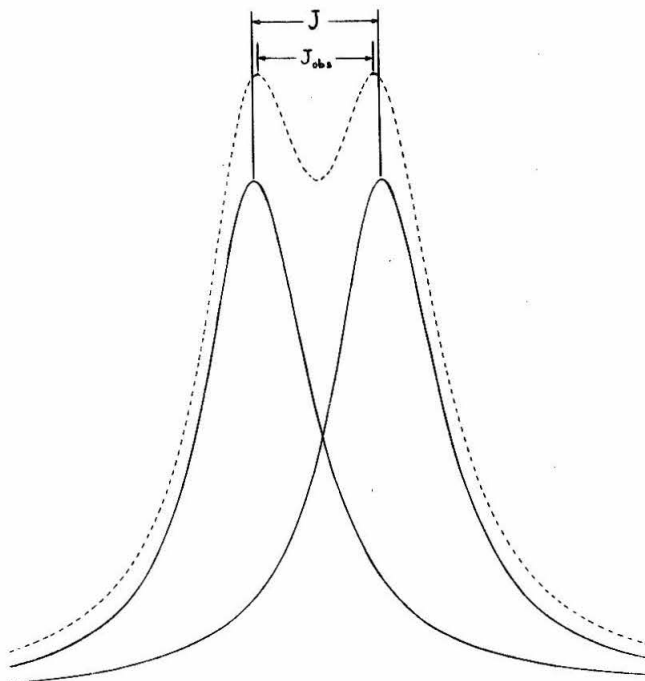


Figure 2.1.2. Two Lorentzians separated by their width at half height.

zero at a finite distance from the maxima. At larger separations the distance between maxima approaches the distance between line positions. At smaller separations the ratio of the distance between maxima to the distance between line positions approaches zero. This ratio equals zero at separations smaller than the resolution line width. There is a systematic error in measuring the separation of overlapping peaks. In order to accurately measure line separations

we must decrease the resolution line width and make the signal approach zero rapidly.

In the case of two triangular peaks (Fig. 2.1.3) the resolution line width is equal to the full width at half height. Since this property

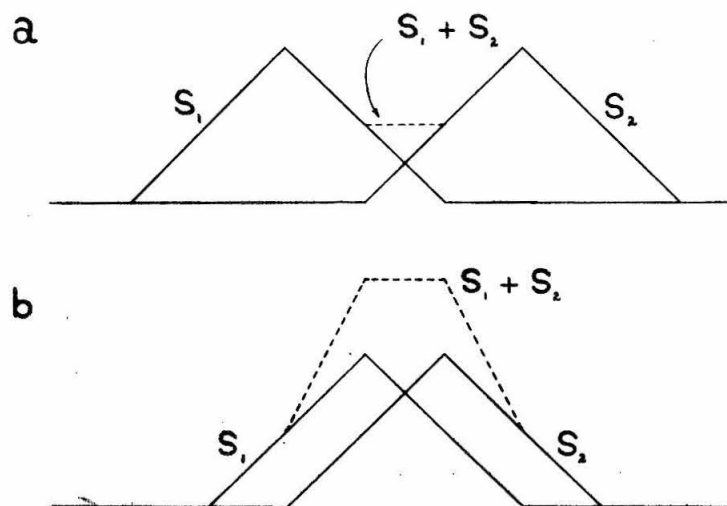


Figure 2.1.3. The resolution of triangular peaks.

is easy to measure for an experimental spectrum, it is widely used. This line width depends upon only two points for a general line shape. It is therefore not amenable to optimization procedures. It is also independent of the "tail" of a line shape and minimizing the full width at half height could lead to increased shifts of the maxima.

It seems reasonable to define a line width as the width of a rectangle which has the same height as the input signal and some other property the same. The most obvious property is the area. The area of an odd function (e. g., a dispersion signal) is zero. A process which minimizes the area could convert a peak to an odd function (e. g., by differentiation) without necessarily decreasing the resolution line width. Fully one half the area of a Lorentzian is outside the full width at half height. The area clearly places too much emphasis on the tail. Using the integral of the absolute value of a function would cure the first problem but not the second. Let us cut off a Lorentzian where it reaches half its height in such manner that the sum of two equal peaks separated by their full width at half height is constant between the maxima (Fig. 2.1.4). This decreases the area by a factor of $\pi/2$. The tail has been removed so well that if two discrete maxima occur, then they correspond to the original peak positions. Unfortunately, the resolution line width has been increased by about 16%. The area places too much emphasis on the tail. A filter based on the area could lead to increased rather than decreased resolution line widths. The first moment is unacceptable since it places even more emphasis on the tail. The second moment may even diverge (e. g., for a Lorentzian line and therefore for an n. m. r. signal). Higher moments offer similar problems.

A practical definition of line width is the energy width.⁷ Energy here refers to the signal energy and not to the absorbed energy that the signal represents. If the signal is a voltage or current, then the

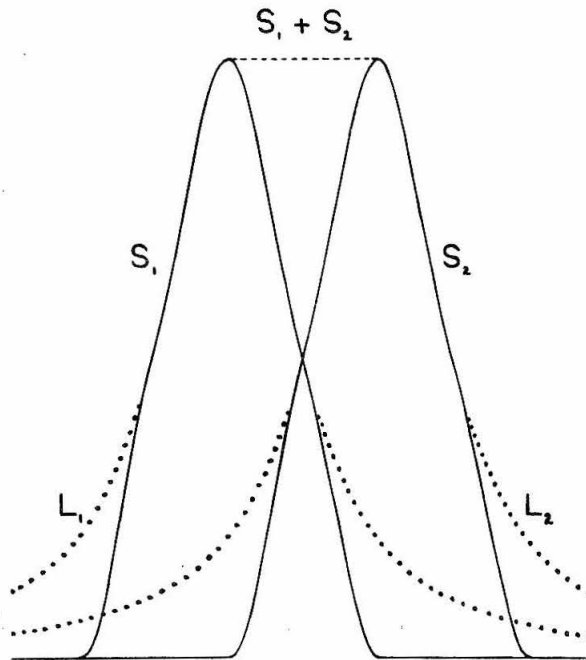


Figure 2.1.4. Two truncated Lorentzians separated by their full width at half height.

square of the signal is the power dissipated. Integration of this power gives the signal energy. The energy width is the width of a rectangle whose height and energy are the same as those of the line. That is:

$$b \equiv \int_{-\infty}^{\infty} s(t)^2 dt / s(0)^2, \quad (2.1.1)$$

where $s(0)$ is the height of the peak.

Only $(\pi-2)/2\pi$, or about one sixth of the energy width for a Lorentzian arises from the portion outside the full width at half height. Truncating a Lorentzian (as in Fig. 2.1.4) decreases the energy width by only a factor of $\pi/(6-\pi)$, or about one sixth the improvement calculated by area. A definition of line width based upon the integral of higher powers of the signal will still give a smaller line width for the truncated line than for the Lorentzian. Only $(1/2 - 4/3\pi)$, or about 7% of the width based upon $s^3(t)$ arises from the portion of a Lorentzian which is outside the full width at half height. This would not seem to place enough emphasis on the tail of the line. Higher powers of $s(t)$ aggravate the problem still further. The best exponent for $s(t)$ would seem to be about two.

The energy width may not be the best definition of line width, but we shall find that it is convenient to optimize and leads to useful filters. When we examine how the resulting filters work we shall find that they use the best method known for accurately measuring positions. It will then be clear that only minor improvements could result from modifying our definition of line width.

We shall define a process which decreases the energy width b . In order to be useful the process must retain sufficient signal to noise that we can still find the n. m. r. signal after filtering. We therefore must consider what happens to the signal height, the energy width of the signal, and the noise level during the filtering operation. This is most easily done by considering the Fourier transform.

2.2 Convolution Integrals and Fourier Transforms

A linear time-independent filter can be represented by an integral; the convolution integral:⁸

$$f_0(t) = \int_{-\infty}^{\infty} h(\tau) f_1(t - \tau) d\tau, \quad (2.2.1)$$

where $h(\tau)$ is called the weighting function of the filter. The problem is to determine the optimum form for $h(\tau)$. This can be done by examining the Fourier transform. We shall define $F(\omega)$ to be the Fourier transform of $f(t)$:

$$f(t) = \frac{1}{2\pi} \int_{-\infty}^{\infty} F(\omega) e^{i\omega t} d\omega, \quad (2.2.2)$$

where:

$$F(\omega) = \int_{-\infty}^{\infty} f(t) e^{-i\omega t} dt. \quad (2.2.3)$$

That is, we shall use lower case for a time function and upper case for the Fourier transform. The angular Fourier frequency ω should not be confused with the frequency of irradiation, ν . They have nothing to do with each other.

We note from examination of Eq. (2.2.3) that if $s(t)$ is even then $S(\omega)$ is real and even. If $s(t)$ is odd, then $S(\omega)$ is imaginary and odd. It follows that for any $s(t)$:

$$S(-\omega) = S^*(\omega), \quad (2.2.4)$$

where the asterisk denotes the complex conjugate. For asymmetric $s(t)$, $S(\omega)$ is complex and asymmetric. Furthermore, the inverse Fourier transform of $S^*(\omega)$ gives $s(-t)$. That is, taking the complex conjugate in frequency space is equivalent to reflecting about $t = 0$ in time space. Finally, we note from Eq. (2.2.2) that $\omega F(\omega)$ is the Fourier transform of $f'(t)$. Multiplying by ω in frequency space provides a convenient method of numerical differentiation. This method is considerably more accurate than simple difference techniques.

Consider a product of the form of Eq. (2.2.1):

$$s_0(t) = \int_{-\infty}^{\infty} h(\tau) s_1(t-\tau) d\tau. \quad (2.2.5)$$

The Fourier transform is:

$$S_0(\omega) = \int_{-\infty}^{\infty} \int_{-\infty}^{\infty} h(\tau) s_1(t-\tau) d\tau e^{-i\omega t} dt, \quad (2.2.6)$$

or:

$$S_0(\omega) = \int_{-\infty}^{\infty} \int_{-\infty}^{\infty} h(\tau) e^{-i\omega\tau} s_1(t-\tau) e^{-i\omega(t-\tau)} d\tau dt. \quad (2.2.7)$$

Reversing the order of integration gives:

$$S_0(\omega) = \int_{-\infty}^{\infty} h(\tau) e^{-i\omega\tau} \left\{ \int_{-\infty}^{\infty} s_i(t-\tau) e^{-i\omega(t-\tau)} d(t-\tau) \right\} d\tau. \quad (2.2.8)$$

Therefore:

$$S_0(\omega) = H(\omega) S_i(\omega) \quad (2.2.9)$$

where $H(\omega)$ (the Fourier transform of the weighting function $h(\tau)$) is called the frequency response function or transfer function of the filter.^{9, 10} A filter simply takes a product in frequency space. This is the first big advantage we gain by working with Fourier transforms. A filtering process can be expressed very simply. Later, we shall see that the properties of noise are also simplified by working in frequency space.

We quote without proof the Plancherel theorem:¹¹

$$\int_{-\infty}^{\infty} f^2(t) dt = \frac{1}{2\pi} \int_{-\infty}^{\infty} |F(\omega)|^2 d\omega. \quad (2.2.10)$$

Applying this to Eq. (2.1.1) for b , the energy line width, gives:

$$b_0 = \frac{1}{2\pi} \int_{-\infty}^{\infty} |S_0(\omega)|^2 d\omega / s_0^2(0). \quad (2.2.11)$$

Substituting the value of $S_0(\omega)$ from Eq. (2.2.9) leads to:

$$b_0 = \frac{1}{2\pi} \int_{-\infty}^{\infty} |H(\omega)|^2 |S_i(\omega)|^2 d\omega / s_0^2(0). \quad (2.2.12)$$

Equations (2.2.9) and (2.2.12) give the output signal and the output energy line width in terms of the input signal and the filter. The properties of noise are more difficult to describe and will be covered in the next section.

2.3 Generalized Harmonic Analysis

Wiener, by developing generalized harmonic analysis, provided the mathematical tools for dealing with random functions.¹² This approach yields a reciprocal relationship between frequency and time. The frequency characteristic is called the power spectrum and the time characteristic the correlation function. We shall use the properties of the power spectrum to develop filters.

Random noise has an infinite period. Let the noise function be $n(t)$. We can define a periodic function, $n_T(t)$, with period T as follows:

$$n_T(t) \equiv n(t); \quad |t| \leq T/2, \quad (2.3.1)$$

and:

$$n_T(t+T) \equiv n_T(t).$$

Taking the limit as T becomes arbitrarily large we obtain:

$$\text{Limit}_{T \rightarrow \infty} n_T(t) = n(t). \quad (2.3.2)$$

We shall first determine some properties of the periodic function, $n_T(t)$, and later take the limit to obtain the desired properties of the

non-periodic function, $n(t)$.

Since $n_T(t)$ is periodic we can expand it in a Fourier Series:

$$n_T(t) = \sum_{j=0}^{\infty} [a_j \cos (\omega_j t) + b_j \sin (\omega_j t)], \quad (2.3.3)$$

where:

$$a_j = 2/T \int_{-T/2}^{T/2} n_T(t) \cos (\omega_j t) dt, \quad (2.3.4)$$

$$b_j = 2/T \int_{-T/2}^{T/2} n_T(t) \sin (\omega_j t) dt, \quad (2.3.5)$$

and $\omega_j = 2\pi j/T$. We shall also use the complex form:

$$n_T(t) = \frac{1}{2\pi} \sum_{j=-\infty}^{\infty} N_T(\omega_j) e^{i\omega_j t} \left(\frac{2\pi}{T} \right), \quad (2.3.6)$$

where:

$$N_T(\omega_j) = \int_{-T/2}^{T/2} n_T(t) e^{-i\omega_j t} dt. \quad (2.3.7)$$

Suppose $n_T(t)$ is a current flowing through a circuit with unit resistance. Then a certain amount of energy, E_T , is dissipated in each cycle. From elementary circuit theory:

$$E_T = \int_{-T/2}^{T/2} n_T^2(t) dt. \quad (2.3.8)$$

Substitution of Eq. (2.3.3) for $n_T(t)$ gives:

$$E_T = \int_{-T/2}^{T/2} \sum_{j=0}^{\infty} \sum_{k=0}^{\infty} [a_j \cos(\omega_j t) + b_j \sin(\omega_j t)] \times [a_k \cos(\omega_k t) + b_k \sin(\omega_k t)] dt. \quad (2.3.9)$$

Rearrangement of this expression leads to:

$$E_T = \sum_{j=0}^{\infty} \sum_{k=0}^{\infty} \left\{ a_j a_k \frac{T}{2\pi} \int_{-\pi}^{\pi} \cos(j\theta) \cos(k\theta) d\theta + a_j b_k \frac{T}{\pi} \int_{-\pi}^{\pi} \sin(j\theta) \cos(k\theta) d\theta + b_j b_k \frac{T}{2\pi} \int_{-\pi}^{\pi} \sin(j\theta) \sin(k\theta) d\theta \right\}. \quad (2.3.10)$$

Integration simplifies this expression to:

$$E_T = \sum_{j=0}^{\infty} \frac{T}{2} (a_j^2 + b_j^2). \quad (2.3.11)$$

We can therefore speak about the component of E_T from the frequency ω_j . The total energy is the sum of these components:

$$E_T = \sum_{j=0}^{\infty} E_T(\omega_j), \quad (2.3.12)$$

where:

$$E_T(\omega_j) = \frac{T}{2} (a_j^2 + b_j^2), \quad (2.3.13)$$

is the energy per cycle from frequency ω_j . The average power for a cycle, ρ_T , is given by E_T/T :

$$\rho_T = \sum_{j=0}^{\infty} E(\omega_j) \frac{1}{T}, \quad (2.3.14)$$

or:

$$\rho_T = \sum_{j=0}^{\infty} \frac{E(\omega_j)}{2\pi} \Delta \omega_j. \quad (2.3.15)$$

A very useful characterization of random functions is the power spectral density:

$$W_T(\omega_j) \equiv E_T(\omega_j)/4\pi; \quad W_T(-\omega_j) \equiv W_T(\omega_j). \quad (2.3.16)$$

This leads to the representation of the total power as:

$$\rho_T = \sum_{j=-\infty}^{\infty} W_T(\omega_j) \Delta \omega_j. \quad (2.3.17)$$

Substituting Eq. (2.3.13) in Eq. (2.3.16) we obtain:

$$W_T(\omega_j) = \frac{T}{8\pi} (a_j^2 + b_j^2), \quad (2.3.18)$$

so that:

$$W_T(\omega_j) = \frac{T}{8\pi} (a_j + i b_j)(a_j - i b_j). \quad (2.3.19)$$

We now substitute Eqs. (2.3.4) and (2.3.5) for a_j and b_j :

$$W_T(\omega_j) = \frac{T}{8\pi} \left\{ \frac{2}{T} \int_{-T/2}^{T/2} n_T(t) [\cos(\omega_j t) + i \sin(\omega_j t)] dt \right\} \\ \times \left\{ \frac{2}{T} \int_{-T/2}^{T/2} n_T(t) [\cos(\omega_j t) - i \sin(\omega_j t)] dt \right\}, \quad (2.3.20)$$

or:

$$W_T(\omega_j) = \frac{1}{2\pi T} \left\{ \int_{-T/2}^{T/2} n_T(t) e^{i\omega_j t} dt \right\} \left\{ \int_{-T/2}^{T/2} n_T(t) e^{-i\omega_j t} dt \right\}. \quad (2.3.21)$$

Substitution of Eq. (2.3.7) for $N_T(\omega_j)$ gives:

$$W_T(\omega_j) = \frac{|N_T(\omega_j)|^2}{2\pi T}. \quad (2.3.22)$$

The root-mean-square value of the noise is defined as:

$$(n_{\text{rms}})_T \equiv \left\{ \frac{1}{T} \int_{-T/2}^{T/2} n_T^2(t) dt \right\}^{1/2}. \quad (2.3.23)$$

This is simply the square root of the total power per cycle. We therefore obtain from Eq. (2.3.17):

$$(n_{\text{rms}})_{\text{T}}^2 = \sum_{j=-\infty}^{\infty} W_{\text{T}}(\omega_j) \Delta \omega_j. \quad (2.3.24)$$

We now examine the result of a filter on n_{rms} . After filtering we have:

$$(n_{\text{rms}})_{\text{T}_0}^2 = \sum_{j=-\infty}^{\infty} W_{\text{T}_0}(\omega_j) \Delta \omega_j, \quad (2.3.25)$$

or, substituting Eq. (2.3.22) for $W_{\text{T}_0}(\omega_j)$ gives:

$$(n_{\text{rms}})_{\text{T}_0}^2 = \sum_{j=-\infty}^{\infty} \left(\frac{1}{2\pi\text{T}}\right) |N_{\text{T}_0}(\omega_j)|^2 \Delta \omega_j. \quad (2.3.26)$$

Since the filter is equivalent to multiplying by $H(\omega_j)$ in frequency space:

$$(n_{\text{rms}})_{\text{T}_0}^2 = \sum_{j=-\infty}^{\infty} \left(\frac{1}{2\pi\text{T}}\right) |H(\omega_j) N_{\text{T}_i}(\omega_j)|^2 \Delta \omega_j. \quad (2.3.27)$$

We again use Eq. (2.3.22) for $W_{\text{T}_i}(\omega_j)$ and obtain:

$$(n_{\text{rms}})_{\text{T}_0}^2 = \sum_{j=-\infty}^{\infty} |H(\omega_j)|^2 W_{\text{T}_i}(\omega_j) \Delta \omega_j, \quad (2.3.28)$$

for the mean-square value of the noise after filtering. This is the crucial relationship which shows the effect of a filter on the noise.

We shall find the time characteristic useful for developing filters based on probability theory. The autocorrelation function, $r_T(t)$, is defined as:

$$r_T(t) = \frac{1}{T} \int_{-T/2}^{T/2} n_T(\tau) n_T(t+\tau) d\tau. \quad (2.3.29)$$

This is a measure of the dependence of $n_T(\tau)$ upon $n_T(t+\tau)$. If $n_T(\tau)$ is independent of $n_T(t+\tau)$ for all t not equal to zero, then $r_T(t)$ approaches a Dirac delta function. Substitution of Eq. (2.3.6) for $n_T(t)$ into Eq. (2.3.29) gives:

$$r_T(t) = \frac{1}{4\pi^2 T} \int_{-T/2}^{T/2} \sum_{j=-\infty}^{\infty} \sum_{k=-\infty}^{\infty} N_T(\omega_j) N_T(\omega_k) e^{i(\omega_j + \omega_k)\tau} e^{i\omega_k t} \left(\frac{2\pi}{T}\right)^2 d\tau. \quad (2.3.30)$$

Rearrangement of this expression leads to:

$$r_T(t) = \sum_{j=-\infty}^{\infty} \sum_{k=-\infty}^{\infty} \frac{N_T(\omega_j) N_T(\omega_k)}{2\pi T} e^{i\omega_k t} \left\{ \frac{1}{2\pi} \int_{-T/2}^{T/2} e^{i(\omega_j + \omega_k)\tau} d\tau \right\}. \quad (2.3.31)$$

The limit as T approaches infinity of the quantity in brackets is the Dirac delta function.¹⁴

We now have derived all the desired relationships for the periodic function $n_T(t)$. We let T approach infinity and we obtain the following relationships for the non-periodic function, $n(t)$ from Eqs. (2.3.6), (2.3.7), (2.3.22), (2.3.29), (2.3.24), (2.3.28), and (2.3.31), respectively:

$$n(t) = \frac{1}{2\pi} \int_{-\infty}^{\infty} N(\omega) e^{i\omega t} d\omega, \quad (2.3.32)$$

$$N(\omega) = \int_{-\infty}^{\infty} n(t) e^{-i\omega t} dt, \quad (2.3.33)$$

$$W(\omega) = \text{Limit}_{T \rightarrow \infty} \frac{|N(\omega)|^2}{2\pi T}, \quad (2.3.34)$$

$$r(t) = \text{Limit}_{T \rightarrow \infty} \frac{1}{T} \int_{-T/2}^{T/2} n(\tau) n(t+\tau) d\tau, \quad (2.3.35)$$

$$n_{\text{rms}}^2 = \int_{-\infty}^{\infty} W(\omega) d\omega, \quad (2.3.36)$$

$$n_{\text{rms}_0}^2 = \int_{-\infty}^{\infty} |H(\omega)|^2 W_i(\omega) d\omega, \quad (2.3.37)$$

and

$$r(t) = \int_{-\infty}^{\infty} W(\omega) e^{i\omega t} d\omega. \quad (2.3.38)$$

It also follows from Eqs. (2.3.32), (2.3.33), and (2.3.38) that:

$$W(\omega) = \frac{1}{2\pi} \int_{-\infty}^{\infty} r(t) e^{-i\omega t} dt. \quad (2.3.39)$$

The autocorrelation function and the power spectral density are related through a Fourier transform. This is called the Wiener-Khinchin relation.

Finally, we note that white noise is defined as having a power spectral density which is frequency independent. That is, $W(\omega)_{\text{white noise}}$ is a constant. All frequencies contribute equally to white noise. Later we shall see that this provides an excellent description of the noise in n. m. r. spectra under normal conditions. The autocorrelation function for white noise is given by:

$$r(t)_{\text{white noise}} = W \int_{-\infty}^{\infty} e^{i\omega t} d\omega = 2\pi W \delta(t), \quad (2.3.40)$$

so that the data points of a spectrum are completely independent for white noise. They are statistically independent only for ergodic Gaussian noise. We shall consider the general significance of $r(t)$ in a later section.

Non-white or colored noise requires assigning a functional form to $W(\omega)$ or $r(t)$. This could be done by measuring either of the two. The resulting filters are significantly more complicated than those for white noise.

This completes our excursion into generalized harmonic analysis. We are now ready to determine $H(\omega)$ for an optimum linear filter.

2.4 Optimum Resolution Enhancement Filters

The optimum resolution enhancement filter gives the minimum energy width for a given signal-to-noise ratio. It is simpler to solve for the filter which gives the maximum signal to noise ratio for a given energy width, which is the same thing. The signal-to-noise ratio is defined as the maximum signal voltage, $s_{0\max}$ divided by the root-mean-square noise voltage. Our definition of the time scale gives the maximum signal voltage as:

$$s_{0\max} = s_0(0). \quad (2.4.1)$$

Taking the Fourier transform we obtain:

$$s_{0\max} = \frac{1}{2\pi} \int_{-\infty}^{\infty} S_0(\omega) d\omega. \quad (2.4.2)$$

Substitution of Eq. (2.2.9) for $S_0(\omega)$ gives:

$$s_{0\max} = \frac{1}{2\pi} \int_{-\infty}^{\infty} H(\omega) S_1(\omega) d\omega, \quad (2.4.3)$$

for the maximum output signal voltage in terms of the input signal.

We maximize the signal-to-noise ratio by holding the signal constant

and minimizing the noise.

The optimum resolution enhancement filter satisfies the conditions:

$$n_{\text{rms}}^2 = \int_{-\infty}^{\infty} |H(\omega)|^2 W_i(\omega) d\omega \quad \text{is a minimum;} \quad (2.4.4)$$

$$s_{0\text{max}} = \frac{1}{2\pi} \int_{-\infty}^{\infty} H(\omega) S_i(\omega) d\omega \quad \text{is a constant;} \quad (2.4.5)$$

and:

$$b_0 = 2\pi \int_{-\infty}^{\infty} |H(\omega)|^2 |S_i(\omega)|^2 d\omega / s_0^2(0) \quad \text{is a constant;} \quad (2.4.6)$$

where the last condition comes from Eq. (2.2.12). Since the denominator of Eq. (2.4.6) appears in Eq. (2.4.5), we can restate the problem. We wish to satisfy the following conditions:

$$\int_{-\infty}^{\infty} |H(\omega)|^2 W_i(\omega) d\omega = \text{a minimum} \quad (2.4.7)$$

$$\int_{-\infty}^{\infty} H(\omega) S_i(\omega) d\omega = c_1 \quad (2.4.8)$$

$$\int_{-\infty}^{\infty} |H(\omega)|^2 |S_i(\omega)|^2 d\omega = c_2. \quad (2.4.9)$$

This problem is readily solved by Lagrange's method of undetermined multipliers.¹³ The general method for an extremal problem with k constraints is as follows;

Let:

$$\int_{x_1}^{x_2} I[x, y(x), y'(x)] dx = \text{an extremum,} \quad (2.4.10)$$

under the k constraints:

$$\int_{x_1}^{x_2} I_j[x, y(x), y'(x)] dx = c_j; \quad j = 1, 2, \dots, k, \quad (2.4.11)$$

and let:

$$K = I + \sum_{j=1}^k \lambda_j I_j, \quad (2.4.12)$$

where the λ_j are constants. Then the solution satisfies:

$$\frac{\partial K}{\partial y} - \frac{d}{dx} \frac{\partial K}{\partial y'} = 0. \quad (2.4.13)$$

When this method is applied to the above problem we obtain:

$$K = |H(\omega)|^2 W_1(\omega) + \lambda_1 H(\omega) S_1(\omega) + \lambda_2 |H(\omega)|^2 |S_1(\omega)|^2. \quad (2.4.14)$$

For this problem K does not depend explicitly upon $H'(\omega)$. Application of Eq. (2.4.13) therefore leads to:

$$2 |H(\omega)| W_i(\omega) + \lambda_1 \frac{H(\omega)}{|H(\omega)|} S_i(\omega) + 2 \lambda_2 |H(\omega)| |S_i(\omega)|^2 = 0, \quad (2.4.15)$$

where we have used $|H(\omega)|$ as $y(x)$ in Eq. (2.4.13). We now multiply by $H^*(\omega)/|H(\omega)|$ and obtain:

$$2 H^*(\omega) W_i(\omega) + \lambda_1 S_i(\omega) + 2 \lambda_2 H^*(\omega) |S_i(\omega)|^2 = 0. \quad (2.4.16)$$

Solving for $H^*(\omega)$ and taking the complex conjugate gives:

$$H(\omega) = \frac{-\frac{\lambda_1}{2} S_i^*(\omega)}{W_i(\omega) + \lambda_2 |S_i(\omega)|^2}, \quad (2.4.17)$$

which is the frequency response function (the Fourier transform of the weighting function) for the optimum linear resolution enhancement filter.

We have held the line width constant by use of the parameter λ_2 . It is clear from its origin in the third term of Eq. (2.4.14) that if $\lambda_2 = 0$ we obtain the filter with the maximum signal-to-noise ratio regardless of line width, since this eliminates consideration of line width in Eq. (2.4.14). If λ_2 approaches infinity we eliminate the first two terms of Eq. (2.4.14) and obtain the minimum line width regardless of the signal-to-noise ratio. First, we take the limit as λ_2 approaches infinity.

The limit of the frequency response function as λ_2 approaches infinity is:

$$\lim_{\lambda_2 \rightarrow \infty} H(\omega) = -\frac{\lambda_1}{2\lambda_2} [S_i(\omega)]^{-1}. \quad (2.4.18)$$

We now substitute this limiting form for $H(\omega)$ in Eq. (2.2.9) giving:

$$S_o(\omega) = \frac{-\lambda_1}{2\lambda_2}. \quad (2.4.19)$$

Taking the Fourier transform of this we obtain:

$$s_o(t) = \frac{-\lambda_1}{4\pi\lambda_2} \int_{-\infty}^{\infty} e^{i\omega t} d\omega. \quad (2.4.20)$$

The integral is easily evaluated¹⁴ giving:

$$s_o(t) = \frac{-\lambda_1}{2\lambda_2} \delta(t). \quad (2.4.21)$$

The signal has been transformed into a Dirac delta function. This indicates that our definition of line width was realistic, since in the limit it leads to a peak with zero resolution line width and no shift of adjacent peaks.

The second situation of interest is the case $\lambda_2 = 0$. This gives:

$$H(\omega) = -\frac{\lambda_1}{2} S_i^*(\omega)/W_i(\omega), \quad (2.4.22)$$

which is the form for a matched filter.⁴ In addition to giving the maximum signal-to-noise ratio, the maximum of the filtered function

is the most probable position of the line.

The parameter λ_2 determines the emphasis of the filter on resolution or sensitivity, while λ_1 determines the normalization. We now assume that the noise power spectral density is a constant (i. e., the noise is white or frequency independent) and rearrange Eq. (2.4.17) to:

$$H(\omega) = \frac{c(q) S_i^*(\omega)}{1 + q |S_i(\omega)|^2}, \quad (2.4.23)$$

where $c(q)$ is the normalization constant and q determines the resolving power of the filter. If we require that:

$$s_0(0) = s_i(0), \quad (2.4.24)$$

so that the filter is height preserving, then:

$$c(q) = s_i(0) \left\{ \int_{-\infty}^{\infty} |S_i(\omega)|^2 / [1 + q |S_i(\omega)|^2] d\omega \right\}^{-1}. \quad (2.4.25)$$

This frequency response function [Eqs. (2.4.23) and (2.4.25)] defines a family of linear resolution enhancement filters which depend only on the input line shape. In the next section we consider the implementation of these filters.

2.5 Numerical Fourier Transforms

The Fourier transform of the weighting function for the optimum linear resolution enhancement filter has the form given in Eq. (2.4.23).

The calculation of this weighting function using the I. B. M. provided subroutine "HARM" has been programmed. This subroutine uses the very efficient numerical Fourier transform algorithm of Cooley and Tukey.¹⁵ The calculation of a Fourier transform at N points using this algorithm requires only $N \log_2 N$ multiplications rather than the N^2 required by a more straightforward approach. The execution time for the complete filtering program is about 10 seconds on an I. B. M. 360/75 computer when the H level compiler is used.

Both linear and non-linear filters require some knowledge about the noise function $n(t)$. We obtained the final form of the linear resolution enhancement filters by assuming that the power spectral density of the input noise $W_1(\omega)$ was not a function of ω . In order to test the validity of this assumption under the operating conditions of our experiments we recorded the noise from the Varian Model DFS-60 spectrometer. The power spectral density was calculated using the above program. The results are shown in Figure 2.5.1. The assumption that the noise is white [$W(\omega)$ is constant] is clearly quite good. There is no systematic variation of $W(\omega)$ with ω (Fig. 2.5.1). The Fourier transform of an n. m. r. signal (Fig. 2.5.2, page 37) does vary with ω . The only assumption made in deriving Eq. (2.4.23) has been verified. We now consider a numerical problem which arises in the use of these filters.

The program requires a table of values of the line-shape function, $s(t)$, from which $h(t)$ is calculated. This line shape function is best determined experimentally. We therefore must make the

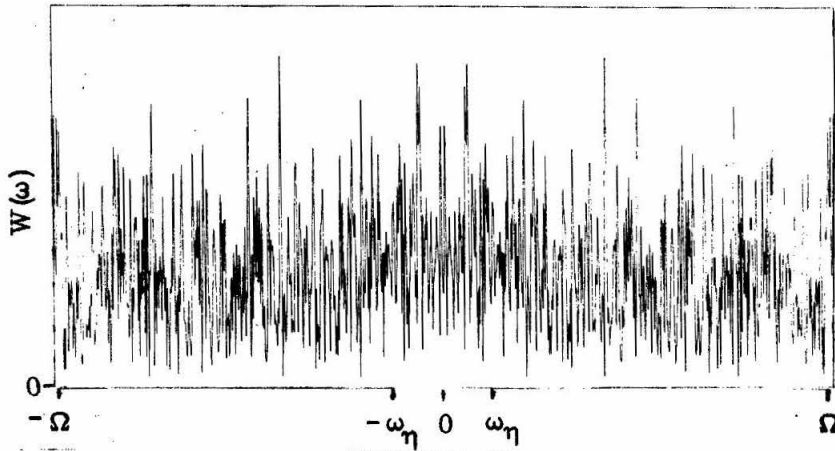


Figure 2.5.1. The power spectral density of noise from the DFS-60 spectrometer.

approximation:

$$s_i(t) \doteq s_i(t) + n_s(t), \quad (2.5.1)$$

where $n_s(t)$ is the noise in the peak we are using for the line shape.

This leads to the approximation for the frequency response function:

$$H(\omega) \doteq \frac{c(q) [S_i^*(\omega) + N_s^*(\omega)]}{1 + q | S_i(\omega) + N_s(\omega) |^2}. \quad (2.5.2)$$

This approximation must be modified to eliminate the domination of high frequency noise. We shall first prove that this is true in principle and then show that it can be important in practice.

The line-shape function at $t = 0$ is given by:

$$s_i(0) = \frac{1}{2\pi} \int_{-\infty}^{\infty} S_i(\omega) d\omega, \quad (2.5.3)$$

which implies that:

$$\text{Limit}_{|\omega| \rightarrow \infty} S_i(\omega) = 0. \quad (2.5.4)$$

The noise frequency response function satisfies the limiting equation:

$$W_S(\omega) = \text{Limit}_{T \rightarrow \infty} |N_S(\omega)|^2 / 2\pi T, \quad (2.5.5)$$

where $W_S(\omega)$ is the power spectral density of the noise. Since the noise is white so that $W_S(\omega)$ is independent of ω , then $|N_S(\omega)|$ is also independent of ω . Therefore the limit of the noise spectrum is:

$$\text{Limit}_{\omega \rightarrow \infty} N_S(\omega) = \eta_S e^{i\theta(\omega)} \neq 0, \quad (2.5.6)$$

where η_S is a constant but θ is not. The limit of the weighting function, Eq. (2.5.2), is therefore:

$$\text{Limit}_{\omega \rightarrow \infty} H(\omega) \doteq \frac{c(q) N_S^*(\omega)}{1 + q |N_S(\omega)|^2}. \quad (2.5.7)$$

We recall that the filtered spectrum is given by:

$$f_o(t) = \frac{1}{2\pi} \int_{-\infty}^{\infty} H(\omega) F_i(\omega) e^{i\omega t} d\omega, \quad (2.5.8)$$

where $F_i(\omega)$ is the Fourier transform of the input spectrum.

Equations (2.5.7) and (2.5.8) show that the noise in the line-shape function will dominate the output spectrum.

Clearly, there exists an $\omega_\eta > 0$ such that:

$$\eta_s > |S(\omega)|; \quad |\omega| \geq \omega_\eta. \quad (2.5.9)$$

If we use Eq. (2.5.2) beyond ω_η we are mainly increasing the noise in the output spectrum. We therefore use ω_η for a cut-off frequency and redefine $H(\omega)$ to be:

$$H(\omega) \doteq \left\{ \begin{array}{ll} \frac{c(q, \omega_\eta) [S^*(\omega) + N_s^*(\omega)]}{1 + q |S(\omega) + N_s(\omega)|^2}; & \omega \leq \omega_\eta \\ 0 & ; \quad \omega > \omega_\eta \end{array} \right\}. \quad (2.5.10)$$

This is equivalent to replacing the limits of integration by ω_η in Eq. (2.5.8).

When performing a numerical Fourier transform, Eq. (2.5.8) must be replaced by the approximation:

$$f_o(t) \doteq \frac{1}{2\pi} \int_{-\Omega}^{\Omega} H(\omega) F_i(\omega) e^{i\omega t} d\omega, \quad (2.5.11)$$

where Ω is determined by the number of data points for $f_i(t)$. The

above discussion would be purely academic if ω_η were larger than Ω . Their relative sizes must be determined experimentally.

Figure 2.5.2 shows a computer drawn plot of the modulus of an experimentally determined line-shape transform $|S(\omega)|$. The signal-to-noise ratio for $s(t)$ was approximately 200/1. It is clear

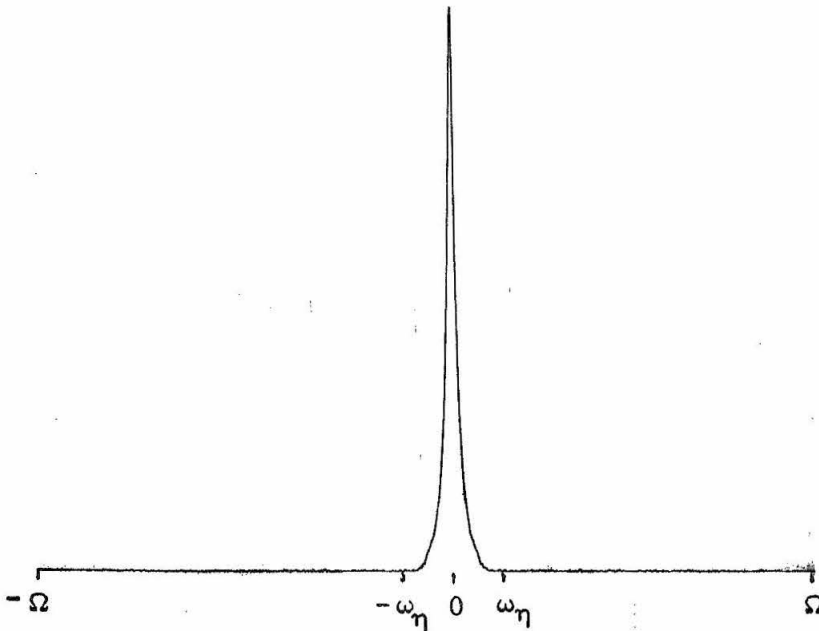


Figure 2.5.2. The modulus of the line-shape transform, $|S(\omega)|$, for an n. m. r. signal.

that in this case ω_η is much less than Ω . A frequency response function which gives high resolution enhancement has been computed from this line shape. The plot of the modulus, $|H(\omega)|$, is shown in Figure 2.5.3 and the corresponding time function, $h(\tau)$, is shown in

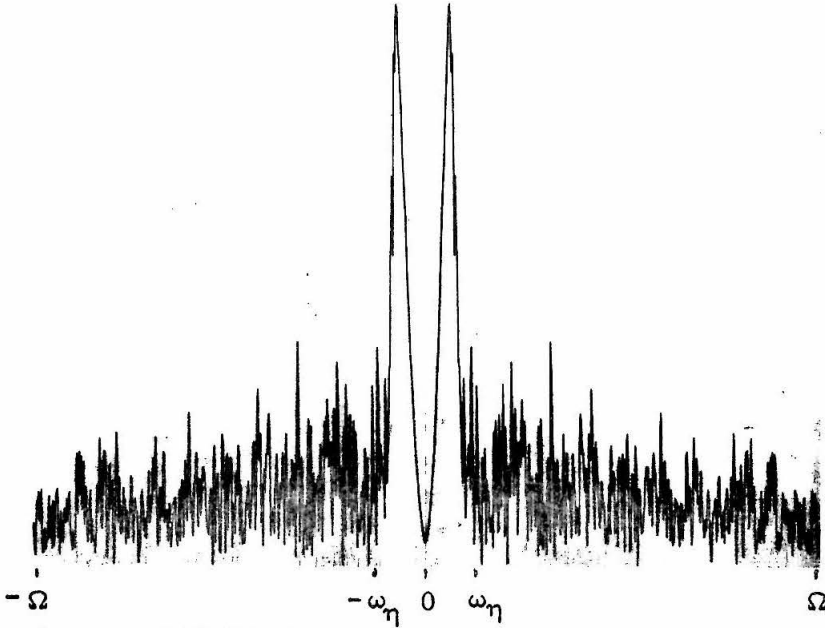


Figure 2.5.3. The modulus of the frequency response function, $|H(\omega)|$, for a high resolution weighting function.

Figure 2.5.4. It is obviously desirable to make use of the cut-off frequency, ω_η .

In practice we compute $\bar{\eta}_S$ as the average value of $|S_i(\omega) + N_S(\omega)|$ for the ten highest frequencies available. We then choose ω_η to be the smallest positive value of ω for which:

$$|S_i(\omega) + N_S(\omega)| \leq 2\bar{\eta}_S. \quad (2.5.12)$$

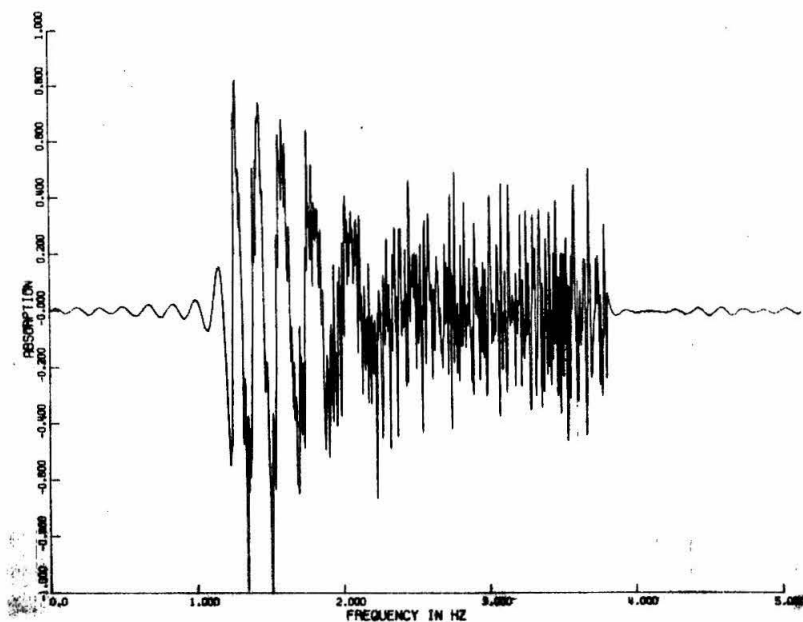


Figure 2.5.4. The weighting function $h(t)$ corresponding to Figure 2.5.3.

This effectively limits the frequency response function to those frequencies for which the signal is greater than the noise.

Figure 2.5.5 shows the results of using this value of ω_η on $|H(\omega)|$. The effect that this has on the weighting function, $h(t)$ is shown in Figure 2.5.6. We have eliminated the problems caused by high frequency noise.

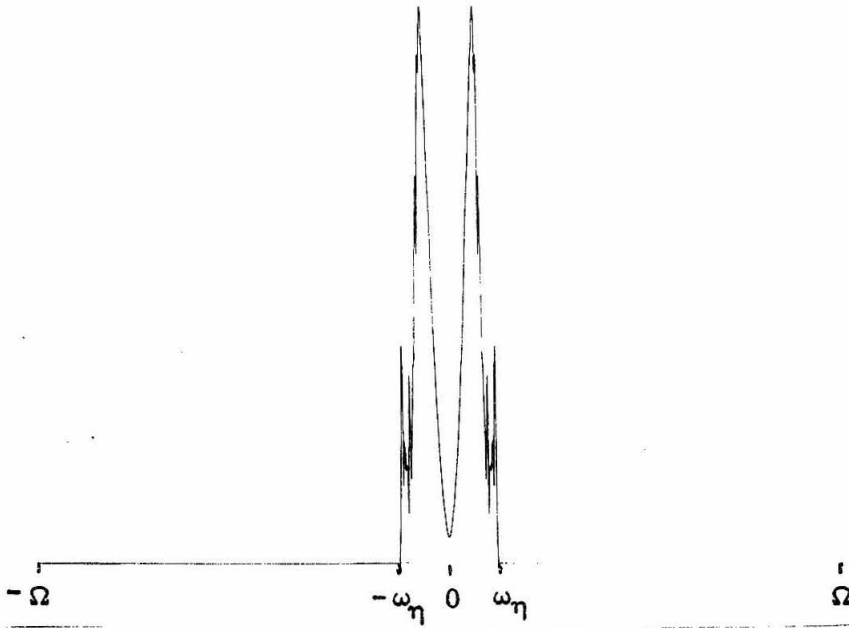


Figure 2.5.5. The modulus of the frequency response function $|H(\omega)|$ using the cut-off frequency ω_η .

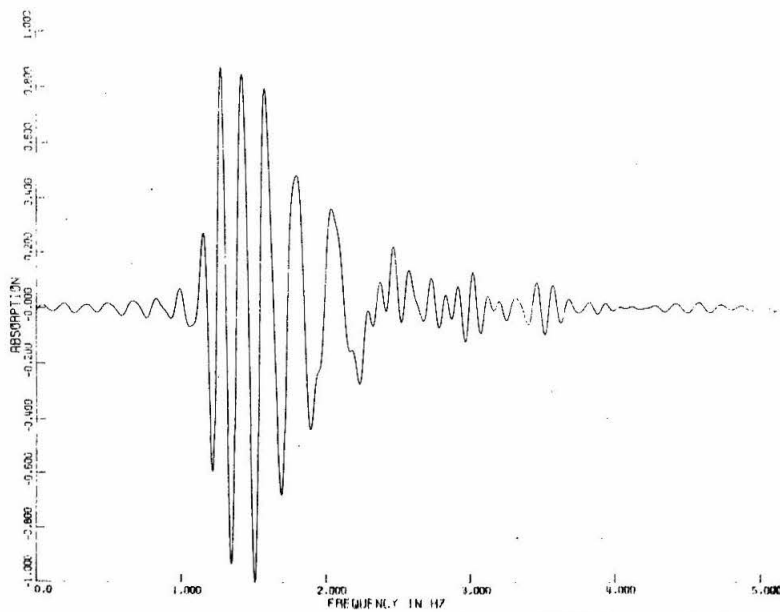


Figure 2.5.6. The weighting function $h(t)$ resulting from the frequency response function in Figure 2.5.5.

The effects of multiple scans on the above frequency response functions are shown in Figure 2.5.7. Comparison with Figures 2.5.2 and 2.5.3 indicates that eliminating the higher frequencies from the single scan data was quite reasonable. The weighting function calculated from the multiple scan data is shown in Figure 2.5.8. The use of the cut-off frequency causes $H(\omega)$ and $h(t)$ to more closely resemble the results which could be obtained by collecting additional data. We note that the high frequency wiggles towards the right in $h(t)$ have been decreased by obtaining better data.

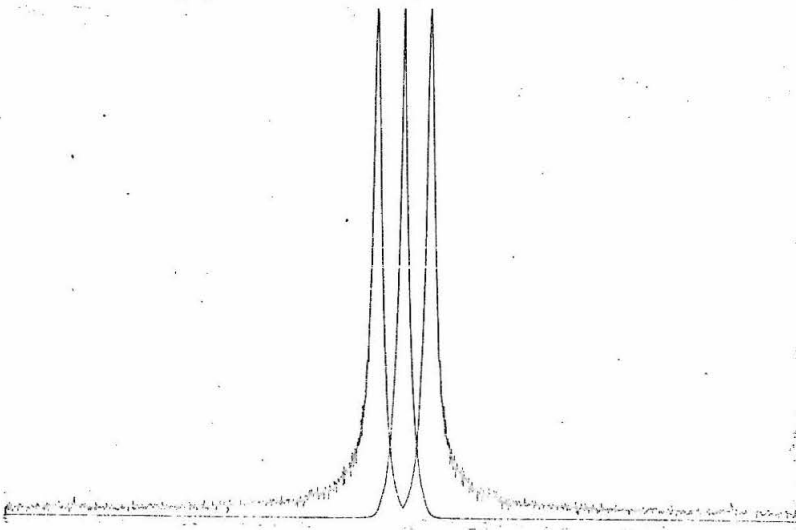


Figure 2.5.7. Frequency response functions obtained from a multiple scan experiment.

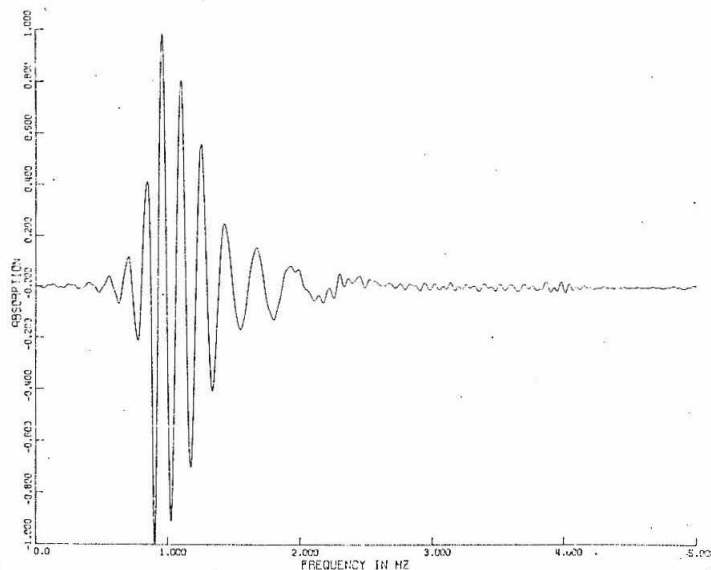


Figure 2.5.8. The weighting function resulting from the high resolution frequency response function shown in Figure 2.5.7.

The elimination of high frequency noise is not obviously important when these weighting functions are used to filter a spectrum. It would be silly to use data for $s_i(t)$ which did not have a significantly higher signal to noise ratio than the input spectrum $f_i(t)$. The high frequency noise in $s_i(t)$ will therefore always be small. However, the high frequency noise in $f_i(t)$ is not necessarily small, and the filter will take the product of the two. The more important application of the cut-off criterion will probably be found in the study of the behavior of $h(t)$. In this case, we clearly eliminate most of the noise.

All weighting functions discussed in the remainder of this thesis have been computed using the above cut-off criterion.

2.6 RC Filters

These simple analog filters are of particular interest since one is built into most commercially available n. m. r. spectrometers. They consist of one or more pairs of resistors and capacitors (Fig. 2.6.1).

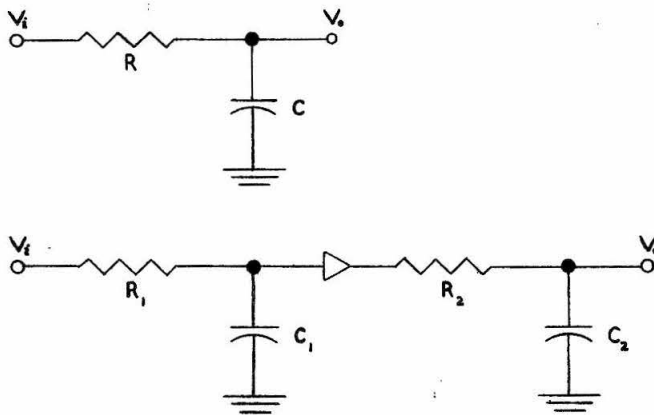


Figure 2.6.1. Single and double section RC filters.

From elementary circuit theory¹⁶ we know that:

$$f_i(t) = I(t)R + Q(t)/C, \quad (2.6.1)$$

where $f_1(t)$ is the input voltage (signal), $I(t)$ is the current, and $Q(t)$ is the charge on the capacitor. Since the current is the rate of change of the charge:

$$f_1(t) = \dot{Q}(t)R + Q(t)/C. \quad (2.6.2)$$

The output voltage (signal) is given by Q/C so that:

$$f_0(t) = RC\dot{f}_0(t) + f_0(t). \quad (2.6.3)$$

The input and output voltages are connected by a first order linear differential equation. We first put it in standard form:

$$\dot{f}_0(t) + \frac{1}{RC} f_0(t) = \frac{1}{RC} f_1(t). \quad (2.6.4)$$

The general solution is:¹⁷

$$f_0(t) = ke^{-t/RC} + e^{-t/RC} \int e^{\tau_1/RC} [1/RC] f_1(\tau_1) d\tau_1 \quad (2.6.5)$$

where k is an arbitrary constant. Since this filter is a real time device it can not use future data. Therefore, $\tau_1 \leq t$. The case of interest also satisfies the initial condition:

$$f_0(-\infty) = f_1(-\infty) = 0. \quad (2.6.6)$$

The result of using a single section RC filter is therefore:

$$f_0(t) = \int_{-\infty}^t e^{-(\tau_1-t)/RC} [1/RC] f_1(\tau_1) d\tau_1. \quad (2.6.7)$$

We now put this in the form of Eq. (2.2.1) by making the substitution

$$\tau = t - \tau_1 :$$

$$f_0(t) = \int_0^{\infty} \left(\frac{1}{RC}\right) e^{-\tau/RC} f_i(t - \tau) d\tau. \quad (2.6.8)$$

This gives the weighting function:

$$h_{RC}(\tau) = \left\{ \begin{array}{ll} \frac{1}{RC} e^{-\tau/RC} & ; \tau \geq 0 \\ 0 & ; \tau < 0 \end{array} \right\} \quad (2.6.9)$$

for a single section RC filter.

When two of these filters are placed in sequence the output function is:

$$f_0(t) = \int_0^{\infty} \left(\frac{1}{RC}\right) e^{-\tau_1/RC} \int_0^{\infty} \left(\frac{1}{RC}\right) e^{-\tau_2/RC} f_i(t - \tau_1 - \tau_2) d\tau_2 d\tau_1. \quad (2.6.10)$$

This can be rearranged to:

$$f_0(t) = \int_0^{\infty} \int_0^{\infty} \left(\frac{1}{RC}\right)^2 e^{-(\tau_1 + \tau_2)/RC} f_i[t - (\tau_1 + \tau_2)] d\tau_2 d\tau_1. \quad (2.6.11)$$

We now make the substitution $\tau = \tau_1 + \tau_2$, giving:

$$f_0(t) = \int_0^{\infty} \int_0^{\tau} \left(\frac{1}{RC}\right)^2 e^{-\tau/RC} f_i(t - \tau) d\tau_2 d\tau, \quad (2.6.12)$$

where the upper limit on τ_2 comes from the fact that τ_1 can not be negative. Integration over τ_2 gives:

$$f_0(t) = \int_0^{\infty} \left(\frac{1}{RC}\right)^2 \tau e^{-\tau/RC} f_1(t - \tau) d\tau. \quad (2.6.13)$$

The weighting function for a double section RC filter is therefore:

$$h(\tau) = \left\{ \begin{array}{ll} \left(\frac{1}{RC}\right)^2 \tau e^{-\tau/RC} & ; \tau \geq 0 \\ 0 & ; \tau < 0 \end{array} \right\}. \quad (2.6.14)$$

This result could also have been obtained by taking the inverse Fourier transform of $H_{RC}^2(\omega)$. That is, by working in frequency space. We shall find this approach particularly helpful when we consider sequences of filters in the next section.

2.7 Sequences of Filters

It is sometimes desirable to use a series of successive filters. One example is the double section RC filter. A second is suggested by the design of an n. m. r. spectrometer. An n. m. r. spectrometer is equipped with a double section RC filter with variable capacitors.¹⁸ We must decide how to set this device, since all data we obtain will have been filtered by it (or not filtered by it if we decide to remove it).

The result of two filters applied in sequence is most easily discussed in frequency space. We therefore take the Fourier

transform of the weighting function:

$$H_{RC}(\omega) = \frac{1}{RC} \int_0^{\infty} e^{-\tau/RC} e^{-i\omega\tau} d\tau, \quad (2.7.1)$$

or

$$H_{RC}(\omega) = \frac{1}{RC} \int_0^{\infty} e^{-(i\omega + 1/RC)\tau} d\tau. \quad (2.7.2)$$

Integration yields:

$$H_{RC}(\omega) = \frac{1}{1 + i\omega RC}, \quad (2.7.3)$$

for the frequency response function of a single section RC filter.

We shall examine single section RC filters in detail. It will be obvious that multiple section filters behave similarly. We recall from Eq. (2.2.9) that the result of a linear filter in frequency space is a simple product:

$$S_{RC}(\omega) = H_{RC}(\omega) S_i(\omega), \quad (2.7.4)$$

where $S_{RC}(\omega)$ is the result of an RC filter on the Fourier transform of the line shape. Similarly:

$$F_{RC}(\omega) = H_{RC}(\omega) F_i(\omega), \quad (2.7.5)$$

where $F_{RC}(\omega)$ is the RC filter output signal in frequency space. If

we use an RC filter on both our signal and our line shape function, and then construct a matched filter [Eq. (2.4.22)] based upon this new line shape, we obtain:

$$F_o(\omega) = c S_{RC}^*(\omega) F_{RC}(\omega). \quad (2.7.6)$$

Substitution of Eq. (2.7.4) for $S_{RC}(\omega)$ and Eq. (2.7.5) for $F_{RC}(\omega)$ gives:

$$F_o(\omega) = c H_{RC}^*(\omega) S_i^*(\omega) H_{RC}(\omega) F_i(\omega), \quad (2.7.7)$$

or:

$$F_o(\omega) = |H_{RC}(\omega)|^2 F_m(\omega), \quad (2.7.8)$$

where $F_m(\omega)$ is the result of a matched filter on the spectrum. We see that this procedure gives the desired result if and only if:

$$|H_{RC}(\omega)|^2 = 1. \quad (2.7.9)$$

From Eq. (2.7.3) and Eq. (2.7.8) we see that:

$$F_o(\omega) = \frac{1}{1 + (RC\omega)^2} F_m(\omega). \quad (2.7.10)$$

We could obtain the results of a matched filter by computing:

$$F_m(\omega) = c [1 + (RC\omega)^2] S_{RC}^*(\omega) F_{RC}(\omega), \quad (2.7.11)$$

but this is considerably more time consuming than carrying out the integration in time space:

$$f_m(t) = \int_{-\infty}^{\infty} s_i(-\tau) f_i(t - \tau) d\tau, \quad (2.7.12)$$

which we can do when no RC filter is used. The simplest procedure is clearly to disconnect the RC filter (frequency response control) on the spectrometer.

The extension of these results to multiple section filters is obvious. We conclude that the results of an optimum filter are recoverable after the use of any RC filter, but that the most efficient procedure is to disconnect the RC filter on the spectrometer. More generally, this is true of any filter for which the inverse exists (i. e., $H(\omega) \neq 0$; for all ω).

The RC filter may be disconnected from the Varian Model DFS-60 (or HR-60) spectrometer by using the "scope" setting. The RC filter on an A-60 type spectrometer may be effectively disconnected by setting the filter bandwidth control at 4. At this setting, RC in Eq. (2.7.11) can be regarded as zero for most purposes.

2.8 Determination of Signal-to-Noise Ratios

The most straightforward method of measuring the signal-to-noise ratio is to take the ratio of the peak height to the rms value of the spectrum where the signal is zero. This method works in some cases. In many of the spectra we deal with, the value of the signal

is greater than the noise level at all points. A less empirical method is therefore necessary.

The output signal-to-noise ratio is given by:

$$(S/N)_o \equiv s_o(t)_{\max} / n_{\text{rms}}, \quad (2.8.1)$$

$$(S/N)_o = s_o(t)_{\max} / \left[\int_{-\infty}^{\infty} |H(\omega)|^2 W_i(\omega) d\omega \right]^{\frac{1}{2}}. \quad (2.8.2)$$

For white noise this becomes:

$$(S/N)_o = \frac{s_o(t)_{\max}}{W_i^{\frac{1}{2}}} \left[\int_{-\infty}^{\infty} |H(\omega)|^2 d\omega \right]^{-\frac{1}{2}}. \quad (2.8.3)$$

Using the Plancherel theorem⁹ gives:

$$(S/N)_o = \frac{s_o(t)_{\max}}{W_i^{\frac{1}{2}}} \left[2\pi \int_{-\infty}^{\infty} h^2(\tau) d\tau \right]^{-\frac{1}{2}}. \quad (2.8.4)$$

The improvement in the signal to noise is then:

$$\frac{(S/N)_o}{(S/N)_i} = \frac{s_o(t)_{\max}}{s_i(t)_{\max}} \left[\int_{-\infty}^{\infty} h^2(\tau) d\tau \right]^{-\frac{1}{2}}, \quad (2.8.5)$$

or approximately:

$$\frac{(S/N)_o}{(S/N)_i} \doteq \frac{f_o(t)_{\max}}{f_i(t)_{\max}} \left[\int_{-\infty}^{\infty} h^2(\tau) d\tau \right]^{-\frac{1}{2}}. \quad (2.8.6)$$

This is true regardless of whether or not $h(\tau)$ is based upon the line shape $s(t)$. We can therefore use this relationship to compare optimum filters with other filters assuming only that the noise is white.

The above equation can also be derived from a statistical approach. Consider the discrete transformation:

$$f_o(t_j) = \sum_k h(\tau_k) f_i(t_j - \tau_k). \quad (2.8.7)$$

The classical statistical equation for the linear propagation of errors¹⁹ is:

$$\sigma_o^2(t_j) = \sum_k \left[\frac{\partial f_o(t_j)}{\partial f_i(t_j - \tau_k)} \right]^2 \sigma_i^2(t_j - \tau_k). \quad (2.8.8)$$

Using Eq. (2.8.7) for $f_o(t_j)$ and assuming that the noise is random we obtain:

$$\sigma_o^2 = \sum_k h^2(\tau_k) \sigma_i^2, \quad (2.8.9)$$

or:

$$\sigma_o = \left[\sum_k h^2(\tau_k) \right]^{\frac{1}{2}} \sigma_i. \quad (2.8.10)$$

The signal-to-noise ratio is given by:

$$(S/N)_o = s_o(t)_{\max} / \sigma_o. \quad (2.8.11)$$

The improvement in the signal-to-noise ratio is therefore:

$$\frac{(S/N)_o}{(S/N)_i} = \frac{s_o(t)_{\max}}{s_i(t)_{\max}} \left(\frac{\sigma_i}{\sigma_o} \right), \quad (2.8.12)$$

or finally:

$$\frac{(S/N)_o}{(S/N)_i} = \frac{s_o(t)_{\max}}{s_i(t)_{\max}} \left[\sum_k h^2(\tau_k) \right]^{-\frac{1}{2}}, \quad (2.8.13)$$

which is the discrete approximation to the result obtained from the information theory approach, Eq. (2.8.5).

This relationship, Eq. (2.8.6), was used to evaluate the signal-to-noise ratio obtained from the filters we later discuss.

3. RESULTS OBTAINED WITH LINEAR FILTERS

The effects of several linear filters on the types of line shapes resulting from an n. m. r. experiment have been studied. The resolution and signal to noise of spectra can be significantly improved with the aid of linear filters. Resolution enhancement requires more detailed knowledge of the line shape than sensitivity enhancement does.

Two line shapes have been studied in detail. The first, an experimental n. m. r. signal, was obtained from the proton-decoupled ^{13}C spectrum of carbon-1 of trans-1,3-pentadiene using a 0.2 Hz/sec. sweep rate. We considered this to be a representative line shape (Fig. 3.1). The second was a Lorentzian line, the form of an n. m. r.

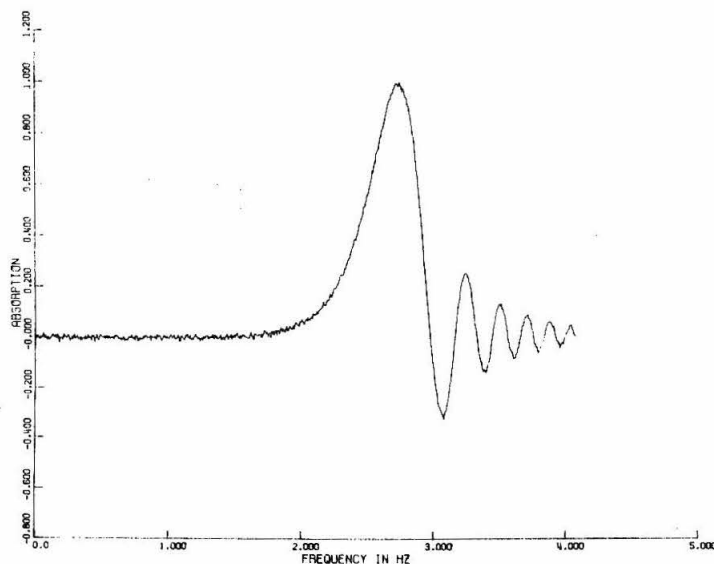


Figure 3.1. The line shape of a typical n. m. r. signal.

signal for infinitely slow passage.²⁰ These line shapes are two members of the family of possible line shapes which result from varying the sweep rate. We shall examine the nature of resolution enhancement by careful consideration of these two line shapes.

Since a filtering device based upon a Lorentzian line shape is commercially available,²¹ we have compared the results obtained by using the correct line shape to filter the above experimental line with those obtained using a Lorentzian line shape. Both these Lorentzian filters and RC filters contain the line width as a variable parameter. It is therefore necessary to optimize this parameter before comparisons can be made.

3.1 Optimum Line Widths of Weighting Functions

The line width of the weighting function, $h(\tau)$ has been varied for several combinations of line-shape function and weighting function. The results of using an RC filter are shown in Fig. 3.1.1 for a Lorentzian line shape and for the above experimental n. m. r. line shape. The use of a double section RC filter on a Lorentzian line can give up to 96.1% of the signal to noise obtainable with a matched filter. The use of a double section RC filter on the experimental signal gave up to 97.1% of the signal to noise obtainable with a matched filter. In the case of an n. m. r. line shape with "wiggles" the signal to noise peaks more sharply, indicating that setting the time constant of the filter is somewhat more critical in this case.

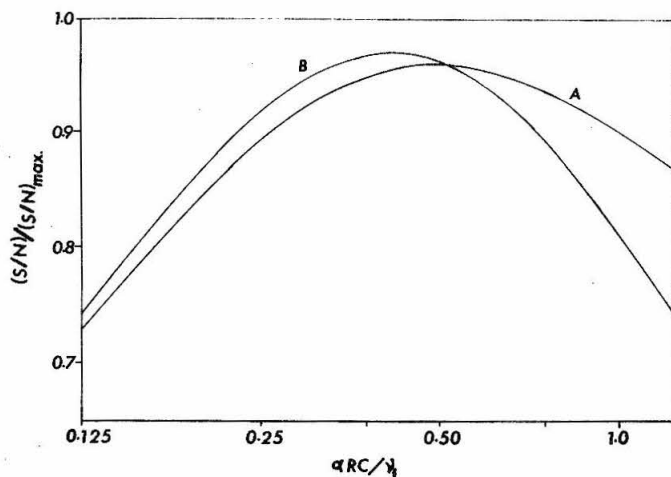


Figure 3.1.1. Signal-to-noise ratios from using a double section RC filter. Curve A results from a Lorentzian line shape and B results from the experimental line shape. ν_1 is the input line width and α is the sweep rate.

Whereas the double section RC filter with the optimum time constant broadens a Lorentzian line by 90%, the experimental n. m. r. signal is broadened by only 26%. This is because the optimum time constant for filtering the experimental signal is only 42% of the line width (full width at half height), while for a Lorentzian line it is 50% of the line width. Our results for filtering a Lorentzian agree with those obtained earlier by Ernst.²²

We have also studied filters using Lorentzian weighting functions of varying half width. The results of using this filter on both the Lorentzian and the experimental line shapes are shown in

Fig. 3.1.2. The Lorentzian function achieves a maximum when the line width of the filter function exactly equals that of the signal. This represents a matched filter. The Lorentzian line is broadened by 100%²³ and the experimental signal by 53% when the optimum line width weighting function is used.

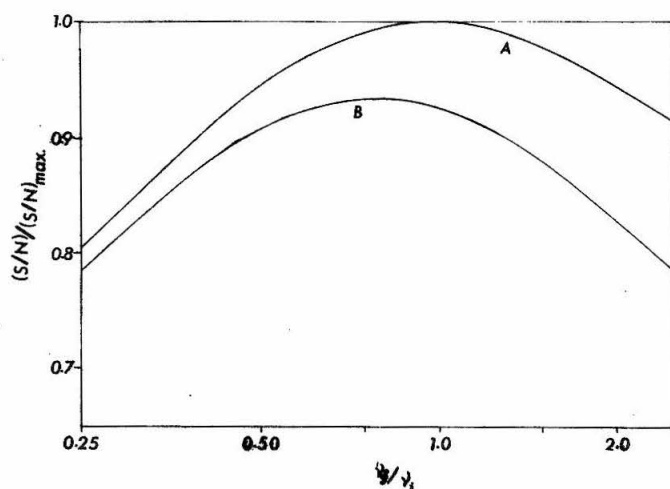


Figure 3.1.2. Signal-to-noise ratios from using a Lorentzian weighting function. Curve A is from Lorentzian line shape and B results from an n. m. r. line shape. ν_i is the input line width and ν_f is the filter line width.

The Lorentzian weighting function which gives the maximum signal-to-noise for the experimental signal had a line width which was 0.79 times the line width of the n. m. r. signal. This is the Lorentzian line width we shall use to evaluate a resolution enhancement filter based upon a Lorentzian line shape but applied to general n. m. r. signals.

3.2 Resolution Enhancement

With the signal-to-noise ratios which are experimentally accessible, one can achieve almost an order of magnitude reduction in the resolution line width. This represents a substantial improvement in the capabilities of the instrument. Figure 3.2.1 shows an example of the results we have achieved in resolution enhancement. The spectrum was obtained by adding together two slightly displaced spectra from carbon-1 of 1,3-pentadiene. The line shape was also taken from pentadiene. It is clear that a high degree of resolution enhancement is possible.

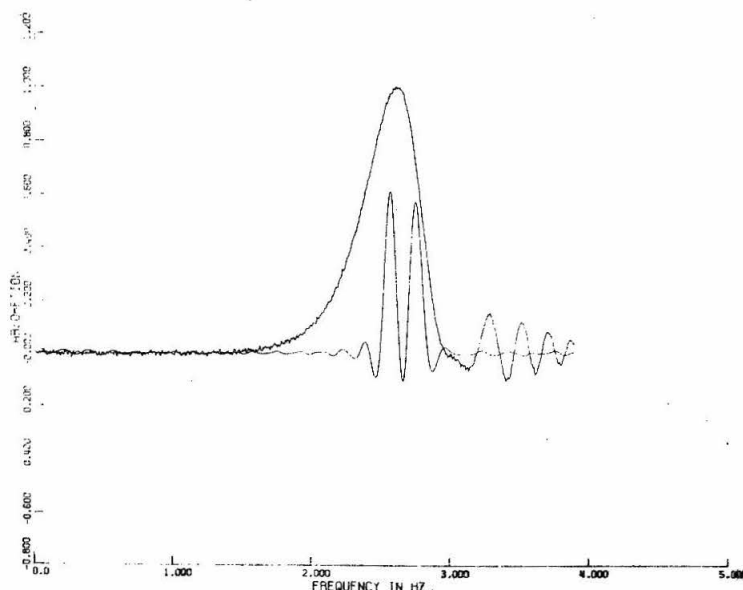


Figure 3.2.1. Resolution enhancement of an n. m. r. signal. The large peak and its "wiggles" are an unresolved doublet. The two smaller peaks are the same doublet after resolution enhancement ($q = 3000$).

We shall now consider the nature of resolution enhancement in some detail and try to achieve a better intuitive understanding of the process. Resolution enhancement is most easily understood in frequency space. We consider the Fourier transform of the weighting function, $h(\tau)$, which is the frequency response function, $H(\omega)$. We recall that this function is given by:

$$H_r(\omega) = \frac{c(q) S_i^*(\omega)}{1 + q |S_i(\omega)|^2}. \quad (3.2.1)$$

The degree of resolution enhancement increases with increasing values of q (see section 2.4). Since $c(q)$ is real and not a function of ω , the phase is unchanged from the phase of the frequency response function for a matched filter, $H_m(\omega)$. However, the amplitude is modified to emphasize higher frequencies. This is clear from the plots of $|H_m(\omega)|$ and $|H_r(\omega)|$ shown in Fig. 3.2.2.

To understand the significance of this shift to higher frequencies, we consider the corresponding weighting functions $h_r(\tau)$ and $h_m(\tau)$, shown in Fig. 3.2.3. In time space, the emphasis has been shifted from the main peak to the "wiggles" and the weighting function has taken on the appearance of a diffraction pattern. When the frequency response function shifts emphasis to higher frequencies, the effective wavelength of the diffraction pattern $h(\tau)$ is decreased. Thus, resolution enhancement can be looked upon as using a higher frequency diffraction pattern to fix positions more accurately.

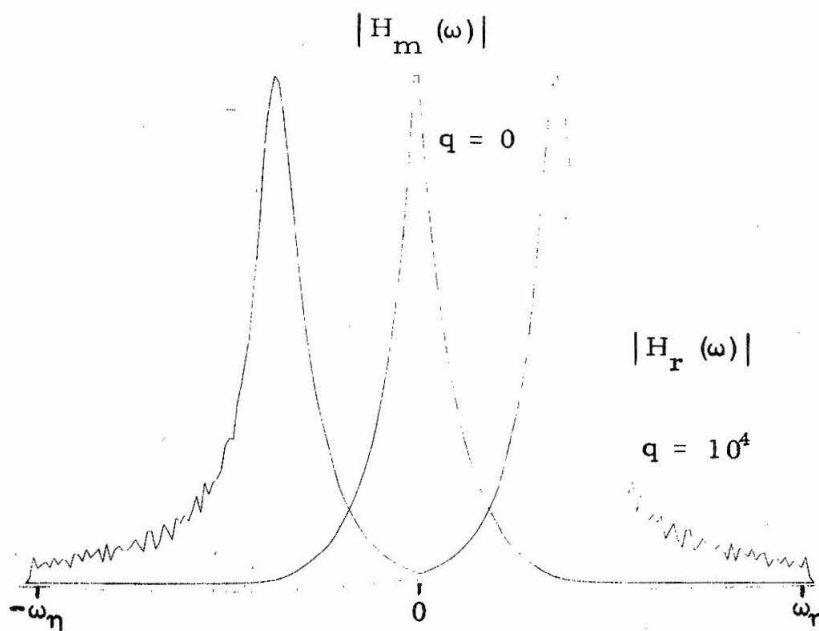


Figure 3.2.2. The modulus of the frequency response functions for a matched filter and for a resolution enhancement filter.

We note from Fig. 3.2.3 that the "wiggles" still line up perfectly. This suggests that unlike sensitivity enhancement, resolution enhancement requires a detailed knowledge of the line shape. We now consider what happens if our knowledge is limited.

One method of determining the importance of the "wiggles" in an n. m. r. line is to eliminate them from the line-shape function and look at the effect on filtering. The above experimental n. m. r.

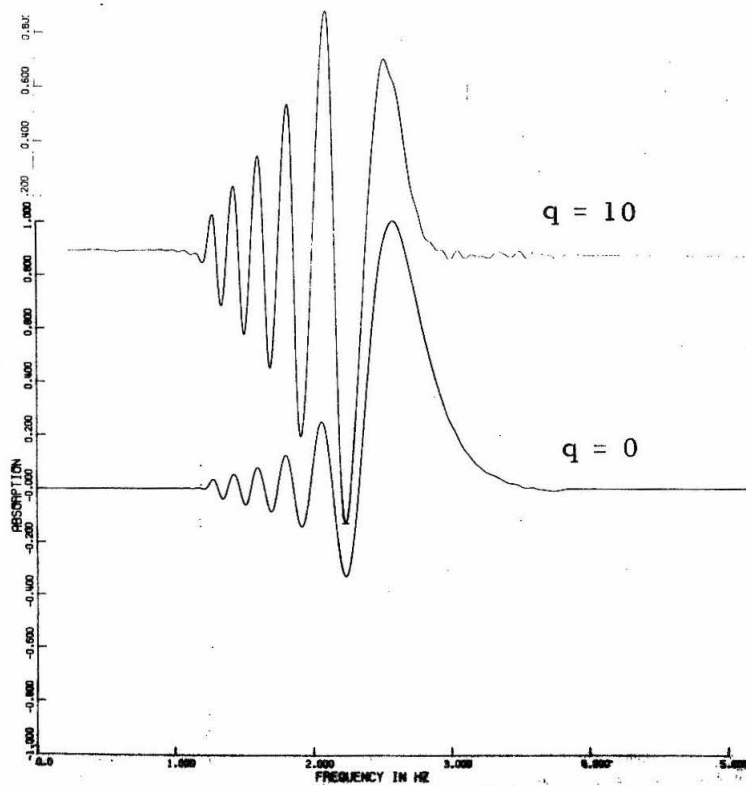


Figure 3.2.3. The weighting function for a matched filter (bottom) and for a resolution enhancement filter (top). The former is the mirror image of the line shape.

spectrum was filtered with a matched filter based upon the correct line shape and with the corresponding filter based upon a line shape with the "wiggles" removed (Fig. 3.2.4). The results are shown in

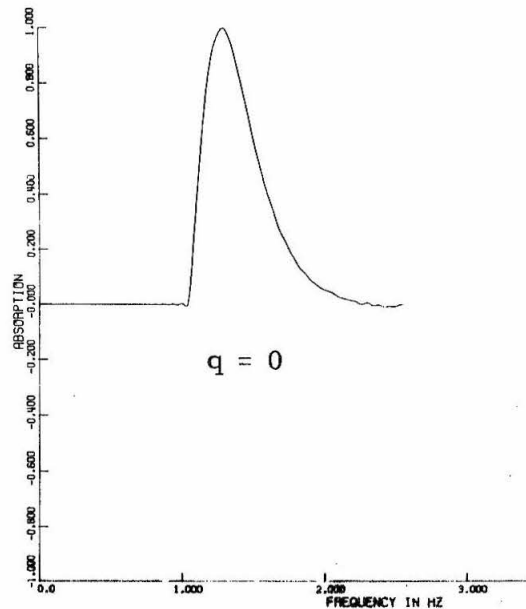


Figure 3.2.4. The weighting function for a matched filter with the "wiggles" removed.

Figure 3.2.5. The signal-to-noise ratios differ by only 2.6% and the spectra look quite similar. This is not the case when resolution enhancement filters based upon these two line shapes are used (Fig. 3.2.6). When the "wiggles" are removed from the line shape the results of resolution enhancement are not even useful. Thus, we see that while 97% of the signal to noise of an n. m. r. signal comes from

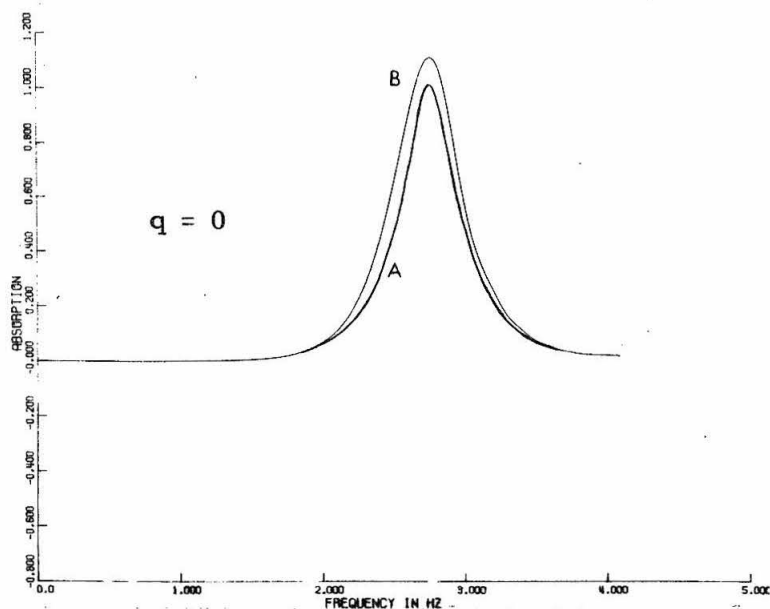


Figure 3.2.5. The results of filtering an n. m. r. signal with a matched filter which: A includes the "wiggles"; and B does not include the "wiggles".

the broad first maximum, the position of the signal (or resolution) is determined almost entirely by the much narrower wiggles.

This raises the question of whether or not we can measure the line shape sufficiently accurately in practice for these techniques to be useful. In an attempt to answer this question we compare the above line shape from pentadiene with a proton-decoupled benzene ^{13}C spectrum taken under identical conditions (Fig. 3.2.7). There is almost no difference between these line shapes; in particular, the

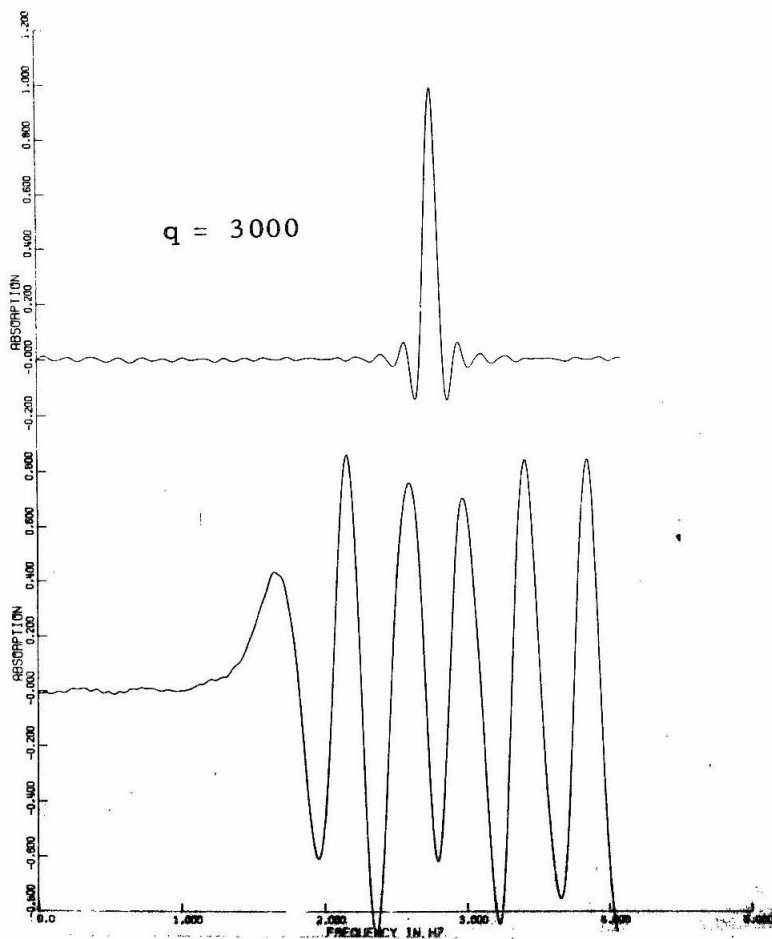


Figure 3.2.6. The results of filtering an n. m. r. signal with a resolution enhancement filter which includes the "wiggles" (top), and with one which does not (bottom).

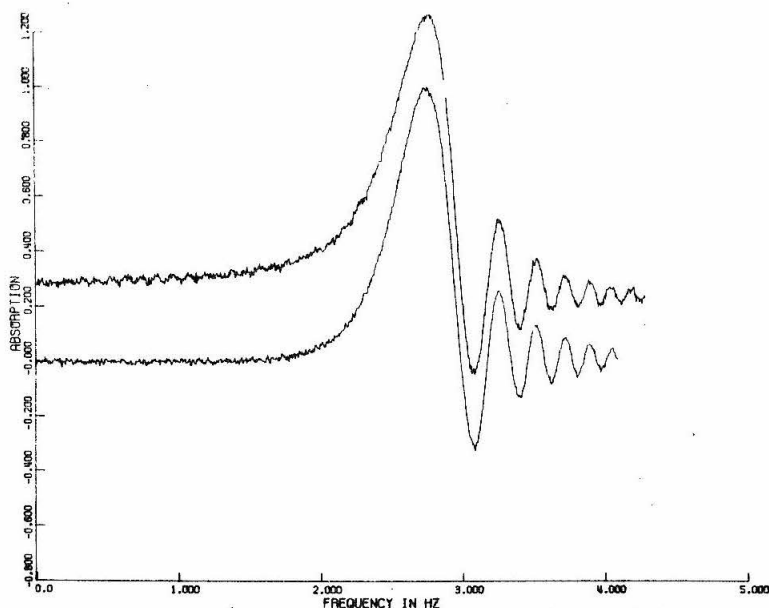


Figure 3.2.7. The proton decoupled ^{13}C spectrum of benzene (top) and the one carbon of trans-1,3-pentadiene (bottom).

"wiggles" line up perfectly. The result of filtering the benzene spectrum with a resolution enhancement filter based upon the line shape from pentadiene (Fig. 3.2.8) does not show any of the difficulties encountered earlier. When we consider the effects of sweep rate we shall see that line shapes generally appear to be sufficiently predictable as to make resolution enhancement based upon the exact line shape practical.

Another case of interest is to assume a Lorentzian line shape,²¹ since this is the exact line shape for an infinitely slow sweep rate.

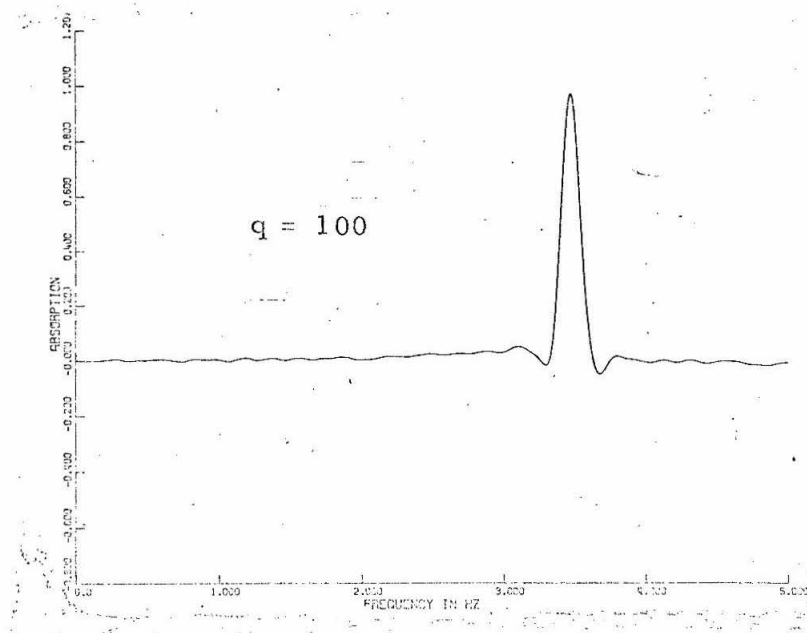


Figure 3.2.8. The result of filtering the above benzene spectrum with a resolution enhancement filter which uses the line shape from pentadiene.

That Lorentzian line width was selected which gave the maximum signal to noise for a filter which uses the Lorentzian as the weighting function to filter the pentadiene signal (see section 3.1). Weighting functions based upon this Lorentzian line shape are shown alongside the equivalent functions based upon the above pentadiene line shape in Fig. 3.2.9. Although both are diffraction patterns, they are drastically different. Most notably, the Lorentzian pattern is symmetric and remains centered at $t = 0$. What effect the differences will have on a filtered signal is not obvious. The results of using

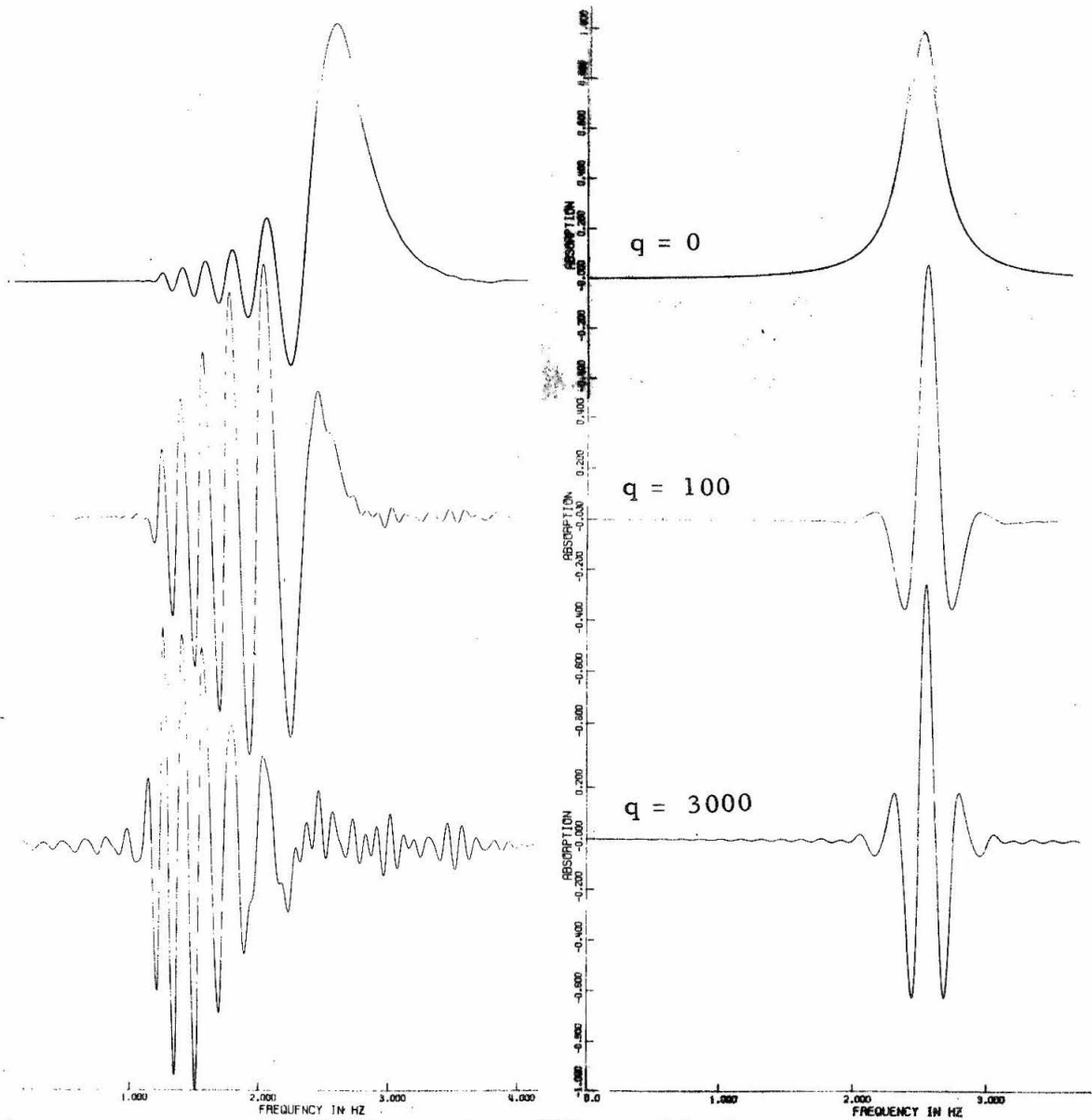


Figure 3.2.9. A comparison of weighting functions based upon the experimental n. m. r. signal (left) with those based upon the Lorentzian line which gives the maximum signal to noise (right).

these two sets of weighting functions to filter n. m. r. spectra are shown in Fig. 3.2.10. For low resolution enhancement the filters based upon a Lorentzian line shape give some improvement in the line width, but for high resolution enhancement they give results which are useless. The Lorentzian results are quite similar to those using the correct line shape, but with the "wiggles" removed.

We should keep in mind that the sweep rate for the original n. m. r. spectrum was only 0.2 Hz/sec. Slower sweep rates than this are often impractical. Under normal conditions of n. m. r. spectroscopy the deviations of the line shape from a Lorentzian are extremely important for resolution enhancement. These deviations are sufficient to make a filter based upon a Lorentzian line shape of questionable value.

Some of the difficulties encountered in filtering an n. m. r. signal with a Lorentzian resolution enhancement filter might be eliminated by first filtering the spectrum with an RC filter to remove the "wiggles". It is clear from section 2.7 that this is not the best method of going about things.

If for some reason (e. g., the sweep rate is sufficiently slow, the magnetic field is inhomogeneous, etc.) the "wiggles" disappear, the Lorentzian assumption is not too bad. Figure 3.2.11 shows the results of using the above Lorentzian resolution enhancement filters on a Lorentzian line. The achievable resolution is not as great as that from filtering an n. m. r. signal containing "wiggles" with the correct filter. This is because the natural diffraction pattern of a Lorentzian

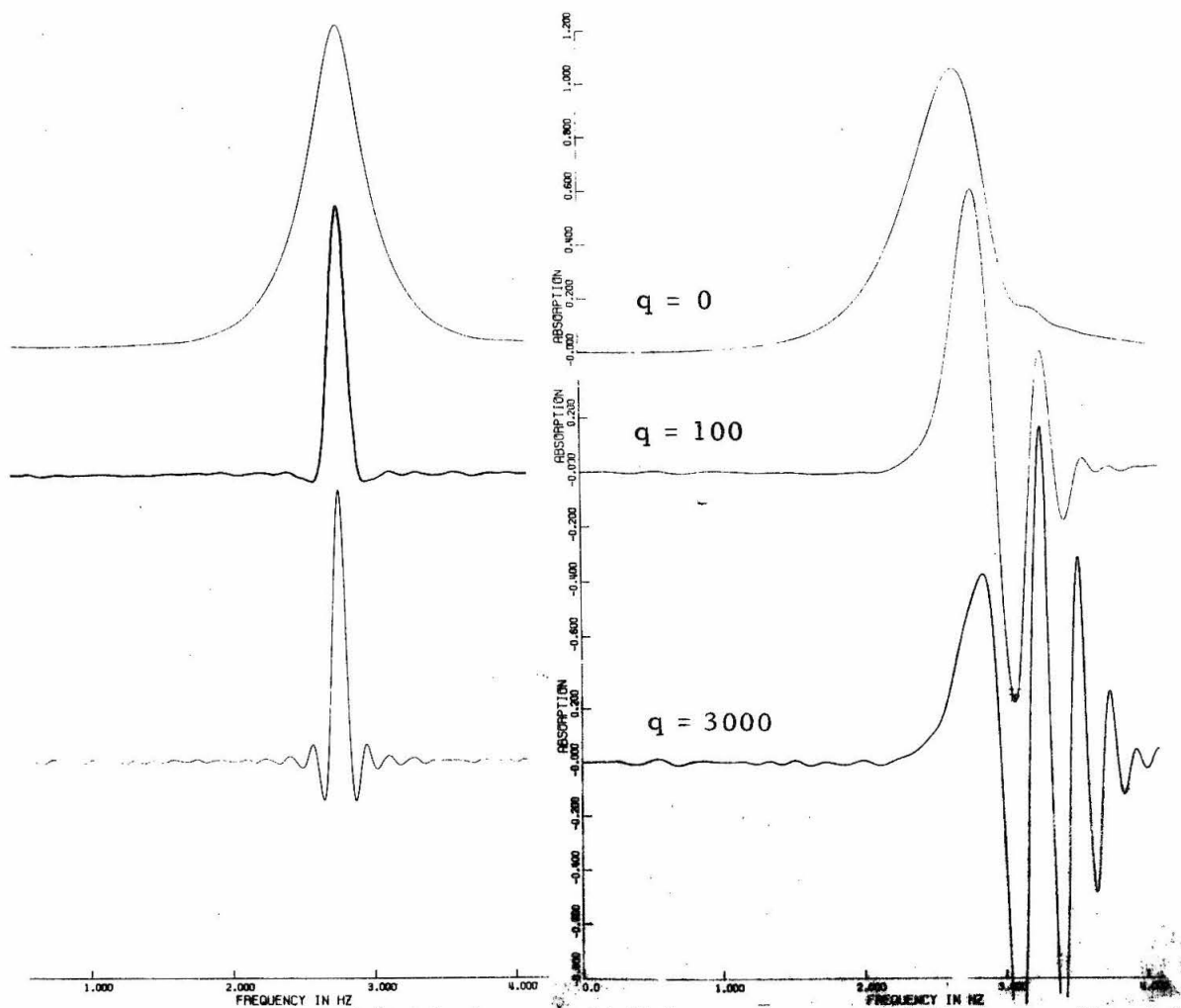


Figure 3.2.10. The results of using the weighting functions based upon the correct n. m. r. line shape (left) and those based upon the Lorentzian line shape (right).

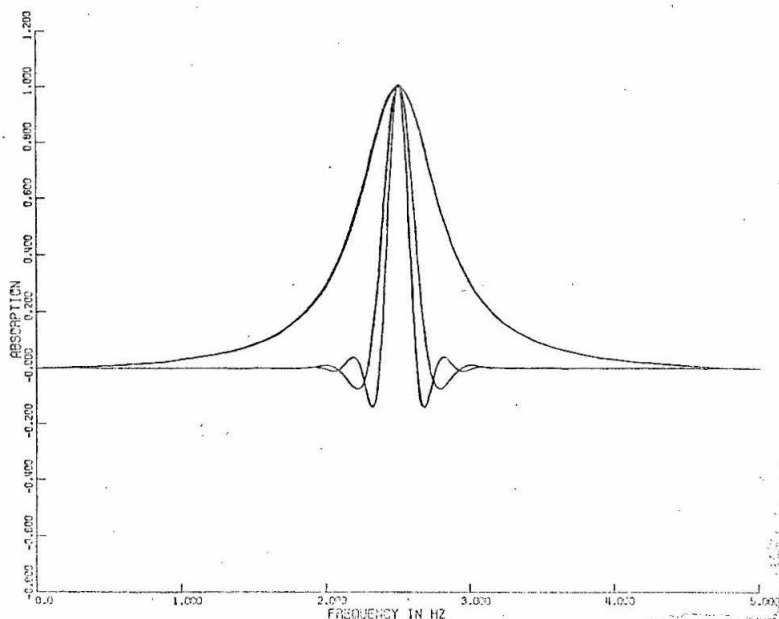


Figure 3.2.11. Resolution enhancement of a Lorentzian line using the correct line shape function. The inner lines represent successively higher resolution enhancement.

line is not as good as that of an n. m. r. signal containing "wiggles". Figure 3.2.11 does indicate however, that these Lorentzian filters can be quite effective if the line shape is similar to a Lorentzian.

The results of using a Lorentzian resolution enhancement filter on the experimental n. m. r. signal (Fig. 3.2.10) are quite similar to the mirror image of a weighting function based upon the same n. m. r. signal (Fig. 3.2.9). The similarity remains even if a Lorentzian line is filtered (see Figs. 3.2.11 and 3.2.9). This similarity is easy to understand in frequency space. The results of using a Lorentzian

resolution enhancement filter are:

$$S_0(\omega) = \frac{c(q_1) L(\omega) S_i(\omega)}{1 + q_1 L^2(\omega)}, \quad (3.2.2)$$

which has the same phase as $H^*(\omega)$, since $L(\omega)$ is real and:

$$H^*(\omega) = \frac{c(q_2) S_i(\omega)}{1 + q_2 |S_i(\omega)|^2}. \quad (3.2.3)$$

It is quite reasonable that these two expressions should be almost equal for some value of q_1/q_2 .

The experimental n. m. r. signal is more closely related to a Lorentzian line shape than the above discussion indicates. In addition to $\ell(t)$ being the limiting form of $s_i(t)$ for slow sweep rates, $L(\omega)$ is an excellent approximation to $|S(\omega)|$ for any sweep rate. We shall first demonstrate that this statement is true, and then use it to determine some general properties of linear resolution enhancement filters.

Consider the normalized Lorentzian function:

$$\ell(t) = \frac{(\pi b_\ell)^{-1}}{1 + (t/b_\ell)^2}, \quad (3.2.4)$$

which has a full width at half height equal to $2 b_\ell$. The Fourier transform of $\ell(t)$ is given by:

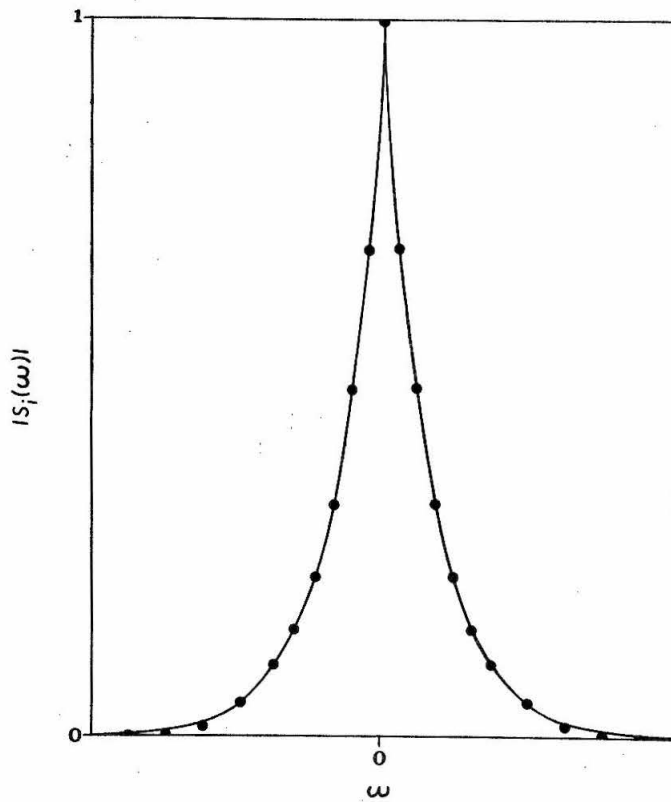


Figure 3.2.12. The Fourier transform of the experimental n. m. r. line. The curve is an exponential.

$$L(\omega) = \frac{1}{\pi b_\ell} \int_{-\infty}^{\infty} \frac{e^{-i\omega t}}{1 + (t/b_\ell)^2} dt. \quad (3.2.5)$$

Integration gives the simple result:

$$L(\omega) = e^{-b_\ell |\omega|}. \quad (3.2.6)$$

The modulus of the Fourier transform of the experimental n. m. r. signal also decays exponentially (Fig. 3.2.12). We can therefore make the approximation:

$$|H(\omega)| \doteq \frac{c(q) e^{-b_S |\omega|}}{1 + q e^{-2 b_S |\omega|}}, \quad (3.2.7)$$

for the frequency response function. The phase of $H(\omega)$ is the same as the phase of $S_i^*(\omega)$. This will depend upon the sweep rate, however, the modulus, $|H(\omega)|$, has a form which is independent of sweep rate. The exponent, b_S , increases with increasing sweep rate, but the form of $|H(\omega)|$ does not change.

If q is between zero and one, this function has a single maximum at $\omega = 0$ (Fig. 3.2.2). If q is greater than one, $|H(\omega)|$ will have two maxima at:

$$\omega_q = \pm \frac{1}{2 b_S} \ln q. \quad (3.2.8)$$

If we define:

$$\omega_1 \equiv |\omega - \omega_q|, \quad (3.2.9)$$

then it follows from Eq. (3.2.7) that:

$$|H(\omega)| \doteq \frac{c(q) q^{-\frac{1}{2}} e^{-b_S \omega_1}}{1 + e^{-2 b_S \omega_1}} \quad (3.2.10)$$

The effect of changing q is simply to change the position of the maximum, ω_q . Each branch of $|H(\omega)|$ is symmetric about this maximum (Fig. 3.2.2).

We shall return to the approximation:

$$|S_1(\omega)| \doteq e^{-b_S |\omega|}, \quad (3.2.11)$$

when we discuss line shapes.

Diffraction patterns have long been used to measure positions accurately. Since the linear filters we have developed make effective use of this technique, it seems rather unlikely that any modification of our definition of line width would lead to a significant improvement in resolution enhancement.

The qualitative conclusions we have reached in this section apply to any n. m. r. signal, whereas the quantitative results are a function of the sweep rate. The two line shapes studied above indicate the nature of the dependence of these results upon the sweep rate. We shall study the details of this dependence later.

3.3 Line Shapes Resulting from Resolution Enhancement

We concluded in section 2.1 that in addition to decreasing the resolution line width we wanted to make the signal approach zero rapidly. Figure 3.3.1 shows the line shapes of filtered spectra for several values of q in Eq. (3.2.1). These lines obviously have both of the desired properties. The line shapes are similar to those resulting from filtering a Lorentzian with an optimum filter²⁴ (Fig. 3.2.11). In both cases "wiggles" are introduced in the tail of the line shape. These "wiggles" grow with increasing resolution enhancement.

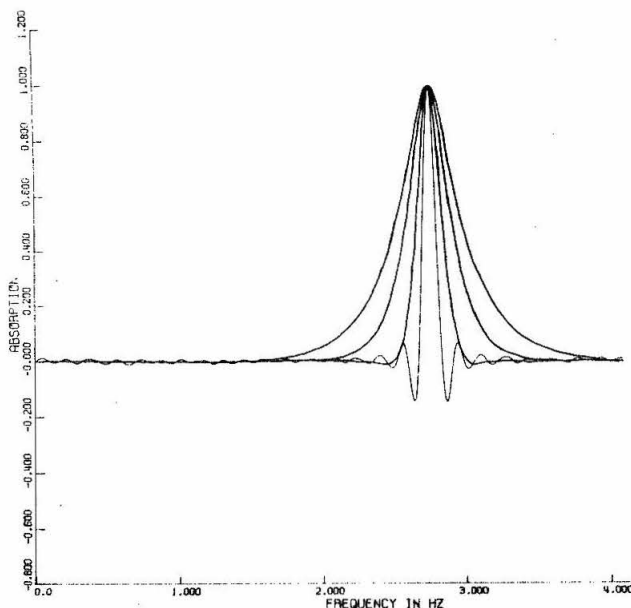


Figure 3.3.1. The line shape of the experimental n. m. r. signal after resolution enhancement. The outside line results from a matched filter. The inside lines result from successively higher values of q in Eq. (3.2.1).

The general features of these line shapes are independent of the sweep rate. The Fourier transform of the line shape resulting from a linear resolution enhancement filter is given by:

$$S_o(\omega) = \frac{c(q) |S_i(\omega)|^2}{1 + q |S_i(\omega)|^2}. \quad (3.3.1)$$

The output from a matched filter ($q = 0$) is then:

$$S_m(\omega) = c(0) |S_i(\omega)|^2. \quad (3.3.2)$$

Substituting the approximate form of $|S_i(\omega)|$ given by Eq. (3.2.11) we find:

$$S_m(\omega) \doteq c(0) e^{-2 b_S |\omega|}. \quad (3.3.3)$$

The output from a matched filter is therefore:

$$s_m(t) \doteq \frac{(2 \pi b_S)^{-1}}{1 + (t/2 b_S)^2}. \quad (3.3.4)$$

That is, if q equals zero, then the output line shape is approximately Lorentzian.

If q is much greater than one, $S_o(\omega)$ is approximately a step function (Fig. 3.3.2). That is, one can make the approximation:

$$\text{Limit}_{q \rightarrow \infty} S_o(\omega) \doteq \left\{ \begin{array}{ll} c(q)/q ; & |\omega| \leq \omega_q \\ 0 ; & |\omega| > \omega_q \end{array} \right\} \quad (3.3.5)$$

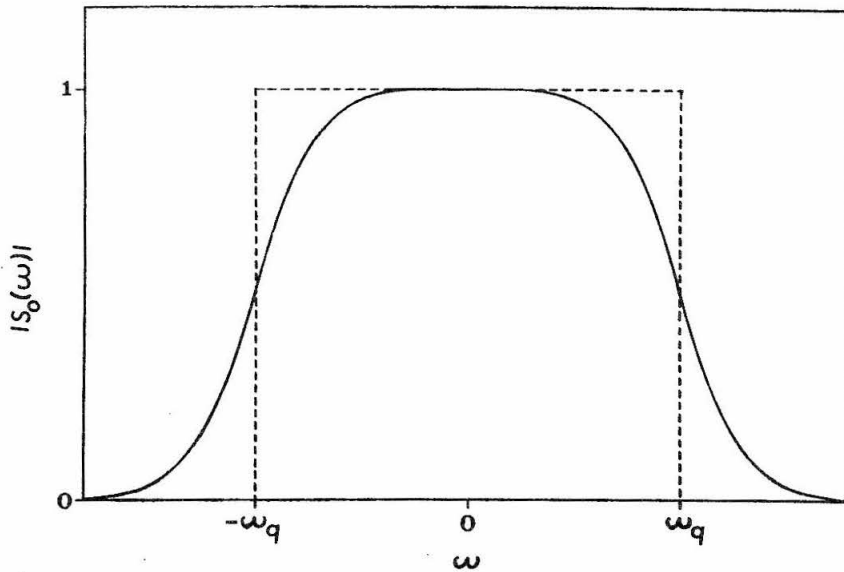


Figure 3.3.2. The Fourier transform of a filtered line.

Taking the Fourier transform gives:

$$\text{Limit}_{q \rightarrow \infty} S_0(t) \doteq \frac{c(q)}{\pi q} \left[\frac{\sin(\omega_q t)}{t} \right], \quad (3.3.6)$$

for the output line shape. As q increases, so does ω_q . This causes the frequency of the wiggles to increase. The full width at half height of this line shape must be determined numerically. The result is:

$$\text{Limit}_{q \rightarrow \infty} \nu_0 \doteq \frac{3.7910}{\omega_q}. \quad (3.3.7)$$

Substitution of Eq. (3.2.8) for ω_q gives:

$$\lim_{q \rightarrow \infty} \nu_0 \doteq \frac{7.5820 b_S}{\ln q} = \frac{1.8955}{\ln q} \nu_m, \quad (3.3.8)$$

since the output line width from a matched filter is $4 b_S$ [Eq. (3.3.4)]. As q approaches infinity, $S_0(t)$ approaches a Dirac delta function according to Eq. (3.3.6). If we wish to resolve two overlapping peaks of greatly differing amplitudes, these "wiggles" may prevent us from doing so. A method of avoiding this problem by using non-linear filters will be discussed later. We shall use linear filters only for lines of comparable magnitude.

A quantitative measure of the desirability of a line shape is the ratio of the observed separation to the exact separation for two closely spaced lines (Fig. 3.3.3). Ideally this ratio should always be one. In practice it is zero when the separation is less than the resolution line width and deviates from one for larger separations. The "wiggles" in a resolution enhancement line shape cause this ratio to oscillate about one. The observed separation is not a lower bound to the true separation, however the magnitude of the deviations has not increased. The resolution line width therefore seems to be an adequate measure of the resolution of these types of line shapes.

The situation is somewhat more complicated for other line shapes. Figure 3.3.4 shows an n.m.r. spectrum of two overlapping lines obtained by adding together two of the above pentadiene spectra.

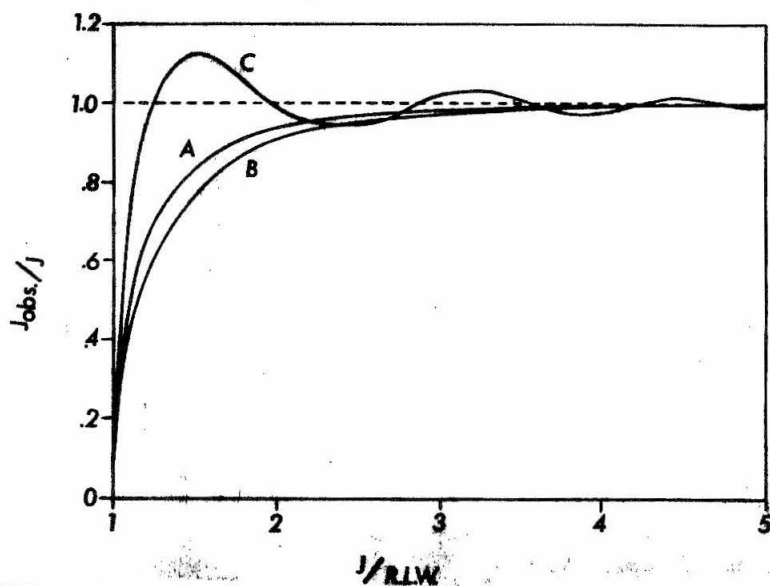


Figure 3.3.3. The observed separation of a symmetric doublet as a function of the actual separation. Curve A results from a Lorentzian line shape. Curves B and C result from the experimental n. m. r. signal using a matched filter and a resolution enhancement filter respectively.

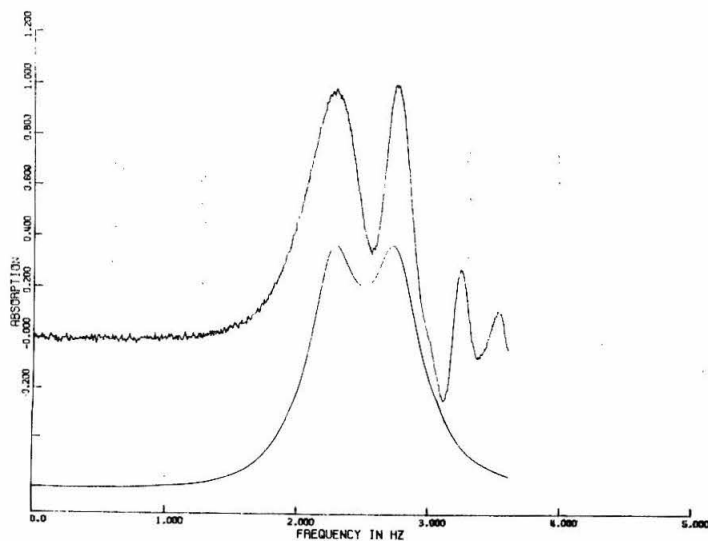


Figure 3.3.4. The n. m. r. spectrum of two overlapping lines before (top) and after (bottom) using a matched filter.

The raw spectrum is rather difficult to interpret. After filtering this spectrum with a matched filter it is obvious that the spectrum represents a symmetric doublet. The matched filter made the line shape symmetric and easy to interpret.

In general, we obtain the Fourier transform of the output line shape by taking the product of the Fourier transform of the input line shape and the frequency response function of the filter:

$$S_o(\omega) = H(\omega) S_i(\omega). \quad (3.3.9)$$

In the case of an optimum linear resolution enhancement filter based upon the correct line shape this leads to the output function:

$$S_o(\omega) = \frac{c(q) S_i^*(\omega) S_i(\omega)}{1 + q |S_i(\omega)|^2}. \quad (3.3.10)$$

Since $S_o(\omega)$ is real, the output line-shape function $s_o(t)$ is symmetric (see Section 2.2). Only a filter based upon the correct line shape can lead to a symmetric filtered line. The above example indicates that using the correct line shape can be important beyond the obvious advantage of a decreased resolution line width.

3.4 Signal-to-Noise Ratios

Now we consider exactly how much signal to noise we must sacrifice for a given improvement in resolution. The signal-to-noise level was calculated using Eq. (2.8.6) and the resolution was

measured using the full width at half height since this quantity is easily obtained. The results for several combinations of line shape and filter are shown in Fig. 3.4.1. The best resolution improvement clearly results when there are "wiggles" in both the signal and the line shape the filter is based upon. An n. m. r. line with "wiggles" gives considerably better results than a Lorentzian line shape when the correct resolution enhancement filter is used for both (A and D

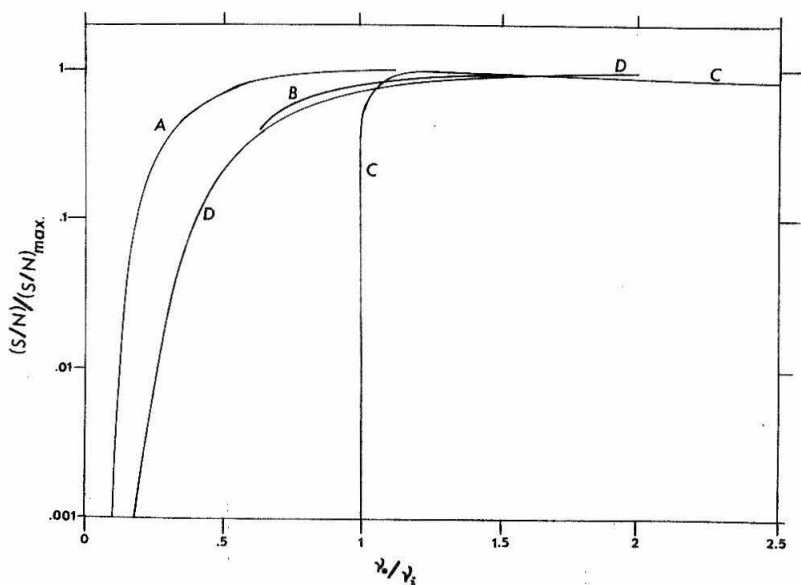


Figure 3.4.1. The output signal to noise as a function of the line width, where ν_1 is the input full width at half height and ν_0 is the output full width at half height. Curves A and B result from filtering the experimental n. m. r. signal with a resolution enhancement filter based upon the correct and Lorentzian line shapes respectively. Curve C results from filtering this n. m. r. signal with an RC filter. Curve D results from filtering a Lorentzian line with a resolution enhancement filter based upon the correct Lorentzian line shape.

in Fig. 3.4.1). Enhancement of the above experimental n. m. r. signal with "wiggles" is roughly equivalent to that of a Lorentzian line with half the full width at half height. The results of filtering this n. m. r. signal with a Lorentzian-based filter (B in Fig. 3.4.1) could not be measured for high resolution enhancement since the resulting line shape (Fig. 3.2.10) becomes too ambiguous to interpret. The line width resulting from using an RC filter (C in Fig. 3.4.1) is never less than the original line width. As RC approaches zero the RC weighting function approaches a Dirac delta function (i. e., it becomes equivalent to not using any filter at all).

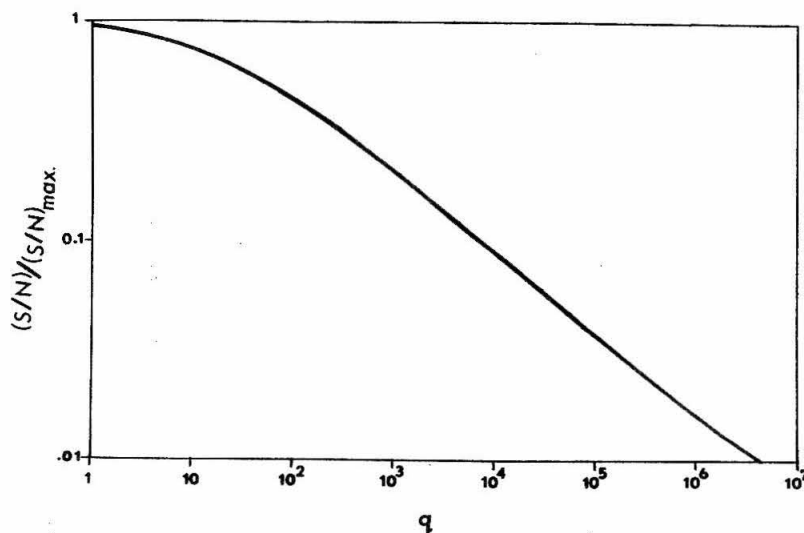


Figure 3.4.2. The relative signal-to-noise ratio as a function of the parameter q in Eq. (3.2.1).

In practice, the resolution enhancement and consequent loss of signal to noise are determined by our choice of the parameter q in the frequency response function [Eq. (3.2.1)]. The loss in signal to noise is a smooth monotonic function of q (Fig. 3.4.2) when the correct line shape is used. The loss in signal to noise varies only slightly between the Lorentzian and the experimental n. m. r. line shapes. That is, it is independent of the sweep rate. Thus, it is possible (and obviously desirable) to know in advance how much signal to noise we shall lose.

We sought a simple expression for the loss of signal to noise as a function of q . The following relationship was empirically determined:

$$(S/N)_{\max}/(S/N) \doteq 1 + \left(\frac{q}{137}\right)^{\frac{1}{2}}. \quad (3.4.1)$$

This equation predicts signal-to-noise losses of up to one thousand to within 30% for all sweep rates of interest. Our program requires only the tolerable signal-to-noise loss $(S/N)_T$ as input. It then calculates q from:

$$q \equiv 137 \left[(S/N)_T - 1 \right]^2. \quad (3.4.2)$$

When using the program one should keep in mind that a matched filter can give an improvement of up to ten to one over the signal-to-noise ratio of the raw data.

The empirical relationship in Eq. (3.4.1) is adequate for the useful range of q . A more accurate relationship between q and the signal-to-noise loss can be obtained from the asymptotic behavior of linear resolution enhancement filters. We shall use the approximate form of $|S_i(\omega)|$ given by Eq. (3.2.11) and the asymptotic form of $S_o(\omega)$ given by Eq. (3.3.5). This leads to the approximation:

$$\lim_{q \rightarrow \infty} |H(\omega)| \doteq \begin{cases} \frac{c(q)}{q} e^{b_s |\omega|} ; & \omega \leq \omega_q \\ 0 & ; \omega > \omega_q \end{cases} \quad (3.4.3)$$

for the asymptotic form of the frequency response function. From Eq. (2.8.3) we see that the loss in signal-to-noise from resolution enhancement is given by:

$$\frac{(S/N)_o}{(S/N)_m} = \frac{s_o(t)_{\max}}{s_m(t)_{\max}} \left\{ \frac{\int_{-\infty}^{\infty} |S_i(\omega)|^2 d\omega}{\int_{-\infty}^{\infty} |H(\omega)|^2 d\omega} \right\}^{\frac{1}{2}}. \quad (3.4.4)$$

Integration using the above approximations for $|S_i(\omega)|$ and $|H(\omega)|$ gives:

$$\text{Limit}_{g \rightarrow \infty} \frac{(S/N)_o}{(S/N)_m} \doteq \frac{[c(q)\omega_q/\pi q]}{[1/2 \pi b_S]} \left\{ \frac{[1/2 b_S]}{\left[\frac{c(q)^2}{2q^2 b_S} (e^{2b_S \omega_q} - 1) \right]} \right\}^{\frac{1}{2}} \quad (3.4.5)$$

Substitution of Eq. (3.2.8) for ω_q gives:

$$\text{Limit}_{q \rightarrow \infty} \frac{(S/N)_o}{(S/N)_m} \doteq \frac{\ell n q}{q^{\frac{1}{2}}}, \quad (3.4.6)$$

for the asymptotic behavior of resolution enhancement filters.

This suggests the approximation:

$$\frac{(S/N)_o}{(S/N)_m} \doteq \frac{1 + \ell n(q+1)}{1 + q^{\frac{1}{2}}} \quad (3.4.7)$$

which is accurate to within 15% for all q greater than or equal to zero. Unfortunately, we cannot solve Eq. (3.4.7) for q as an explicit function of the signal-to-noise loss. We therefore retain Eq. (3.4.2) as our basis for selecting q .

We have used the full width at half height to compare several filters. A more realistic comparison would use the resolution line

width (sec. 2.1) for two equal lines. The resolution line widths of some typical line shapes are given in Table 3.4.1. Although they vary

TABLE 3.4.1

Line Shape	(R. L. W.)/(F. W. H. H.)
Lorentzian	0.864
Experimental N. M. R.	0.664
Exp. Matched Filter	0.511
Exp. Res. Enhc. ($q = 3000$)	0.950

by almost a factor of two, they do not effect any of the qualitative conclusions reached on the basis of the full width at half height. The variation of signal-to-noise ratio with line width (Fig. 3.4.1) has been recalculated on the basis of Table 3.4.1. The two cases of principal interest are filtering the experimental n. m. r. line and the Lorentzian line with the correct resolution enhancement filters. Figure 3.4.3 shows the variations in signal to noise with resolution line width for these two cases. The Lorentzian curve (B) is almost unchanged from that in Fig. 3.4.1. The curve (A) for an n. m. r. line with "wiggles" shows greater improvement for low resolution enhancement. Even a matched filter can give an improvement in the resolution line width. The curves shown in Fig. 3.4.3 are two members of the family of

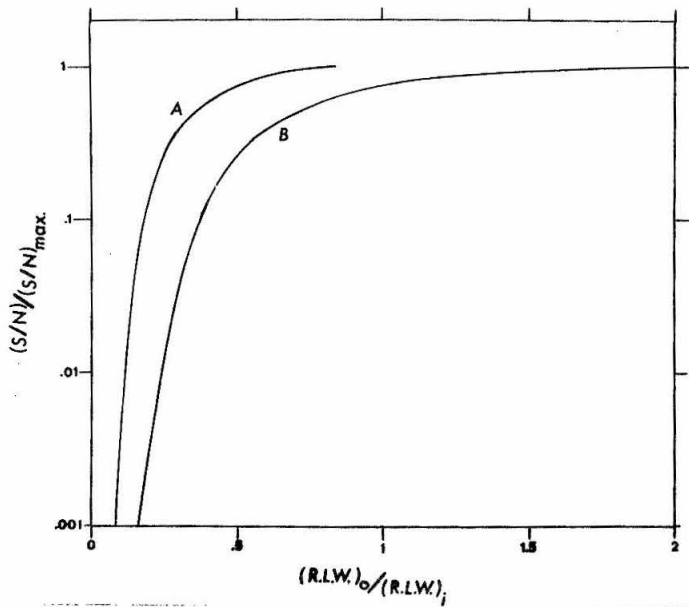


Figure 3.4.3. The output signal to noise as a function of the resolution line width. Curve A results from filtering the n. m. r. signal with "wiggles" using the correct resolution enhancement filter. Curve B results from filtering a Lorentzian signal using the correct resolution enhancement filter.

possible curves for resolution enhancement in an n. m. r. experiment with varying sweep rate. Curve B ($\alpha = 0$) appears to be the limiting worst case. Significant improvement in resolution can be achieved in any n. m. r. experiment for which we can measure the line shape. We shall now consider the effects of sweep rate in more detail.

3.5 The Effects of Sweep Rate

Changing the sweep rate has dramatic effects upon all aspects of an n. m. r. experiment. To understand the effects involved we consider briefly the physical nature of a typical n. m. r. experiment.

If nuclei are placed in a homogeneous magnetic field in the z direction, they tend to align themselves with the field and precess about this direction with the Larmor frequency ν_0 (Fig. 3.5.1).

A net magnetization \underline{M}_0 develops in the z direction, with the characteristic time constant T_1 . If the magnetic field is turned on at $t = 0$, then:

$$\underline{M}_Z = \underline{M}_0 (1 - e^{-t/T_1}), \quad (3.5.1)$$

where \underline{M}_Z is the instantaneous magnetization in the z direction. If an rf field, $2H_1$, of frequency ν_0 is applied in the x direction, it will have components of magnitude H_1 and frequency ν_0 rotating clockwise and counter-clockwise in the xy plane. The clockwise component is stationary with respect to the nuclei, while the counter-clockwise

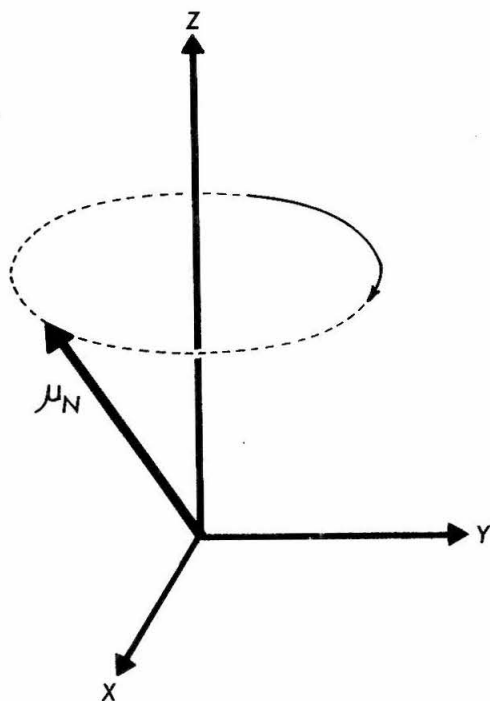


Figure 3.5.1. Precession of a nuclear magnetic moment μ_N about a magnetic field in the z direction.

component rotates with frequency $2\nu_0$ with respect to the nuclei and has no effect on them. The nuclei will precess about the "stationary" clockwise component. This leads to an induced magnetization in the xy plane, \underline{M}_{xy} , which trails the clockwise component of the rf field by 90° (Fig. 3.5.2). If \underline{H}_1 is turned off, \underline{M}_{xy} decays with characteristic time constant T_2 . That is:

$$||\underline{M}_{xy}|| = ||\underline{M}_{xy}||_{t=0} e^{-t/T_2}, \quad (3.5.2)$$

where \underline{H}_1 was turned off at $t = 0$. The torque exerted by \underline{H}_1 on \underline{M}_{xy} leads to absorption.

If the frequency of the rf field, ν_{rf} , is slightly different from ν_0 , \underline{H}_1 will slowly rotate with respect to \underline{M}_{xy} . If ν_{rf} has been increased sufficiently past ν_0 , then \underline{H}_1 no longer affects \underline{M}_{xy} and \underline{M}_{xy} will rotate at exactly ν_0 . The rate of change of θ (Fig. 3.5.2) is then given by:

$$\dot{\theta} = 2\pi(\nu_{rf} - \nu_0), \quad (3.5.3)$$

where θ is measured in radians. If the frequency (or field) sweep is linear and we passed through resonance at $t = 0$, then:

$$(\nu_{rf} - \nu_0) = \alpha t, \quad (3.5.4)$$

where α is the sweep rate in Hz. Combining these two equations and integrating we obtain:

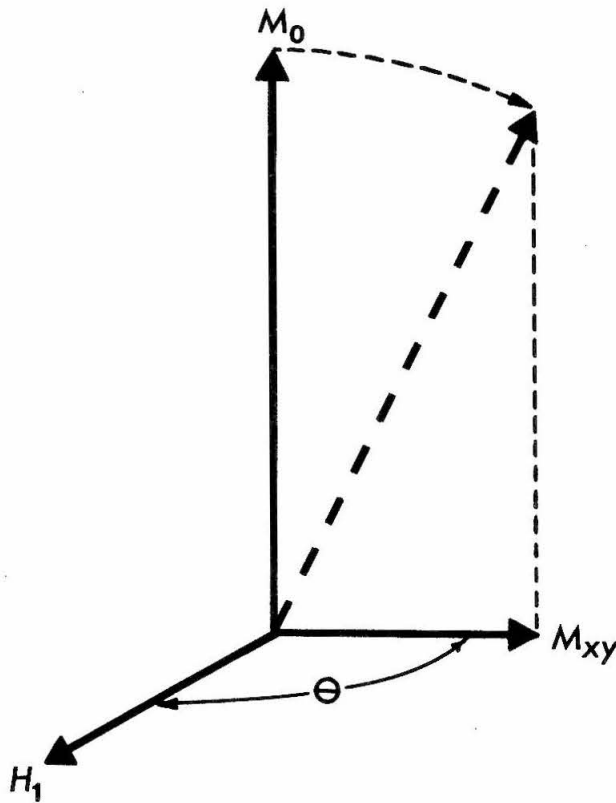


Figure 3.5.2. The rf field leads to an induced magnetization in the xy plane.

$$\theta = \pi \alpha t^2 + \theta_0, \quad (3.5.5)$$

or:

$$\theta = \frac{\pi}{\alpha} (\nu_{\text{rf}} - \nu_0)^2 + \theta_0. \quad (3.5.6)$$

The torque exerted by H_1 on \tilde{M}_{xy} depends upon the sine of θ . We observe alternating absorption and emission, or "wiggles". The

maxima are determined by the condition $\sin \theta = 1$. Since θ_0 is approximately $\pi/2$:

$$\theta_{\max} - \theta_0 = \frac{\pi}{\alpha} (\nu_{\text{rf}} - \nu_0)^2 \doteq 2\pi n, \quad (3.5.7)$$

where n is an integer. The maxima of the "wiggles" therefore occur when:

$$(\nu_{\text{rf}} - \nu_0) \doteq \sqrt{2n\alpha}; \quad n = 0, 1, 2, \dots \quad (3.5.8)$$

The positions of the "wiggles" depend only upon the sweep rate and not on the relaxation times or the magnetogyric ratio of the nuclei (Fig. 3.5.3). Therefore, for purposes of resolution enhancement,

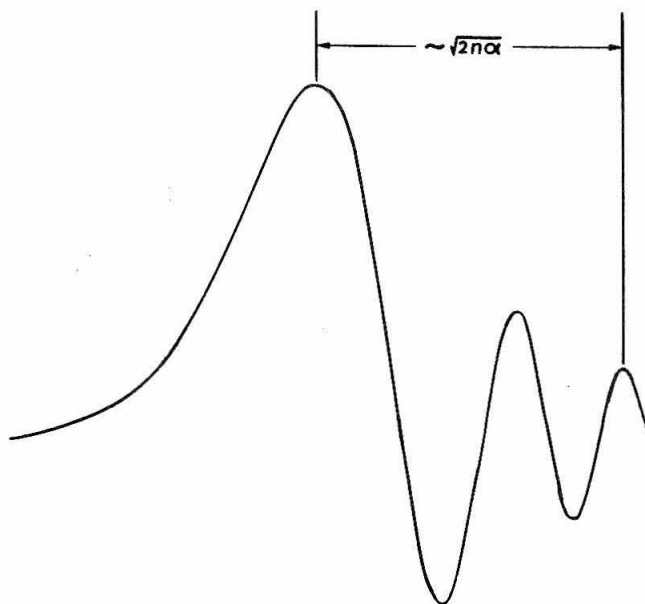


Figure 3.5.3. The approximate positions of the maxima in an n. m. r. experiment.

line shapes may be measured by using standard samples. We shall have problems only if either the standard or the unknown is sufficiently broadened to make the "wiggles" disappear.

The full width at half height of these "wiggles" is roughly the time it takes for θ to change by $2\pi/3$ (Fig. 3.5.4), so that:

$$\nu_n \doteq \sqrt{2(n + 1/3)\alpha} - \sqrt{2n\alpha}; \quad n = 0, 1, 2, \dots \quad (3.5.9)$$

Although this relationship is not accurate for small n , it does give a rough approximation for the full width at half height of the first maximum:

$$\nu_1 \doteq 0.817 \sqrt{\alpha}. \quad (3.5.10)$$

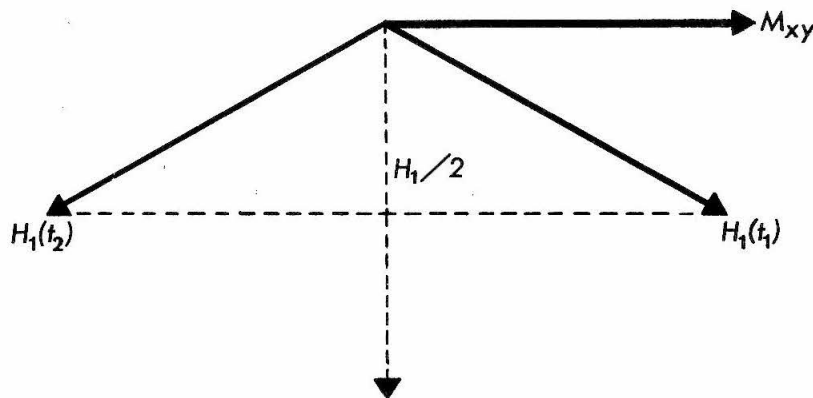


Figure 3.5.4. The projection of \tilde{H}_1 perpendicular to \tilde{M}_{xy} .
Note that: $\theta(t_2) - \theta(t_1) = 2\pi/3$.

This approximation should be more accurate for large α , since ν_{rf} becomes larger than ν_0 very quickly.

Ernst and Anderson²⁵ have solved the Bloch equations²⁰ numerically by the Runge-Kutta technique²⁶ and found that:

$$\text{Limit}_{\alpha \rightarrow \infty} \nu_i \doteq 0.66 \sqrt{\alpha}. \quad (3.5.11)$$

Our simplified model is really then not too bad in that ν_i turns out to be proportional to $\sqrt{\alpha}$, even though with a different proportionality constant than shown in Eq. (3.5.11). In order to determine the detailed effects of sweep rate on filtering n. m. r. spectra, we return to a somewhat more pragmatic approach.

We have recorded the line shape of the proton signal from chloroform over a wide range of sweep rates. The observed line widths are shown in Fig. 3.5.5. The asymptotic form [Eq. (3.5.9)] is an excellent approximation at the faster sweep rates.

This experimental curve agrees very closely with the theoretical curve obtained by Ernst and Anderson²⁵ if we assume that $T_1 = T_2 \doteq 3$ sec. The two relaxation times will in general be equal for a non-viscous isotropic sample, and 3 sec is a reasonable relaxation time for protons.²⁷ The relaxation times of other nuclei with $I = \frac{1}{2}$, and whose chemical environments are comparable to those of protons are given by:²⁷

$$T_N/T_{1H} \doteq (\gamma_H/\gamma_N)^2. \quad (3.5.12)$$

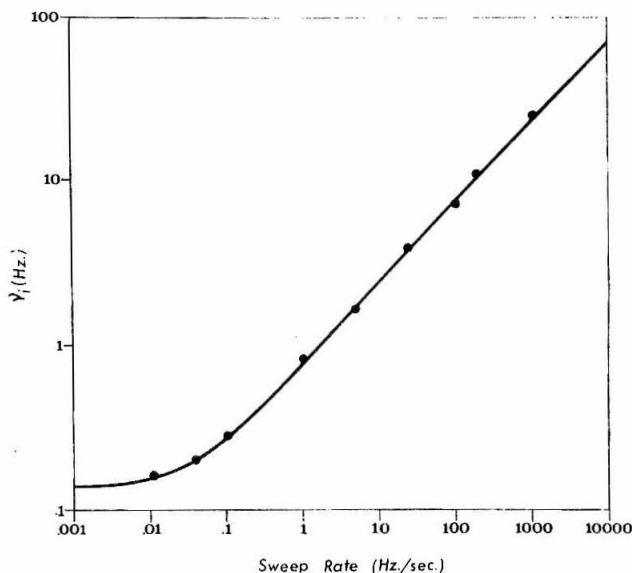


Figure 3.5.5. The line width of the proton signal from chloroform as a function of sweep rate.

Thus, ^{13}C relaxation times should be about 16 times as large as proton relaxation times. This leads to ^{13}C line widths which would be much narrower than the homogeneity of the magnetic field.

Fortunately, an inhomogeneous field has approximately the same effect as decreasing the relaxation times.²⁸ We can rationalize this by considering an inhomogeneous field to be a random field with a long correlation time.²⁹ If we calibrate our sweep rates in terms of line shapes (e.g., the number of "wiggles") rather than Hz, the ratio of T_1/T_2 will have only minor effects upon these line shapes. In this sense, the conclusions we reach below will be quite general.

The signal-to-noise ratio of an unfiltered spectrum varies considerably with the sweep rate. The nature of this variation depends upon how we change the other parameters of our n. m. r. experiment. We shall assume that we are interested in a given region of the spectrum, from ν_1 to ν_2 . We therefore keep the sweep width constant and vary only the sweep time. We shall also assume that we have a constant amount of total instrument time available, so that the number of scans we record is proportional to the sweep rate. Finally, we assume that we carefully adjust the strength of the rf field for the maximum signal-to-noise ratio at each sweep rate.

Ernst and Anderson²⁵ have determined the theoretical variation of the signal-to-noise level with sweep rate under these conditions (Fig. 3.5.6). For sweep rates above or below the region where saturation varies, the signal-to-noise ratio of an unfiltered spectrum approaches a constant value. If we calibrate the sweep rate as discussed above, this curve shows the same general behavior for any ratio of T_1/T_2 . We shall use this theoretical variation of the input signal-to-noise level since the noise produced during amplification is strongly dependent upon instrument design.

The signal-to-noise ratio of a filtered spectrum is of considerably greater interest. The signal-to-noise improvement from a matched filter is proportional to the square root of the number of data points under the line (Sec. 1.1). The signal-to-noise ratio resulting from the use of a matched filter is therefore approximately:

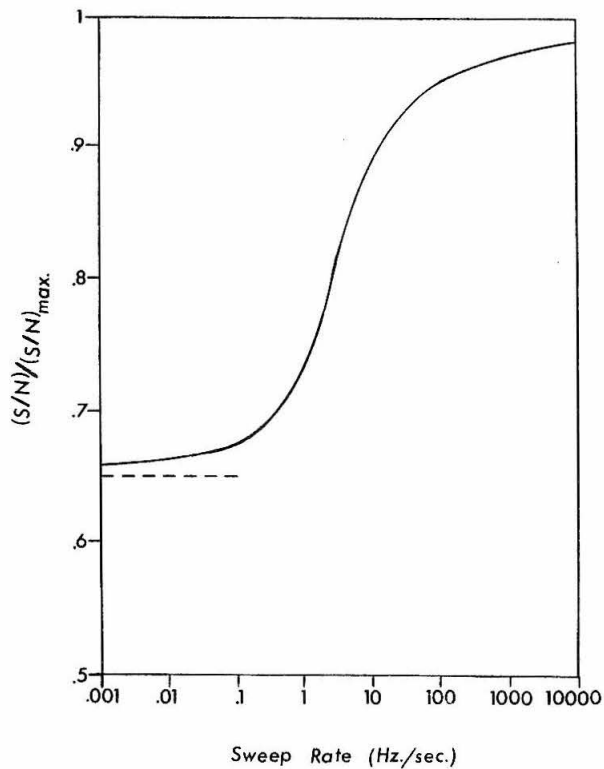


Figure 3.5.6. The theoretical variation of the input signal-to-noise ratio with the sweep rate.

$$(S/N)_m \doteq k_1 (S/N)_i \nu_i^{\frac{1}{2}} \quad (3.5.13)$$

where k_1 is a constant. Although the "wiggles" will dominate the signal-to-noise ratio at extremely fast sweep rates, they do not make an important contribution at the sweep rates available with our spectrometers. Recalling that the input signal-to-noise ratio approaches a constant value for large sweep rates and using Eq. (3.5.11) for the input line width we find that:

$$(S/N)_m \doteq k_2 \alpha^{\frac{1}{4}}. \quad (3.5.14)$$

This approximation is valid for moderately large values of α . The general variation with sweep rate of the signal-to-noise ratio resulting from using a matched filter was calculated from Eq. (2.8.5) using Fig. 3.5.6 for the input signal-to-noise ratio (Fig. 3.5.7).

We previously observed that lines with "wiggles" were not broadened by matched filters as much as Lorentzian lines were. This is essentially an artifact caused by our restriction of the definition of

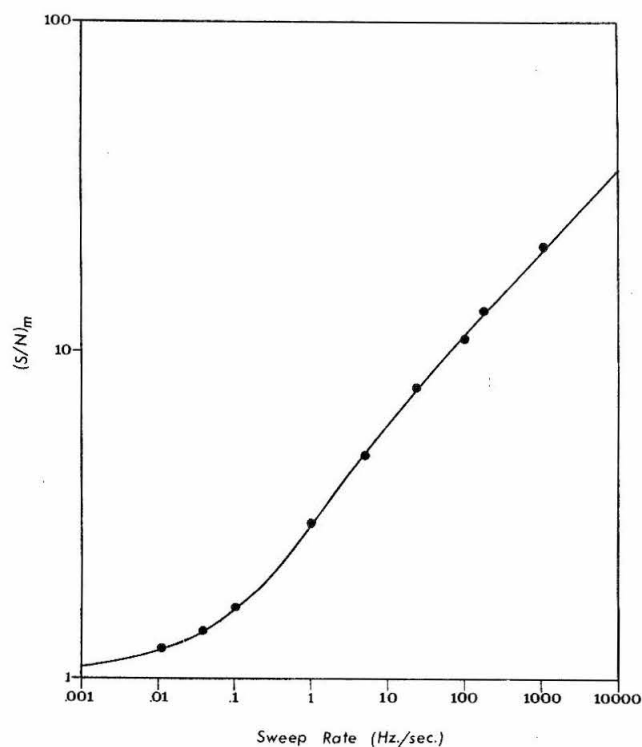


Figure 3.5.7. The signal-to-noise ratio resulting from using a matched filter on the proton signal from CHCl_3 .

line width to the first maximum. As we increase the sweep rate and more "wiggles" appear, the "average" width of a "wiggle" decreases relative to the width of the first maximum [Eq. (3.5.9)]. Since a matched filter uses the entire line shape, the line width resulting from use of a matched filter depends upon the "average" line width of the input line shape. The ratio of the width of the first maximum to the line width after using a matched filter therefore decreases with increasing sweep rate (Fig. 3.5.8).

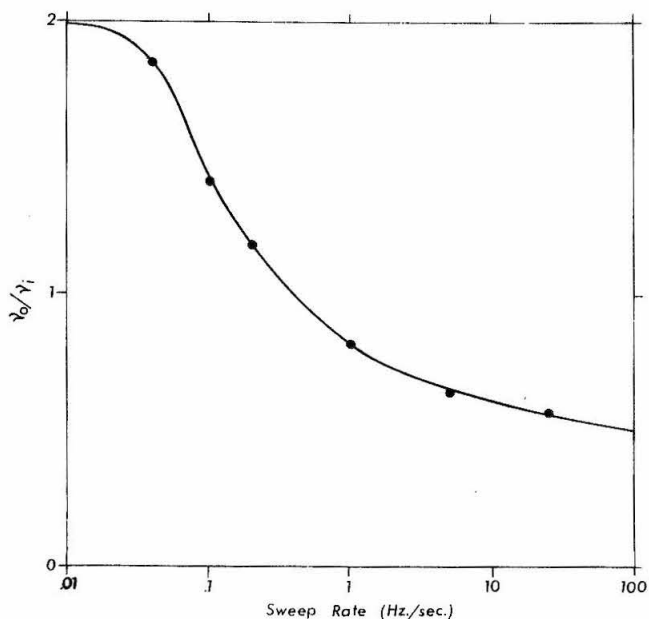


Figure 3.5.8. The ratio of the full width at half height after using a matched filter to the width of the first maximum before filtering for the proton signal from CHCl_3 as a function of sweep rate.

The effects of sweep rate on resolution enhancement filters may be determined by considering the filtering process in frequency space. The Fourier transform of the line shape resulting from a resolution enhancement filter is given by:

$$S_o(\omega) = \frac{c(q) S_i^*(\omega) S_i(\omega)}{1 + q |S_i(\omega)|^2}, \quad (3.5.15)$$

where $S_i(\omega)$ is the Fourier transform of the input line shape. Since filters take simple products in frequency space we can easily break this filter down into a sequence of two filters:

$$S_o(\omega) = \left[\frac{c(q)/c(0)}{1 + q |S_i(\omega)|^2} \right] \left[c(0) S_i^*(\omega) \right] S_i(\omega), \quad (3.5.16)$$

where the first filter is a matched filter. The Fourier transform of the output line shape is therefore:

$$S_o(\omega) = \left[\frac{c(q)/c(0)}{1 + q |S_i(\omega)|^2} \right] S_m(\omega), \quad (3.5.17)$$

where $S_m(\omega)$ is the Fourier transform of the line shape resulting from using a matched filter.

The line shape resulting from a matched filter is always symmetric (see Sec. 3.3) and except for changes in line width shows little variation with sweep rate (Figs. 3.2.11, 3.3.1, and 3.3.3). The frequency response function in Eq. (3.5.17) can also be expressed

in terms of $S_m(\omega)$. The Fourier transform of the output line shape is then:

$$S_o(\omega) = \frac{c(q) S_m(\omega)}{c(o) + q S_m(\omega)} \quad (3.5.18)$$

It is clear that the only effect of sweep rate on resolution enhancement filters is through the line width obtained by using a matched filter.

If we plot the signal-to-noise ratio as a function of the line width as in section 3.4, but normalize the line width to that obtained by the use of a matched filter, then the resulting curve shows no observable trend with changes in the sweep rate (Fig. 3.5.9). The asymptotic form of these curves is easily determined by substituting Eq. (3.3.8) for $\ln q$ in Eq. (3.4.6). We find:

$$\text{Limit}_{q \rightarrow \infty} \frac{(S/N)_o}{(S/N)_m} \doteq 1.8955 \left(\frac{\nu_m}{\nu_o} \right) e^{-1.8955 \nu_m / 2 \nu_o} \quad (3.5.19)$$

which is accurate to within 30% for all q greater than or equal to zero.

The sweep rate has an important effect on resolution enhancement which does not explicitly involve the filtering process. Both the signal-to-noise ratio and the line width of the input signal vary with the sweep rate (Figs. 3.5.5 and 3.5.6). If we plot the signal-to-noise level resulting from use of a matched filter as a function of the line width after using a matched filter, we obtain a curve indicating how the resolution may be enhanced by decreasing the sweep rate. At any sweep rate the resolution may be further enhanced by filtering (Fig.

3.5.9). The possible results of the combination of these two resolution enhancement processes is indicated in Fig. 3.5.10. The curve which is tangent to each of the smaller curves indicates a procedure in which we optimize both the sweep rate and the filter. First, we estimate the line width which will permit observation of a coupling. Then we select the sweep rate (using Fig. 3.5.10) such that a

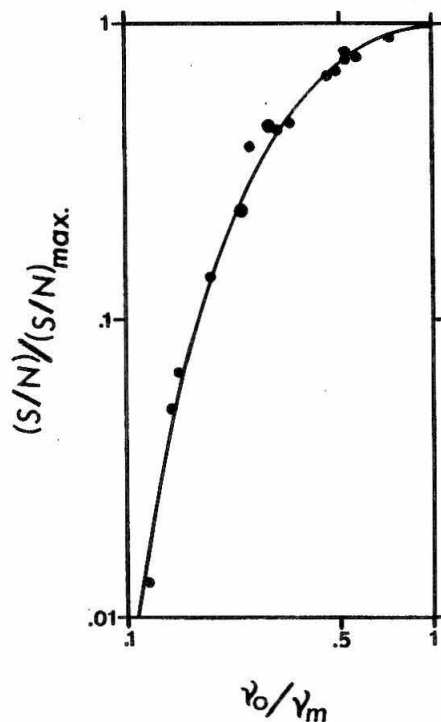


Figure 3.5.9. The loss in signal-to-noise ratio resulting from resolution enhancement. The solid line was obtained by filtering a Lorentzian. The points shown were obtained by filtering the above CHCl_3 spectra. ν_0 is the output full width at half height and ν_m is the width resulting from using a matched filter.

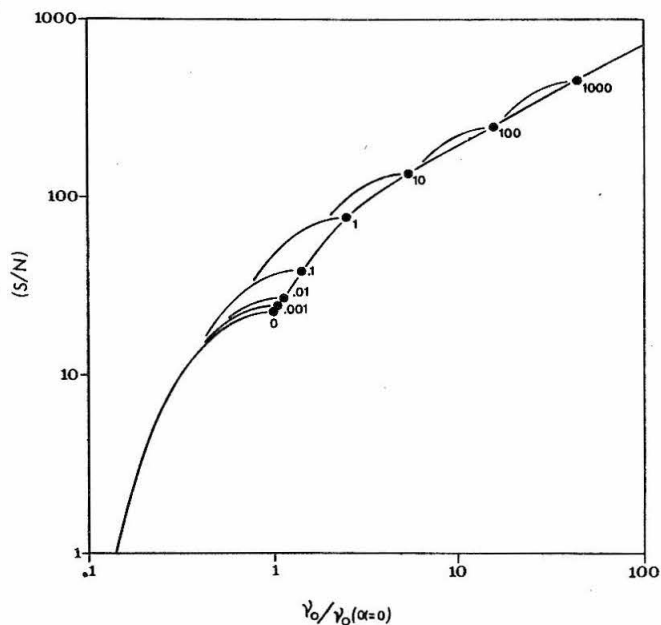


Figure 3.5.10. Resolution enhancement in which we vary both the sweep rate and the filter. The numbers at the points indicate the sweep rate in Hz. This curve was obtained from the above CHCl_3 spectra with the exception of the point $\alpha = 0$, which was obtained from the asymptotic form.

resolution enhancement filter can bring us to the tangent curve at the desired line width. After collecting the data we then filter the spectrum using the proper value of q so that we achieve the desired line width. This procedure gives the maximum signal-to-noise for a given line width when linear filters are used for n. m. r. signals.

When we select the sweep rate we must keep in mind that it cannot be so fast that the nuclei will not return to equilibrium for the

next scan, nor so slow that we cannot see a peak to "tune" on in a single scan. The latter consideration seriously limits the use of extremely slow sweep rates for ^{13}C n. m. r. In this case, it is critical that we can use the correct line shape for resolution enhancement (see Sec. 3.2).

Although Fig. 3.5.10 was obtained from experiments using a specific sample, the basic form of this curve is quite general. The only important variation is in the scale for the sweep rate. This scale can be adjusted by considering the point labeled 0.1 to represent the minimum sweep rate for which the first downward "wiggle" goes below zero.

4. NON-LINEAR FILTERS

These filters are easier to describe than linear filters, but are in general more difficult to apply. The effect of a filter on a single line is given by:

$$s_0(t) = \underline{H}[s_i(t)], \quad (4.1)$$

where $s_i(t)$ is the input line shape and $s_0(t)$ is the output line shape. The effect of this filter on a spectrum composed of two lines is then:

$$\underline{H}[s_i(t)_1 + s_i(t)_2] = s_0(t)_1 + s_0(t)_2 + \underline{H}_{1,2}[s_i(t)_1, s_i(t)_2], \quad (4.2)$$

where $\underline{H}_{1,2}$ is the non-linear interaction term. This interaction term may be comparable to the linear terms. We therefore must know (or assume) the multiplicity of a spectrum before we can apply non-linear filters. Although we could filter a spectrum assuming several different multiplicities and afterwards select the best one, linear filters are clearly simpler to apply in this case. In the discussion which follows we shall assume that the number of lines is known.

4.1 The Principle of Maximum Likelihood

A very useful group of filters is obtained by a statistical approach. We seek a basis for deciding that some quantity, x , lies in a certain interval.

$$x_1 \leq x \leq x_2. \quad (4.1.1)$$

This decision is clearly valid only if:

$$P(x_1 \leq x \leq x_2) > 1/2 \quad (4.1.2)$$

where $P(X)$ is the probability that X is true. Since this condition does not uniquely define x_1 and x_2 , any method of measuring x must include additional conditions. There is no rigorous approach to defining the best set of additional conditions. A reasonable approach might be to find the smallest interval which satisfies Eq. (4.1.2).

This does not appear to be very practical since it does not suggest any method of finding this interval. A very common approach is the principle of maximum likelihood.³⁰ We select x_0 such that

$P(x_0 \leq x \leq x_0 + dx)$ is a maximum. That is, we use the most probable value of x as an estimate of the true value. We then use the limits to which we can determine x_0 for the values of x_1 and x_2 . It is only the interval (x_1, x_2) that has any statistical significance. Although x_0 is the most probable value of x , the interval (x_1, x_2) is not generally the smallest interval satisfying Eq. (4.1.2). There is no justification for assuming that the principle of maximum likelihood is the most powerful approach to measuring x . Later, we shall examine an important example for which it is not the most powerful approach.

If we wish to determine f , we can do an experiment and obtain a value f_1 which will differ from f by the error or noise. The probability that the error, $f_1 - f$, lies between f' and $f' + df$ is given by:

$$P(f' \leq f_1 - f \leq f' + df) = \phi(f') df, \quad (4.1.3)$$

where $\phi(f')$ is the probability density function³¹ of the noise. If we measure f a total of N_T times, then the definition of the above probability is:

$$P(f' \leq f_i - f \leq f' + df) \equiv \text{Limit}_{N_T \rightarrow \infty} \left[\frac{N(f' \leq f_i - f \leq f' + df)}{N_T} \right], \quad (4.1.4)$$

where $N(X)$ is the number of measurements that satisfy X . From Eqs. (4.1.3) and (4.1.4) we see that we can measure $\phi(f')$ by using the following approximation:

$$\phi\left(f' + \frac{\Delta f}{2}\right) \doteq \left[\frac{N(f' \leq f_i - f \leq f' + \Delta f) \pm \sqrt{N(f' \leq f_i - f \leq f' + \Delta f)}}{N_T \Delta f} \right], \quad (4.1.5)$$

if we know f . The probability density function of the noise spectrum referred to in section 2.5 is shown in Fig. 4.1.1. The true value of the zero point was assumed to be the average value \bar{n} . The probability density function of this noise is not distinguishable from a Gaussian. This is the probability density function for the noise measured at different times. In a multiple-scan experiment, the value of the signal at any point in the spectrum is the average of measurements made at many different times (the individual scans). The average over this ensemble of scans is therefore in reality a time average. That is, regardless of the nature of the noise in a single scan, the noise in a multiple-scan experiment is effectively ergodic. We can therefore assume that the noise at each data point of an n. m. r. spectrum has a Gaussian probability density function:

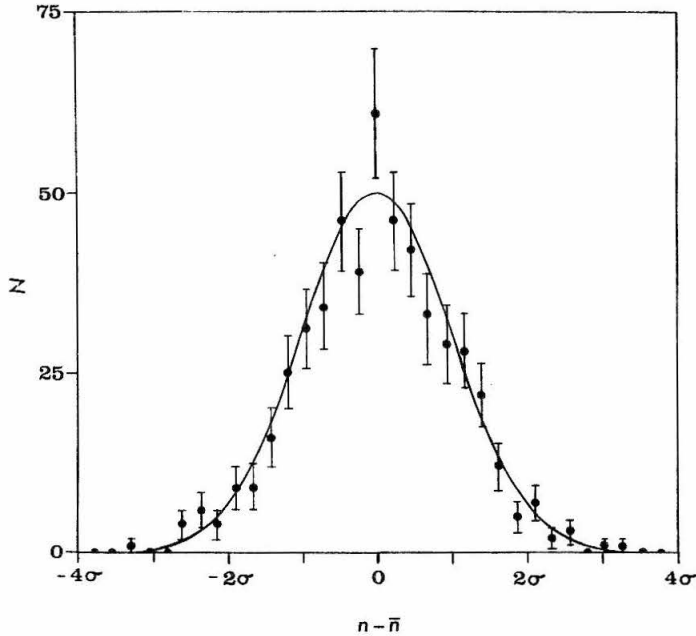


Figure 4.1.1. The points are the probability density function of noise from the DFS-60 spectrometer. The curve is a Gaussian.

$$\phi[f_i(t) - f(t)] = \frac{1}{\sqrt{2\pi} \sigma} e^{-[f_i(t) - f(t)]^2 / 2 \sigma^2}, \quad (4.1.6)$$

where σ is the variance of the noise. The probability density function for the N data points of the spectrum is thus:³²

$$\phi(\underline{\hat{f}}_i - \underline{\hat{f}}) = \frac{1}{(2\pi)^{\frac{1}{2}N} \sqrt{|\underline{\hat{C}}|}} e^{-\frac{1}{2}(\underline{\hat{f}}_i - \underline{\hat{f}})^t \underline{\hat{C}}^{-1}(\underline{\hat{f}}_i - \underline{\hat{f}})}, \quad (4.1.7)$$

where $\underline{\hat{f}}$ is the vector with components $f(t_j)$, $\underline{\hat{f}}_i$ is the vector with components $f_i(t_j)$ and $\underline{\hat{f}}^t$ is the transpose of $\underline{\hat{f}}$. The covariance matrix,

\underline{C} , has components:

$$C_{jk} \equiv \int_{-\infty}^{\infty} [f_i(t_j) - f(t_j)][f_i(t_k) - f(t_k)] \phi(\underline{f}_i - \underline{f}) \underline{df}. \quad (4.1.8)$$

This is an ensemble average. Since the noise is effectively ergodic we can substitute a time average:

$$C_{jk} = \int_{-\infty}^{\infty} [f_i(t_j) - f(t_j)][f_i(t_k) - f(t_k)] dt_j, \quad (4.1.9)$$

or:

$$C_{jk} = \int_{-\infty}^{\infty} [f_i(\tau) - f(\tau)][f_i(t_k - t_j + \tau) - f(t_k - t_j + \tau)] d\tau. \quad (4.1.10)$$

The last expression is simply the autocorrelation function $r(t_k - t_j)$ for the noise (Sec. 2.3). In section 2.5, it was shown that the noise in an unfiltered n. m. r. spectrum is white. The autocorrelation function is therefore a delta function (Sec. 2.3).

We can check this by calculating this integral using the above experimental noise spectrum. The result (Fig. 4.1.2) clearly indicates that the assumption that $r(t_k - t_j)$ is a delta function is quite good. The components of the covariance matrix are simply:

$$C_{jk} = \delta_{jk} \sigma^2, \quad (4.1.11)$$

and the determinant, $|\underline{C}|$, is equal to σ^{2N} .

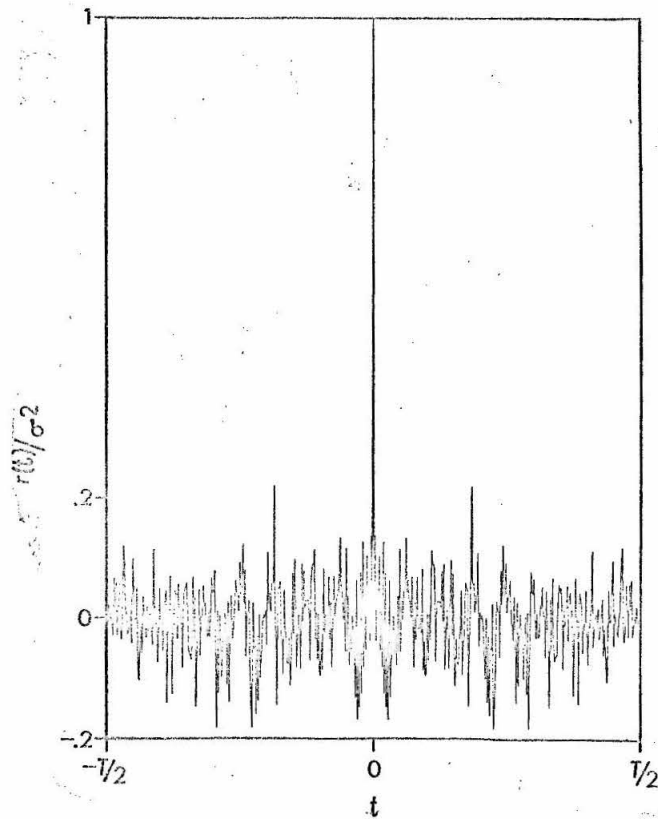


Figure 4.1.2. The autocorrelation function [Eq. (2.3.35)] of noise from the DFS-60 spectrometer.

The total probability of the spectrum is:

$$P = \frac{df}{\sigma N (2\pi)^{\frac{1}{2}N}} e^{-\sum_{j=1}^N [f_i(t_j) - f(t_j)]^2 / 2 \sigma^2}, \quad (4.1.12)$$

which is the product of the probabilities of the individual data points. The data points are therefore independent for white ergodic Gaussian noise. The probability is a maximum when the exponent in Eq. (4.1.12) is a minimum. The principle of maximum likelihood leads to a simple least-squares procedure for white Gaussian ergodic noise. We have shown that the noise in an unfiltered n. m. r. spectrum has these properties. The principle of maximum likelihood therefore gives the form of \hat{f} which minimizes the function:

$$\Phi = \sum_{j=1} [f_i(t_j) - f(t_j)]^2, \quad (4.1.13)$$

as the most probable form, \hat{f}_0 , for a multiple-scan n. m. r. spectrum.

The situation is more complicated if the noise is not white. If an RC filter were used, the noise would still be Gaussian³³ and ergodic, but not white. We should then have to minimize the exponent in Eq. (4.1.7). That is, we must find the minimum of the more general function:

$$\Phi = (\hat{f}_i - \hat{f})^t \hat{C}^{-1} (\hat{f}_i - \hat{f}), \quad (4.1.14)$$

in order to determine \hat{f}_0 , the most probable \hat{f} . We shall limit our discussion to the simpler case of white noise.

4.2 Least-Squares Filters

Let a spectrum be composed of n lines with k_j variable parameters for the line shape of line j , where $j = 1, 2, \dots, n$. These parameters may include position, height, width, etc. There are M variable parameters in all, where:

$$M = \sum_{j=1}^n k_j. \quad (4.2.1)$$

Let \underline{b} be a vector of dimension M whose components are the line-shape parameters. Then the spectrum is composed of the sum of the n lines, $f(t, \underline{b})$, and random noise. The function, $f(t, \underline{b})$ may be known either analytically or through a table of numerical values. The most probable value of \underline{b} is the value which minimizes the function:

$$\Phi = \int_{-\infty}^{\infty} [f_1(t) - f(t, \underline{b})]^2 dt, \quad (4.2.2)$$

where $f_1(t)$ is the experimental spectrum. This is in general a non-linear problem which is ill-conditioned. That is, the b_j are strongly coupled, and the problem is difficult to solve numerically. This approach does have the advantage that there is no systematic error in the result³⁴ as with linear filters (Sec. 3.3). If the signal-to-noise ratio is sufficiently large, then the observed separation of two lines exactly equals the calculated separation. The values of the peak positions obtained in \underline{b} are the most probable values. If the number and relative size of the lines is known, then the statistical approach

is feasible. We shall use two simple filters to illustrate the above remarks.

We first examine filtering an input spectrum $f_i(t)$ composed of a single line with known line-shape function $s_i(t)$. The only unknown parameters are the position and amplitude of the line. The theoretical spectrum is therefore given by:

$$f(t, \underline{b}) = a s_i(t - \delta), \quad (4.2.3)$$

where $a s_i(0)$ is the amplitude and δ is the position of the maximum of $f(t)$. Substituting Eq. (4.2.3) in Eq. (4.2.2) we obtain:

$$\Phi = \int_{-\infty}^{\infty} [f_i(t) - a s_i(t - \delta)]^2 dt. \quad (4.2.4)$$

Expansion of the integrand gives:

$$\Phi = \int_{-\infty}^{\infty} f_i^2(t) dt - 2a \int_{-\infty}^{\infty} s_i(t - \delta) f_i(t) dt + a^2 \int_{-\infty}^{\infty} s_i^2(t) dt. \quad (4.2.5)$$

The value of a which minimizes Φ satisfies the condition:

$$\frac{\partial \Phi}{\partial a} = 0 = 2a \int_{-\infty}^{\infty} s_i^2(t) dt - 2 \int_{-\infty}^{\infty} s_i(t - \delta) f_i(t) dt, \quad (4.2.6)$$

so that:

$$a_{\min} = \left[\int_{-\infty}^{\infty} s_i^2(t) dt \right]^{-1} \int_{-\infty}^{\infty} s_i(t - \delta) f_i(t) dt. \quad (4.2.7)$$

Substituting this value of a in Eq. (4.1.5) gives:

$$\Phi_{a_{\min}} = \int_{-\infty}^{\infty} f_i^2(t) dt - \left[\int_{-\infty}^{\infty} s_i^2(t) dt \right]^{-1} \left[\int_{-\infty}^{\infty} s_i(t - \delta) f_i(t) dt \right]^2. \quad (4.2.8)$$

This function is clearly a minimum when the second term is a maximum, but the second term is a maximum when the output from a matched filter [Eq. (1.1.6)] is a maximum. The position of a single line obtained by the method of least-squares is therefore identical to that obtained with a matched filter. The amplitude obtained by the method of least squares is given by:

$$f_o(\delta_o) = a_{\min} s_i(0) = s_i(0) \left[\int_{-\infty}^{\infty} s_i^2(t) dt \right]^{-1} \int_{-\infty}^{\infty} s_i(t - \delta_o) f_i(t) dt, \quad (4.2.9)$$

which is precisely the amplitude obtained by using a matched filter. Since Eq. (4.2.9) gives the most probable amplitude of a line with a maximum at δ_o , for any δ_o , we have simply given an alternate derivation of Eq. (1.1.6).

If the input spectrum is composed of a single line (or several lines which do not overlap), the non-linear interaction term in Eq. (4.2) vanishes and the method of least-squares is equivalent to using a matched filter.

It is of interest to consider the more general case of filtering a single line when the noise is not white. The principle of maximum likelihood then leads to seeking the minimum of Φ in Eq. (4.1.14).

From Eq. (4.1.10), we see that if the noise is colored, but still Gaussian and ergodic, then we must find the minimum of the function:

$$\Phi = \int_{-\infty}^{\infty} \int_{-\infty}^{\infty} [f_1(t_1) - f(t_1)][f_1(t_2) - f(t_2)] r^{-1}(t_2 - t_1) dt_1 dt_2, \quad (4.2.10)$$

rather than Eq. (4.2.2). The inverse of the autocorrelation function, r^{-1} , is defined by:

$$\int_{-\infty}^{\infty} r(\tau) r^{-1}(t - \tau) d\tau = \delta(t). \quad (4.2.11)$$

where $\delta(t)$ is the Dirac delta function. Taking the Fourier transform of both sides, we find:

$$R(\omega) R^{-1}(\omega) = 1 \quad (4.2.12)$$

where we have used Eqs. (2.2.9) and (2.3.33). Substituting Eq. (2.3.39) for $R(\omega)$ we see that:

$$R^{-1}(\omega) = \frac{1}{2\pi W(\omega)}. \quad (4.2.13)$$

This suggests that these "generalized least-squares" filters [Eq. (4.2.10)] are described more concisely in frequency space.

We now substitute Eq. (4.2.3) for $f(t)$ in Eq. (4.2.10). By the same arguments used to obtain Eq. (4.2.9), we see that we can determine the most probable value of δ by finding the maximum of the function:

$$f_0(\delta) = \frac{s_i(0) \int_{-\infty}^{\infty} \int_{-\infty}^{\infty} f_i(t_1) s_i(t_2 - \delta) r^{-1}(t_2 - t_1) dt_1 dt_2}{\int_{-\infty}^{\infty} \int_{-\infty}^{\infty} s_i(t_1) s_i(t_2) r^{-1}(t_2 - t_1) dt_1 dt_2}. \quad (4.2.14)$$

Since the denominator is a constant, independent of δ , we can rearrange Eq. (4.2.14) to give:

$$f_0(\delta) = c \int_{-\infty}^{\infty} s_i(t_2 - \delta) \int_{-\infty}^{\infty} f_i(t_1) r^{-1}(t_2 - t_1) dt_1 dt_2. \quad (4.2.15)$$

We define the intermediate function $f_1(t_2)$ by:

$$f_1(t_2) \equiv \int_{-\infty}^{\infty} f_i(t_1) r^{-1}(t_2 - t_1) dt_1 dt_2, \quad (4.2.16)$$

so that:

$$f_0(\delta) = c \int_{-\infty}^{\infty} f_1(t_2) s_i[-(\delta - t_2)] dt_2. \quad (4.2.17)$$

As suggested by the properties of r^{-1} , we now take Fourier transforms of Eqs. (4.2.16) and (4.2.17) giving:

$$F_0(\omega) = \frac{c S_i^*(\omega)}{2\pi W(\omega)} F_1(\omega). \quad (4.2.18)$$

This is the general form of a matched filter [Eq. (2.4.22)]. For Gaussian ergodic noise, the principle of maximum likelihood leads to a "generalized least-squares" procedure. In the case of

non-overlapping lines, this procedure is equivalent to a matched filter, regardless of the power spectral density of the noise.

We now examine filtering an input spectrum composed of two closely spaced lines of equal size, such as we find in either half of an AX spectrum. The theoretical spectrum is given by:

$$f(t, \underline{b}) = a[s_1(t - \delta + J/2) + s_1(t - \delta - J/2)], \quad (4.2.19)$$

where δ is the chemical shift and J is the spin-spin coupling constant. The chemical shift can be measured by using a matched filter and so we assume that it is known. The only unknowns are a and J . Substituting this in Eq. (4.2.2) we obtain:

$$\begin{aligned} \Phi = \int_{-\infty}^{\infty} f_1^2(t) dt - 2a \int_{-\infty}^{\infty} [s_1(t - \delta + J/2) + s_1(t - \delta - J/2)] f_1(t) dt \\ + a^2 \int_{-\infty}^{\infty} [s_1(t - \delta + J/2) + s_1(t - \delta - J/2)]^2 dt. \end{aligned} \quad (4.2.20)$$

The last two integrals can be expressed in terms of the convolution integrals for a matched filter:

$$s_m(t) \equiv c(0) \int_{-\infty}^{\infty} s_1(-\tau) s_1(t - \tau) d\tau, \quad (4.2.21)$$

and:

$$f_m(t) \equiv c(0) \int_{-\infty}^{\infty} s_1(-\tau) f_1(t - \tau) d\tau. \quad (4.2.22)$$

The function we wish to minimize is then:

$$\begin{aligned} \Phi = & \int_{-\infty}^{\infty} f_i^2(t) dt - \frac{2a}{c(0)} [f_m(\delta + J/2) + f_m(\delta - J/2)] \\ & + \frac{2a^2}{c^2(0)} [s_m(0) + s_m(J)]. \end{aligned} \quad (4.2.23)$$

It follows that Φ is a minimum only if:

$$a = c(0) \frac{f_m(\delta + J/2) + f_m(\delta - J/2)}{2 [s_m(0) + s_m(J)]}. \quad (4.2.24)$$

Substituting this value of a in Eq. (4.2.23) we find:

$$\Phi_{a_{\min}} = \int_{-\infty}^{\infty} f_i^2(t) dt - \frac{[f_m(\delta + J/2) + f_m(\delta - J/2)]^2}{2 [s_m(0) + s_m(J)]}. \quad (4.2.25)$$

The most probable value of J is clearly the one for which the second term on the right is a maximum. We shall call this term $g^2(J)$. The most probable amplitude of lines with chemical shift δ and spin-spin coupling constant J is given by:

$$a_{\min} s_i(0) = c(0) s_i(0) \frac{f_m(\delta + J/2) + f_m(\delta - J/2)}{2 [s_m(0) + s_m(J)]}. \quad (4.2.26)$$

This function is not necessarily a maximum when $g^2(J)$ is a maximum. Both $g^2(J)$ and $a(J)_{\min}$ were calculated for the spectrum shown in

Fig. 3.2.1. The most probable value of a , a_0 , is not the maximum value. It is the value of $a(J)_{\min}$ which corresponds to the maximum of $g^2(J)$ (Fig. 4.2.1). Rather than study $g^2(J)$, we shall find it more convenient to determine the maximum of the function:

$$g(J) \equiv \frac{f_m(\delta + J/2) + f_m(\delta - J/2)}{\sqrt{2} [s_m(0) + s_m(J)]^{\frac{1}{2}}} . \quad (4.2.27)$$

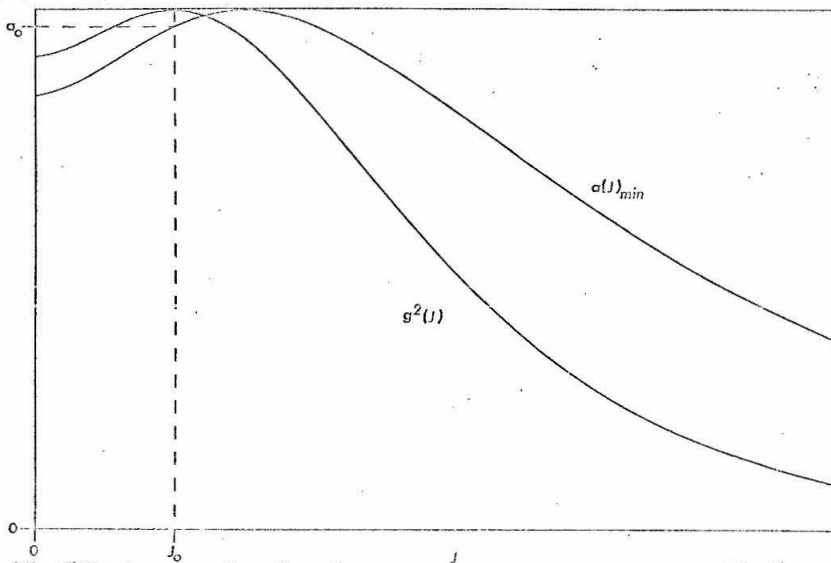


Figure 4.2.1. The normalized functions, $g^2(J)$ and $a(J)_{\min}$ corresponding to the spectrum shown in Figure 3.2.1.

This function takes an average of $f_m(\delta + J/2)$ and $f_m(\delta - J/2)$. That is, it averages the output of a matched filter about the center ($t = \delta$).

This is because we assumed that $f_i(t)$ should be symmetric about $t = \delta$. If we define the "non-averaged" function $h(t)$ as:

$$h(t) \equiv \sqrt{2} f_m(t) \{s_m[0] + s_m[2(t - \delta)]\}^{-\frac{1}{2}}, \quad (4.2.28)$$

then:

$$g(J) = \frac{1}{2} [h(\delta + J/2) + h(\delta - J/2)]. \quad (4.2.29)$$

From Eqs. (4.2), (4.2.9), and (4.2.19) we see that the non-linear interaction term is given by:

$$\widetilde{H}_{1,2}[s_i(t)_1, s_i(t)_2] = \frac{\sqrt{2} - \{1 + s_m[2(t - \delta)]/s_m[0]\}^{\frac{1}{2}}}{\{s_m[0] + s_m[2(t - \delta)]\}^{\frac{1}{2}}} \{s_o(t)_1 + s_o(t)_2\}. \quad (4.2.30)$$

Least-squares filters are non-linear for the case of overlapping lines. Interaction terms appear in both the position and the amplitude functions. Neither is the sum of two analogous expressions involving the individual lines.

If a closely spaced doublet is processed with a matched filter, the maxima in the output spectrum are too close together (Sec. 3.3). A least-squares filter multiplies the matched filter output by the function:

$$x(t, \delta) = \sqrt{2} \{s_m[0] + s_m[2(t - \delta)]\}^{-\frac{1}{2}}, \quad (4.2.31)$$

to give a spectrum with the maxima in the most probable positions.

A least-squares filter produces maxima in the most probable positions even if a matched filter gives only one maximum at $t = \delta$. Since $x(t, \delta)$ varies by only a factor of $\sqrt{2}$ between $t = \delta$ and $t = \infty$, the maxima of the output spectrum are not much greater than the output at $t = \delta$ (Fig. 4.2.1). We would not expect the simple expedient of multiplying the matched filter output by $x(t, \delta)$ to be as powerful a technique as using the linear resolution enhancement filters developed earlier. In the next section we shall make a quantitative comparison between the two.

4.3 Comparison of Linear and Non-Linear Filters

We shall examine non-linear filters first. The signal-to-noise ratio of $g(J)$ determines whether or not we can measure J and with what accuracy. From Eq. (4.2.28) we see that the signal-to-noise ratio of $g(J)$ is given by:

$$(S/N)_g = \sqrt{2} (S/N)_m \quad (4.3.1)$$

where $(S/N)_m$ is the signal-to-noise ratio resulting from a matched filter. This signal-to-noise level is a measure of the ratio of $[g(J_0) - g(\infty)]$ to the root-mean-square noise level. This is the signal-to-noise level available to distinguish between two lines separated by J_0 and two lines separated by ∞ (or no lines at all). We are interested in the signal-to-noise level available to measure J . That is, we wish to distinguish between two lines separated by J_0 and a single line

($J = 0$). From Fig. 4.2.1 it is clear that the signal-to-noise level available to measure J is given by:

$$(S/N)_J = \frac{g(J_0) - g(0)}{g(J_0)} (S/N)_g. \quad (4.3.2)$$

The factor of $\sqrt{2}$ in Eq. (4.3.1) arises from the averaging effect discussed in the previous section. In order to make a valid comparison with linear filters we shall omit this factor and consider the function:

$$(S/N)_{J_0} \equiv \frac{g(J_0) - g(0)}{g(J_0)} (S/N)_m. \quad (4.3.3)$$

This function has been calculated for both a Lorentzian line shape ($\alpha = 0$) and for the line shape shown in Fig. 3.1 ($\alpha = 0.2$). The results (Fig. 4.3.1) are almost identical for the two cases, if we normalize the separation, J_0 , to the full width at half height resulting from a matched filter. Just as we previously found for linear filters (Fig. 3.5.9), non-linear resolution enhancement filters give results which are independent of the sweep rate if we normalize to the line width from a matched filter.

We are now ready to examine linear filters. The output of a linear filter is given by:

$$f_q(t) = \int_{-\infty}^{\infty} h_q(\tau) f_i(t - \tau) d\tau \quad (4.3.4)$$

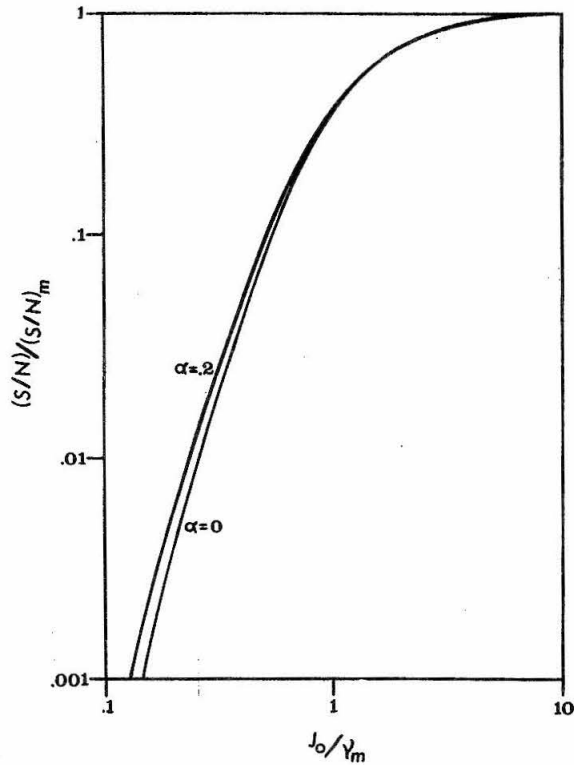


Figure 4.3.1. The signal-to-noise ratio available to measure a spin-spin coupling constant as a function of the coupling, J_0 . The line width resulting from a matched filter is ν_m , and α is the sweep rate in Hz.

where q determines the degree of resolution enhancement (Sec. 3.4). This function has a signal-to-noise ratio which is approximately given by:

$$(S/N)_q \doteq \frac{1}{1 + \left(\frac{q}{137}\right)^{\frac{1}{2}}} (S/N)_m, \quad (4.3.5)$$

where $(S/N)_m$ is the signal-to-noise ratio resulting from a matched filter. In order to improve our accuracy, we shall determine $(S/N)_q$ numerically (Sec. 2.8), rather than use Eq. (4.3.5). This is the signal-to-noise ratio available to determine whether or not there are any lines in the spectrum. We are interested in the signal-to-noise level available to measure J . It is clear from Fig. 2.1.2 that this is approximately given by:

$$(S/N)_{q,J} \doteq \frac{[s_q(0) + s_q(J)] - 2[s_q(J/2)]}{s_q(0)} (S/N)_q, \quad (4.3.6)$$

where $s_q(t)$ is the output line shape of a single line with a maximum at $t = 0$. This function is independent of the sweep rate, α , since the line shape resulting from resolution enhancement is independent of α (Sec. 3.3). We therefore computed $(S/N)_{q,J}$ only for the case $\alpha = 0$. The results show considerable variation with q (Fig. 4.3.2). The "wiggles" in these curves for large q result from the "wiggles" in the line shape (Fig. 3.3.1).

The signal-to-noise ratio, $(S/N)_q$, decreases with increasing q [Eq. (4.3.5)]. The line width, ν_q , also decreases with increasing q (Fig. 3.5.9). Combining these relations, we obtain the family of curves shown in Fig. 4.3.3. We can use Fig. 4.3.3 to determine the optimum value of q . The signal-to-noise level available to measure J with this optimized process is given by the envelope (the dashed line in Fig. 4.3.3) of the family of curves, $(S/N)_{q,J}$.

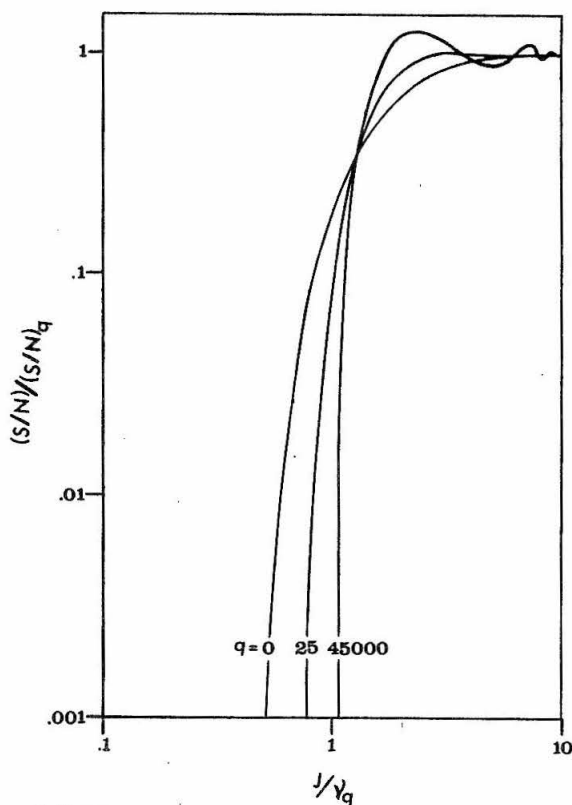


Figure 4.3.2. The fraction of the signal-to-noise level available to measure J using linear resolution enhancement filters. The output line width is ν_q .

Finally, we are ready to compare the linear and non-linear filters for the resolution of two identical lines separated by J (Fig. 4.3.4). We have also included the results obtainable with a matched filter. The resolution enhancement of a filter is essentially any improvement over a matched filter.

It seems clear that no filter can resolve two lines separated by J , if the position of a single line cannot be measured to within $\pm J$. We therefore include the signal-to-noise level available to measure

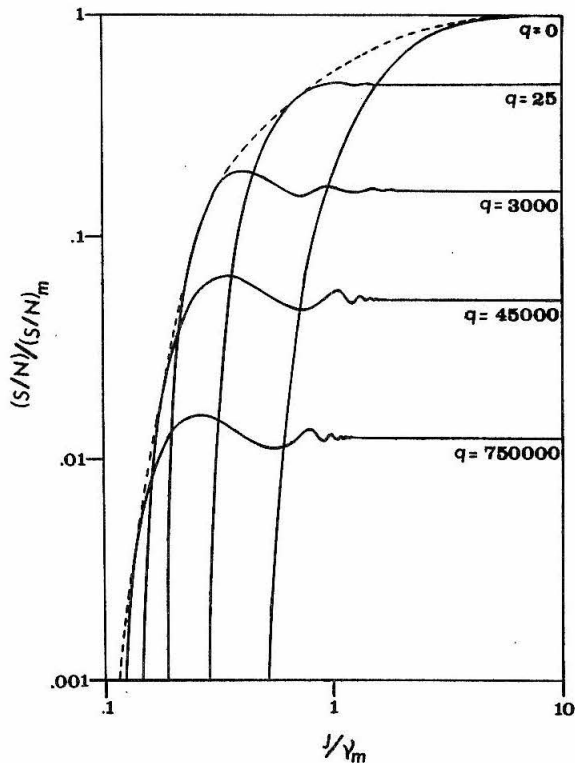


Figure 4.3.3. The signal-to-noise level available to measure J when linear resolution enhancement filters are used.

a peak position of a single line to within $\pm J$ in Fig. 4.3.4. This is essentially an upper bound on the resolution which should be possible. Linear resolution enhancement filters come very close to this upper bound in the region of primary interest. They are more powerful than least-squares filters for any reasonable loss in the signal-to-noise ratio.

Least-squares filters perform well under two conditions. The first is the trivial case of large separation between lines.

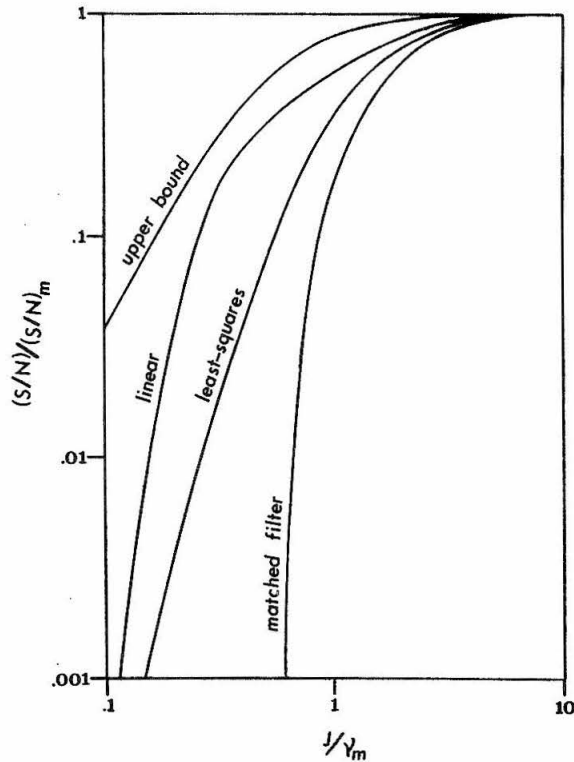


Figure 4.3.4. The signal-to-noise level available to measure J by various methods.

The least-squares filter is then a matched filter and is identical to the linear resolution enhancement filter. The second case is of practical importance. If we wish to resolve two lines of drastically different size, the "wiggles" in the tail of the line shape from linear filters will interfere (Fig. 3.2.8). A least-squares filter does not suffer from this problem. Resolving lines of drastically different size is considered in the next section.

It is convenient to assign a line width to non-linear filters, in order to discuss the effects of varying sweep rates on these filters.

We define the effective line width as follows:

$$\nu_{\text{eff. x}} \equiv \left\{ \left(\frac{J_x}{J_q} \right) \nu_q \right\} \text{const. (S/N)/(S/N)}_m, \quad (4.3.7)$$

where J_x is the minimum separation which can be measured by method x, J_q is the minimum separation which can be measured with linear resolution enhancement filters, and ν_q is the line width resulting from the optimum linear filter. Suppose we have sufficient signal-to-noise that we can afford to reduce the signal-to-noise ratio to 0.1 times that available with a matched filter. We can then measure a coupling greater than or equal to $0.25 \nu_m$ with linear resolution enhancement filters. Using least-squares filters we can measure a coupling greater than or equal to $0.55 \nu_m$. The linear resolution enhancement filter has an output line width of approximately $0.17 \nu_m$ when the signal-to-noise ratio is reduced by a factor of 10. The effective line width of the least-squares filter is therefore:

$$\nu_{\text{L.S.}} \doteq \left\{ \left(\frac{0.55}{0.25} \right) 0.17 \nu_m \right\} (\text{S/N}) = 0.1 (\text{S/N})_m. \quad (4.3.8)$$

We have calculated $\nu_{\text{L.S.}}$ for several values of the available signal-to-noise ratio and obtained a curve similar to that previously obtained for linear resolution enhancement filters (Fig. 3.5.9). We then determined the envelope of these curves as the sweep rate is varied, just as we had previously done for linear resolution enhancement filters (Fig. 3.5.10). This envelope (Fig. 4.3.5) gives the

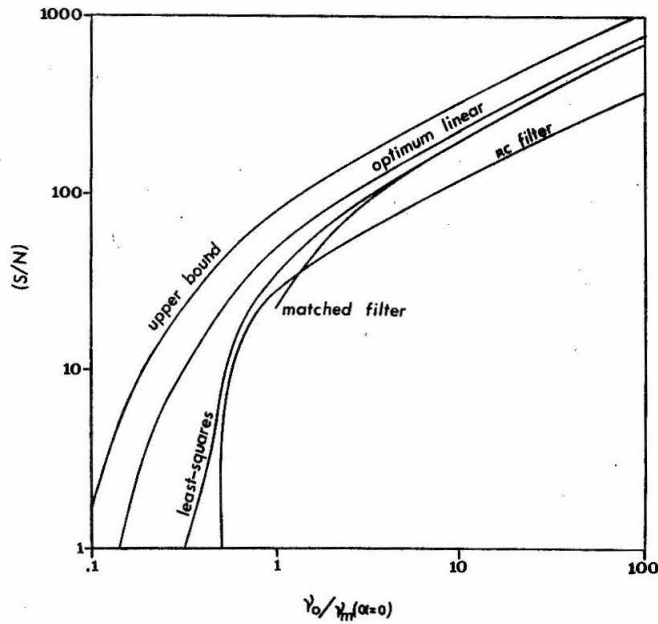


Figure 4.3.5. Resolution enhancement by various methods in which the sweep rate is varied (see Figure 3.5.10).

maximum signal-to-noise level available as a function of the effective line width of a least-squares filter. The upper bound shown in Fig. 4.3.5 was obtained by performing the identical calculations for the upper bound in Fig. 4.3.4.

The time constant of an RC filter can be used as a resolution enhancement parameter analogous to q (Fig. 3.4.1), however the output line width is never less than the input line width. We can therefore obtain a curve similar to that in Fig. 3.5.9 for an RC filter. Although the resulting curve for an RC filter varies with the sweep rate since these filters are not based upon the exact line shape, we can

still determine the envelope of these curves as the sweep rate is varied. The result is shown in Fig. 4.3.5.

We have also reproduced the analogous curves for matched filters and for optimum linear resolution enhancement filters in Fig. 4.3.5. We can now compare all the important filters that we have discussed so far. First, we should note that our definition of the effective line width [Eq. (4.3.7)] was somewhat arbitrary and therefore the details of the curves for the upper bound and the least-squares filters are also somewhat arbitrary. They are qualitatively significant however. Least-squares filters are definitely intermediate between optimum linear resolution enhancement filters and matched filters. We should also keep in mind that we have no reason to believe that the upper bound in Fig. 4.3.5 is the smallest upper bound.

The simple RC filter which is built into most commercially available n. m. r. spectrometers is clearly adequate for all routine work. There are two general circumstances when it should not be used. The first is the obvious case of the resolution of lines separated by less than the "natural line width" [$J < \nu_m (\alpha = 0)/2$]. The "natural line width" is usually determined by the inhomogeneity of the magnetic field (Sec. 3.5). The second case is that of spectra with inherently low signal-to-noise levels, such as natural abundance ^{13}C or ^{15}N spectra. For the sweep rates considered (Fig. 3.5.10), optimum linear resolution enhancement filters give an improvement in the signal-to-noise level of about a factor of 2 over RC filters (Fig. 4.3.5). This represents a reduction of the number of scans

which must be recorded by a factor of 4. Optimum linear resolution enhancement filters are the most powerful filters we presently have for dealing with lines of comparable size. We now consider the problem of filtering lines of drastically different size.

5. RESOLUTION OF SATELLITE PEAKS

Let X be a magnetic nucleus (e. g., ^{13}C) whose natural abundance is small. Let Y be a nucleus which is coupled only to X. If we measure the absorption spectrum of Y, we find a large parent peak at δ_Y and two small satellite peaks at approximately $\delta_Y \pm J_{XY}/2$. The parent peak results from those molecules which do not contain an X nucleus (e. g., they have a ^{12}C nucleus with spin 0 rather than a ^{13}C nucleus with spin 1/2). The satellite peaks arise from the small percentage of molecules which contain X.

If X and Y have similar resonance frequencies, the satellites will not be symmetric about δ_Y . We shall therefore adopt the following notation for spin-spin coupling constants: the upfield "shift" shall be labeled J_+ and the downfield "shift" J_- (Fig. 5.1). That is:

$$J = J_+ - J_- \quad (5.1)$$

If J is large, the optimum linear filters discussed earlier give the maximum signal-to-noise available to measure J. We shall examine two approaches for resolving satellite peaks when J is small. The first is a least-squares method. The second is a non-linear method which is closely related to linear resolution enhancement filters. The detection of satellite peaks which overlap the parent peak requires extremely accurate knowledge of the line shape of the parent peak. It is not practical to attempt a separate measurement of the line shape with sufficient accuracy (Figs. 3.2.7 and 3.2.8) to detect

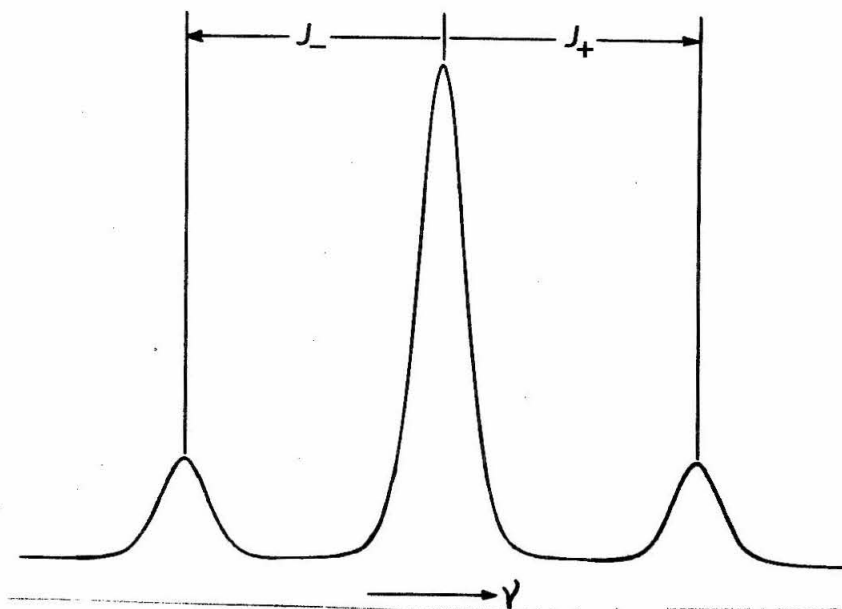


Figure 5.1. The definition of J_- and J_+ .

the small satellites. Both approaches we consider therefore determine the line shape from the spectrum of the sample.

5.1 The Least-Squares Approach

The intensity of a satellite peak such as that from ^{13}C in natural abundance is of the order of 0.5% of the intensity of the parent peak. To first order we can ignore the satellite and perform a least-squares fit to the parent peak [i. e., we can minimize Φ in Eq. (4.2.2) while omitting the satellite from $f(t, b)$].

The shape of a resonance signal will depend upon the sweep rate and the relaxation times. The qualitative variation of the line shape with the sweep rate, α , was considered in section 3.5. Jacobsohn and Wangsness³⁵ have calculated the exact line shapes of n. m. r. absorption signals when a small rf field is applied (Fig. 5.1.1). The asymptotic form of these line shapes is identical to the form for adiabatic passage³⁵ ($\alpha = 0$). This form is:

$$\text{Limit}_{\Delta\nu \rightarrow -\infty} g(\nu) = \frac{|\gamma| H_1 T_2}{1 + (\Delta\nu T_2)^2}, \quad (5.1.1)$$

where $|\gamma|$ is the absolute value of the gyromagnetic ratio, ν_0 is the resonance frequency, ν is the frequency of the rf field, $\Delta\nu \equiv \nu - \nu_0$,

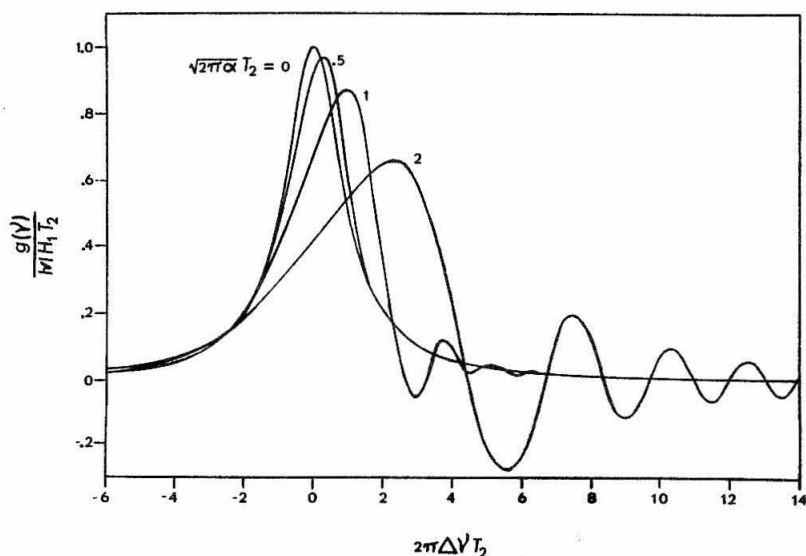


Figure 5.1.1. Line shapes of n. m. r. absorption signals for varying sweep rates (Jacobsohn and Wangsness³⁵).

$2H_1$ is the amplitude of the rf field, and T_2 is the total relaxation time (i. e., T_2 takes into account broadening due to inhomogeneity of the strong magnetic field).

In an actual experiment it is difficult to avoid mixing in a small amount of dispersion mode. In fact, this can be helpful, by reducing the line width. The proper asymptotic form is therefore:³⁵

$$\text{Limit}_{\Delta\nu \rightarrow -\infty} g(\nu) = \frac{|\gamma|H_1T_2}{1 + (\Delta\nu T_2)^2} [1 - d(\Delta\nu T_2)], \quad (5.1.2)$$

where d determines the amount of dispersion mode. From Fig. 5.1.1 we see that this approximation is fairly good if:

$$\Delta\nu T_2 < -2. \quad (5.1.3)$$

We therefore make the approximation:

$$g(\nu) \doteq \frac{a}{1 + b(\Delta\nu)^2} [1 - d_b(\Delta\nu)]; \quad \nu \leq \nu_{\max}, \quad (5.1.4)$$

where a , b , d_b , and ν_0 are determined by least-squares fitting.

The value of ν_{\max} is chosen so that:

$$.05 \leq g(\nu_{\max})/g(\nu)_{\max} \leq 0.5. \quad (5.1.5)$$

That is, we are able to fit the experimental curve with Eq. (5.1.4) up to the point where it reaches 0.05 to 0.5 of the peak height. The procedure for the least-squares fit is discussed in the next section.

5.2 Least-Squares Fitting with Non-Linear Parameters

We wish to approximate a set of N experimental points $f_i(x_j)$, $j = 1, 2, \dots, N$ by the function $f(\underline{x}, \underline{b})$. The vector \underline{b} is a set of M parameters we shall vary so as to minimize:

$$\Phi = \sum_j |f_i(x_j) - f(x_j, \underline{b})|^2. \quad (5.2.1)$$

A necessary condition for Φ to be a minimum is that:

$$\frac{\partial \Phi}{\partial b_k} = 0; \quad k = 1, 2, \dots, M. \quad (5.2.2)$$

If the parameters, \underline{b} , are non-linear, this problem cannot in general be solved directly. The most common approach is the Taylor series method of linear approximation. This is the method currently used by most crystallographers.³⁶ It consists of taking only the linear term in the Taylor series expansion of the function f :

$$f(\underline{x}, \underline{b}_0 + \underline{\delta}_T) \doteq f(\underline{x}, \underline{b}_0) + \sum_{k=1}^M \frac{\partial f(\underline{x}, \underline{b}_0)}{\partial b_k} \delta_k. \quad (5.2.3)$$

This gives the approximation for Φ :

$$\Phi \doteq \sum_{j=1}^N \left\{ f_i(x_j) - f(x_j, \underline{b}_0) - \sum_{k=1}^M \frac{\partial f(x_j, \underline{b}_0)}{\partial b_k} \delta_k \right\}^2. \quad (5.2.4)$$

The set of conditions, Eq. (5.2.2), then becomes:

$$0 = 2 \sum_{j=1}^N \left\{ f_1(x_j) - f(x_j, \underline{b}_0) - \sum_{k=1}^M \frac{\partial f(x_j, \underline{b}_0)}{\partial b_k} \delta_k \right\} \left\{ - \frac{\partial f(x_j, \underline{b}_0)}{\partial b_\ell} \right\};$$

$$\ell = 1, 2, \dots, M. \quad (5.2.5)$$

Rearranging this, we obtain the set of linear equations:

$$\sum_{k=1}^M \sum_{j=1}^N \frac{\partial f(x_j, \underline{b}_0)}{\partial b_\ell} \frac{\partial f(x_j, \underline{b}_0)}{\partial b_k} \delta_k =$$

$$\sum_{j=1}^N [f_1(x_j) - f(x_j, \underline{b}_0)] \frac{\partial f(x_j, \underline{b}_0)}{\partial b_\ell}; \quad \ell = 1, 2, \dots, M. \quad (5.2.6)$$

These equations can be written more concisely in the matrix form:

$$\underline{\underline{A}} \underline{\underline{\delta}}_T = \underline{\underline{g}}, \quad (5.2.7)$$

where:

$$A_{\ell k} \equiv \sum_{j=1}^N \frac{\partial f(x_j, \underline{b}_0)}{\partial b_\ell} \frac{\partial f(x_j, \underline{b}_0)}{\partial b_k}, \quad (5.2.8)$$

and:

$$g_k \equiv \sum_{j=1}^N [f_1(x_j) - f(x_j, \underline{b}_0)] \frac{\partial f(x_j, \underline{b}_0)}{\partial b_k}. \quad (5.2.9)$$

The solution of these equations is then:

$$\underline{\underline{\delta}}_T = \underline{\underline{A}}^{-1} \underline{\underline{g}}. \quad (5.2.10)$$

After solving for δ_{Γ} , we then set \underline{b} equal to $\underline{b}_0 + \delta_{\Gamma}$, and iterate until \underline{b} converges. This set of equations can in principle be solved by Gaussian elimination; however, in practice we find that for the problem of interest the matrix \underline{A} is ill-conditioned and the method does not work. This is because the diagonal elements of \underline{A} are small compared to the off diagonal elements.³⁷

Another common approach is the gradient technique which iteratively moves in the direction of steepest descent on the Φ surface. That is:

$$\delta_{\underline{g}} \equiv - \begin{pmatrix} \partial \Phi / \partial b_1 \\ \partial \Phi / \partial b_2 \\ \cdot \\ \cdot \\ \cdot \end{pmatrix} . \quad (5.2.11)$$

Substitution of Eq. (5.2.1) for Φ gives:

$$\delta_k = 2 \sum_{j=1}^N [f_i(x_j) - f(x_j, \underline{b})] \left[- \frac{\partial f(x_j, \underline{b})}{\partial b_k} \right]. \quad (5.2.12)$$

Substituting Eq. (4.5.9) for g_k we find:

$$\delta_k = - 2 g_k , \quad (5.2.13)$$

so that:

$$\delta_{\underline{g}} = - 2 \underline{g} . \quad (5.2.14)$$

This method suffers from extremely slow convergence near the minimum. The Taylor series method converges rapidly only near the minimum. Ideally, we should use the gradient method first, and switch to the Taylor series method near the minimum. In order to do this we must find a way to get around the ill-conditioning of \underline{A} . The most obvious way to make \underline{A} "better conditioned" is to construct:

$$(\underline{A} + \lambda \underline{I}) \underline{\delta}_0 = \underline{g}, \quad (5.2.15)$$

and decrease λ as we approach the minimum. Marquardt³⁸ has shown that: 1) $\underline{\delta}_0$ minimizes Φ on the "sphere" of radius $\|\underline{\delta}_0\|$; 2) $\|\underline{\delta}_0\|$ is a continuous decreasing function of λ , such that as $\lambda \rightarrow \infty$, $\|\underline{\delta}_0\| \rightarrow 0$; 3) let γ be the angle between $\underline{\delta}_0$ and $\underline{\delta}_g$. Then γ is a continuous decreasing function of λ such that as $\lambda \rightarrow \infty$, $\gamma \rightarrow 0$; i. e., $\underline{\delta}_0$ rotates toward $\underline{\delta}_g$ as $\lambda \rightarrow \infty$. Hence, this method is an interpolation between the above methods. Since $\underline{\delta}_T$ is independent of scale, but $\underline{\delta}_g$ is not, we must rescale \underline{A} and \underline{g} to be dimensionless. A convenient scale is the root-mean-square value of $[\partial f_0(\underline{x}_j)/\partial b_k]$. This leads to the definition of the scaled quantities:

$$A_{jk}^* = \frac{A_{jk}}{\sqrt{A_{jj}} \sqrt{A_{kk}}}, \quad (5.2.16)$$

$$g_j^* = g_j / \sqrt{A_{jj}}, \quad (5.2.17)$$

and:

$$\delta_j = \delta_j^* / \sqrt{A_{jj}}, \quad (5.2.18)$$

where δ^* for the r^{th} iteration is obtained from the solution of:

$$(\underline{A}^{*(r)} + \lambda^{(r)} \underline{I}) \underline{\delta}^{*(r)} = \underline{g}^{*(r)}. \quad (5.2.19)$$

The only question remaining is the selection of an appropriate value for $\lambda^{(r)}$. It is clear that $\Phi^{(r+1)}$ must be less than $\Phi^{(r)}$ or the process will not converge. A procedure which has been found to work well is as follows:³⁸

Let $q = 10$

1. If $\Phi(\lambda^{(r-1)}/q) \leq \Phi^{(r-1)}$, let $\lambda^{(r)} = \lambda^{(r-1)}/q$.
2. If $\Phi(\lambda^{(r-1)}/q) > \Phi^{(r-1)}$, and $\Phi(\lambda^{(r-1)}) \leq \Phi^{(r-1)}$, let $\lambda^{(r)} = \lambda^{(r-1)}$.

3. If $\Phi(\lambda^{(r-1)}/q) > \Phi^{(r-1)}$, and $\Phi(\lambda^{(r-1)}) > \Phi^{(r-1)}$,

increase λ by successive multiplication by q until for some smallest m , $\Phi(\lambda^{(r-1)} q^m) \leq \Phi^{(r-1)}$, let

$$\lambda^{(r)} = \lambda^{(r-1)} q^m.$$

4. If Eq. (4.5.19) is ill-conditioned and cannot be solved, increase λ by successive multiplication by q until for some smallest m , we can solve Eq. (5.2.19), let $\lambda^{(r)} = \lambda^{(r-1)} q^m$.

The non-linear least-squares procedure involves the calculation of many thousands of quantities $\partial f(x_j, \underline{b}) / \partial b_k$. It is essential that these quantities be calculated in a reasonably efficient manner. Let

the function, f , be given by:

$$f(x) = y_0 + a \left[\frac{1 - DB(x - x_0)}{1 + b(x - x_0)^2} \right]. \quad (5.2.20)$$

We then calculate the necessary quantities according to the following algorithm.

	<u>Number of Multiplications</u>
1. $B2 = b + b$	
2. $ADB = a * DB$	
3. DO 12 $j = 1, 2, \dots, N$	
4. $XJ = x(j) - x_0$	
5. $BX2 = 1. / (1. + B * XJ^2)$	2
6. $\partial f_j / \partial a = (1. - DB * XJ) * BX2$	2
7. $f_j = a * (\partial f_j / \partial a) + y_0$	1
8. $\partial f_j / \partial DB = -a * XJ * BX2$	2
9. $DFF = (\partial f_j / \partial a) * (\partial f_j / \partial DB)$	1
10. $\partial f_j / \partial b = XJ * DFF$	1
11. $\partial f_j / \partial x_0 = ADB * BX2 - B2 * DFF$	2
12. $\partial f_j / \partial y_0 = 1.$	1
	11

Thus, there are a total of approximately $11N$ multiplications required to evaluate these quantities. This leads to an efficient and practical program for filtering spectra. The values of the parameters, \underline{b} , which we obtain have a high degree of uncertainty. This uncertainty results from the ill-conditioning of \underline{A} , which is caused by the large

correlations between the parameters, \hat{b} . It is irrelevant for our present purposes, since the important point is that the deviations between f_i and f should be small. This condition can be satisfied.

5.3 Filtering the Satellite Peak

After performing the least-squares fit of the parent peak, we are ready to search for the satellite peak. We remove the parent peak by subtracting the Lorentzian we have determined by least-squares fitting from the experimental spectrum:

$$f_1(t) = f_i(t) - f(t, \hat{b}), \quad (5.3.1)$$

where $f_i(t)$ is the set of data points. The line shape of the satellite peak is significantly distorted, because the fitting procedure attempts to remove the satellite. The least-squares fit and the resulting distorted line shape are shown in Fig. 5.3.1 where the size of the satellite peak is exaggerated for clarity.

This distortion can be eliminated. The approximate position of the satellite can be determined from $f_1(t)$ (Fig. 5.3.1). We then construct:

$$f_{i_1}(t) = f_i(t) - f_s(t), \quad (5.3.2)$$

where $f_s(t)$ is the satellite. A new $f_1(t, \hat{b})$ is then determined by least-squares fitting to $f_{i_1}(t)$. We remove the parent peak from $f_1(t)$ again:

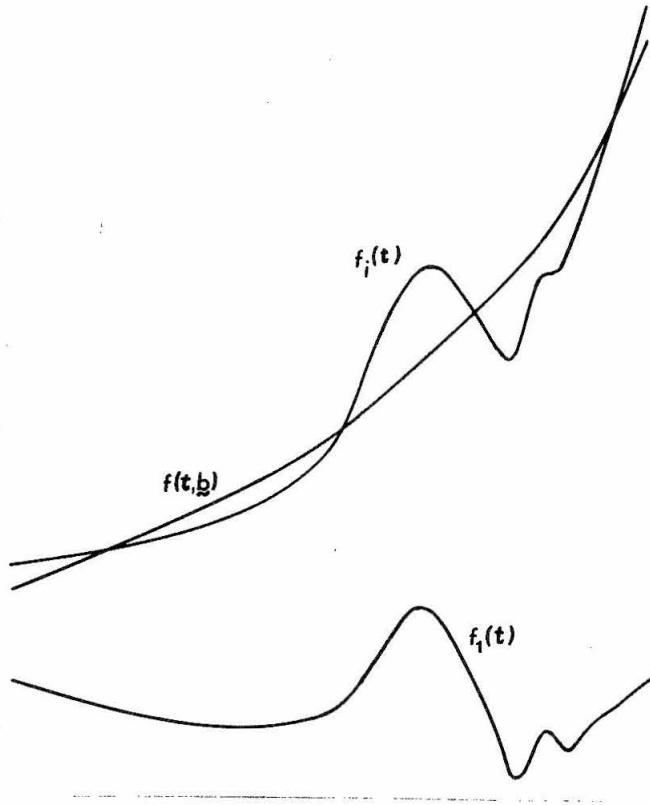


Figure 5.3.1. The line shape of the satellite peak is distorted by removing the parent peak.

$$f_2(t) = f_i(t) - f_1(t, \underline{b}), \quad (5.3.3)$$

and obtain a new spectrum of the satellite peak. Additional iterations are possible but not necessary.

If $f(t, \underline{b})$ fits the parent peak exactly, then the sum of the squares of the residues, Φ , is given by:

$$\Phi = \int_{t_1}^{t_2} [f_s(t) + n_i(t)]^2 dt, \quad (5.3.4)$$

where $f_s(t)$ is the satellite peak and $n_i(t)$ is the input noise. From Fig. 5.3.1 we see that in practice the value of Φ after the first iteration, Φ_1 is somewhat better described by:

$$\Phi_1 \doteq \int_{t_1}^{t_2} \left[\pm \frac{1}{2} f_s(t) + n_i(t) \right]^2 dt. \quad (5.3.5)$$

If $f_s(t)$ and $n_i(t)$ are of the same order of magnitude, we can make the further approximation:

$$\Phi_1 \doteq \frac{1}{4} \int_{t_1}^{t_2} [f_s(t)]^2 dt + \int_{t_1}^{t_2} [n_i(t)]^2 dt, \quad (5.3.6)$$

since the cross terms, $f_s(t) n_i(t)$ and $f_s(t+\tau) n_i(t+\tau)$ tend to cancel when the noise is white. We can express Φ_1 more concisely as:

$$\Phi_1 \doteq \frac{1}{4} E_s + E_n \quad (5.3.7)$$

where E_s and E_n are the energy of the satellite peak and the noise respectively [Eq. (2.3.8)]. If we determine the exact position of the satellite peak from the first iteration, then $f_{i_1}(t)$ in Eq. (5.3.2) will contain only the parent peak and noise. The sum of the squares of the residues would then be given by:

$$\Phi_2 \doteq E_n. \quad (5.3.8)$$

Combining Eqs. (5.3.7) and (5.3.8) we obtain a useful condition for the existence of a satellite at the position we determined from the

first iteration:

$$\Phi_1 - \Phi_2 \doteq 0.25 E_S. \quad (5.3.9)$$

The only remaining problem is the determination of the position of the satellite peak in the presence of random noise. The least-squares position of the satellite peak can be determined by using a matched filter (Sec. 4.2). The parent peak can frequently be used for the line shape function. The examples we shall treat are all in this category. This iterative procedure leads to a least-squares estimate of the satellite and parent peak parameters. We have used what is essentially a perturbation approach.

A very high signal-to-noise spectrum of the proton resonance from chloroform was recorded using a Varian Associates Model A-60 spectrometer (Fig. 5.3.2). The Lorentzian least-squares function [Eq. (5.2.20)] provides a very accurate description of this experimental spectrum in the region of interest. If $f_1(t) \leq 0.5 f_1(\delta)$, then $|f_1(t) - f(t, \underline{b})| < 0.0005 f_1(\delta)$. A comparison of Figs. 5.1.1 and 5.3.2 indicates that the parameters, \underline{b} , are not very good estimates of the parameters in Eq. (5.1.2). In order to determine whether or not the excellent fit we obtain using a Lorentzian is real, we have also performed a least-squares fit of the same data using a Gaussian:

$$f(x) = y_0 + a \left[\frac{1 - DB(x - x_0)}{e^{b(x - x_0)^2}} \right]. \quad (5.3.10)$$

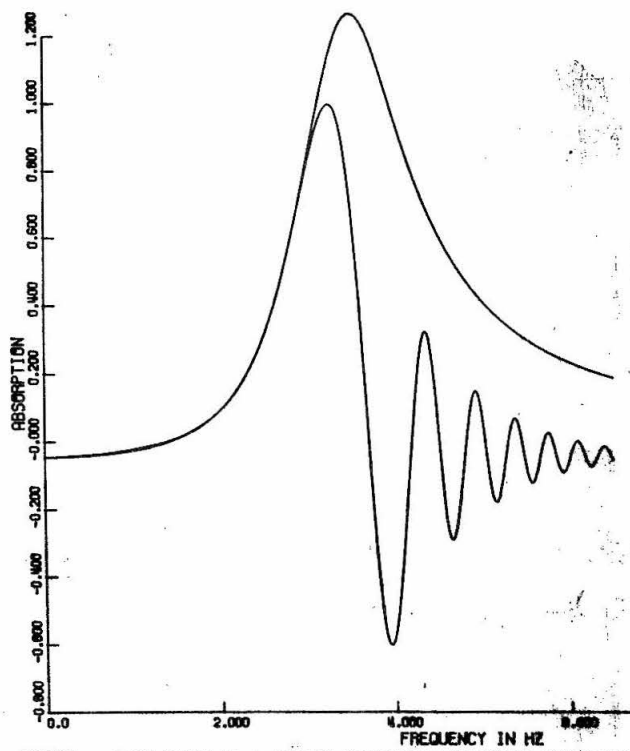


Figure 5.3.2. The least-squares fit of the proton resonance of CHCl_3 ($\alpha = 1.0$) using a Lorentzian line shape function [Eq. (5.2.20)].

The result (Fig. 5.3.3) is clearly unsatisfactory. In the region of interest, $|f_1(t) - f(t, \underline{b})|$ can be greater than $0.005 f_1(\delta)$ which is the amplitude of a ^{13}C satellite. The parameters, \underline{b} , are even less realistic than those obtained using a Lorentzian line shape. The parameter a in Eq. (5.3.10) is approximately $7.5 f_1(\delta)$. Recalling the correlation of the Lorentzian parameters, we conclude that the asymptotic form [Eq. (5.1.2)] is a valid approximation in the region

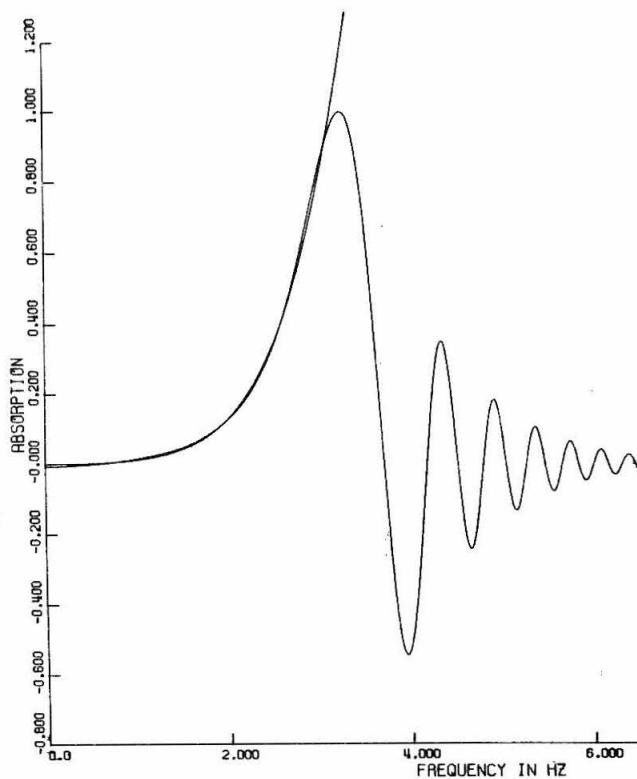


Figure 5.3.3. The least-squares fit of the proton resonance of CHCl_3 ($\alpha = 1.0$) using a Gaussian line shape function [Eq. (5.3.10)].

of interest although the parameters are not well defined.

In order to determine the resolving power of these filters we have artificially added satellite peaks to the spectrum shown in Fig. 5.3.2. If we set J_- equal to -1.90 Hz, the maximum of $f_1(t)$ falls at -1.95 Hz (Fig. 5.3.4). We then set the maximum of $f_s(t)$ at -1.95 Hz [Eq. (5.3.2)] and calculate $f_{i_1}(t)$. A second least-squares fit gives $f_2(t)$ [Eq. (5.3.3)]. The maximum of $f_2(t)$ falls at -1.90 Hz and the

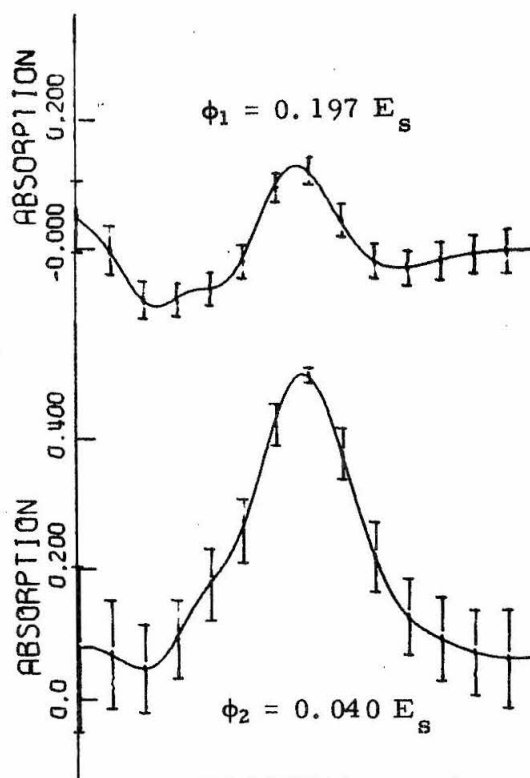


Figure 5.3.4. The functions $f_1(t)$ (top) and $f_2(t)$ (bottom) [Eqs. (5.3.1) and (5.3.3)] resulting from the above CHCl_3 spectrum. A matched filter has been used and the scale is such that $f_1(\delta) = 100$. The error bars represent one standard deviation (Sec. 6).

amplitude is within a few per cent of the correct value for the satellite. The condition in Eq. (5.3.9) is approximately satisfied (Fig. 5.3.4) and we have successfully resolved our artificial ^{13}C satellite. By varying where we place this artificial satellite, we find that this filter can resolve a ^{13}C satellite if the spin-spin coupling is

greater than about four times the line width of the parent peak.

When using this filter, there is some danger reporting a satellite which is not real. In order to assess this danger we have studied the above chloroform spectrum with no satellite added. The initial filtered spectrum, $f_1(t)$ shows nothing remotely resembling a satellite (Fig. 5.3.5). If however, we assume the existence of a ^{13}C satellite with J_- equal to -1.95 Hz, we obtain something strongly resembling a satellite peak at approximately -1.80 Hz in $f_2(t)$ (Fig. 5.3.5). The sum of the squares of the residues has increased

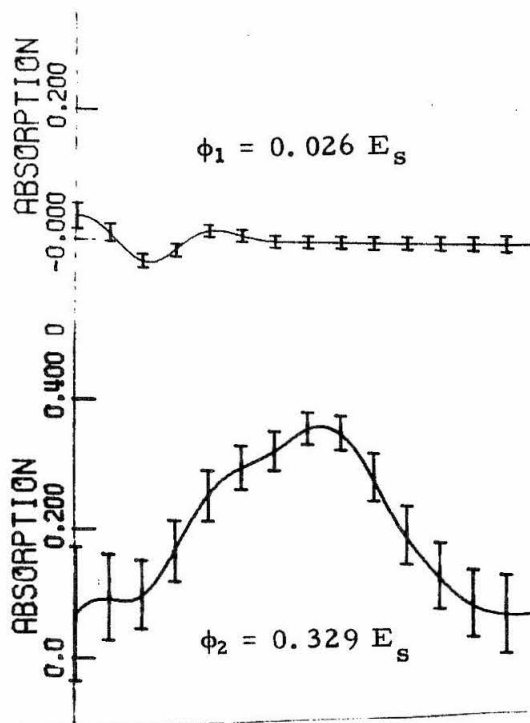


Figure 5.3.5. The functions $f_1(t)$ and $f_2(t)$ [Eqs. (5.3.1) and (5.3.3)] in the absence of a satellite peak. Note that $f_1(t)$ (top) is almost entirely within one standard deviation from zero.

however, and we therefore conclude that there is no satellite peak at -1.80 Hz in $f_1(t)$. The second output spectrum, $f_2(t)$, is useful only for the refinement of our estimate of the exact value of J_{\pm} . From Fig. 5.3.4 we see that the signal-to-noise level available to measure a small coupling constant when this least-squares filter can be used is approximately half that available with a matched filter for an infinitely large coupling.

A. ^{13}C spin-spin coupling constant greater than four line widths can be measured using this least-squares filter based upon the asymptotic form of the line shape. The loss in signal-to-noise from resolution enhancement is rather modest. Since the "wiggles" in the line shape obscure the satellite at high frequency, we must measure J_+ separately by sweeping from high frequency to low frequency. Although this doubles the work we must do, it does provide an important check on the results.

5.4 The Pseudo-Linear Approach

We shall now consider a class of filters which are conceptually derived from linear resolution enhancement filters, but are actually non-linear. A linear filter requires an independent measurement of the line shape. Since this is not practical for the resolution of satellite peaks, we shall derive some pseudo-linear filters which determine the line shape from the spectrum itself.

Consider a spectrum composed of n lines, all of which have the same line shape. If there is no noise, the spectrum is given by:

$$f_i(t) = \sum_{j=1}^n a_j s_i(t - \delta_j), \quad (5.4.1)$$

where δ_j and $a_j s_i(0)$ are the position and amplitude of the j^{th} line.

The Fourier transform of the spectrum is then:

$$F_i(\omega) = S_i(\omega) \sum_{j=1}^N a_j e^{-i\omega \delta_j}. \quad (5.4.2)$$

If a_k is much greater than all the other a_j we can make the approximation:

$$S_i(\omega) \doteq S_f(\omega) \equiv F_i(\omega) \frac{e^{i\omega \delta_k}}{a_k}, \quad (5.4.3)$$

for the Fourier transform of the line shape. The output of a matched filter is given by:

$$F_m(\omega) = c(0) S_i^*(\omega) F_i(\omega). \quad (5.4.4)$$

This suggests the construction of the self-filter:

$$F_o(\omega) = c(0) F_i^*(\omega) \frac{e^{-i\omega \delta_k}}{a_k} F_i(\omega). \quad (5.4.5)$$

Substituting Eq. (5.4.2) for $F_i(\omega)$, we find that:

$$F_o(\omega) = c(0) S_i^*(\omega) S_i(\omega) \sum_{j=1}^n \sum_{\ell=1}^n \frac{a_j a_\ell}{a_k} e^{i\omega(\delta_j - \delta_k - \delta_\ell)}. \quad (5.4.6)$$

Taking the Fourier transform gives:

$$f_0(t) = \sum_{j=1}^n \sum_{\ell=1}^n \frac{a_j a_\ell}{a_k} s_m(t - \delta_k + \delta_j - \delta_\ell), \quad (5.4.7)$$

where $s_m(t)$ is the line shape resulting from a matched filter. If a_k is indeed much greater than all the other a_j , then $a_j a_\ell / a_k$ will be very small unless j or ℓ or both are equal to k . The output of a self-filter is therefore approximately:

$$f_0(t) \doteq \sum_{j=1}^n a_j [s_m(t - \delta_j) + s_m(t + \delta_j - 2\delta_k)] - a_k s_m(t - \delta_k). \quad (5.4.8)$$

The output spectrum is symmetric about $t = \delta_k$. For each line in the input spectrum at $t = \delta_j$ there is a line in the output spectrum at both $t = \delta_j$ and at $t = \delta_k + (\delta_k - \delta_j)$. These two lines are located symmetrically with respect to δ_k .

The simplest case of a self filter is that of a spectrum containing only one line and no noise. The output spectrum [Eq. (5.4.7)] is then:

$$f_0(t) = a_1 s_m(t - \delta_1), \quad (5.4.9)$$

which is the output from a matched filter. If the input spectrum contains two lines, the output spectrum becomes:

$$f_0(t) = \left[a_1 + \frac{a_2^2}{a_1} \right] s_m(t - \delta_1) + a_2 s_m(t - \delta_2) + a_2 s_m[t - \delta_1 - (\delta_1 - \delta_2)], \quad (5.4.10)$$

where $a_1 s_1(t - \delta_1)$ is the larger of the two input lines. From Eq. (4.2) we see that the non-linear interaction term is given by:

$$\underline{H}_{12}[s_1(t)_1, s_1(t)_2] = \left(\frac{a_2}{a_1}\right)^2 s_0(t)_1 + s_0[t - 2(\delta_1 - \delta_2)]_2. \quad (5.4.11)$$

The self-filter is not a linear filter. The first term in Eq. (5.4.11) may be neglected when filtering satellite peaks, however, the second term is quite important. If J_+ and J_- are unequal, the output spectrum will have four satellite peaks located at $\delta + J_+$, $\delta - J_+$, $\delta + J_-$, and $\delta - J_-$. If J_+ and J_- are equal, the output spectrum will have two satellite peaks located at $\delta + J/2$ and $\delta - J/2$, and the output amplitudes of the satellites will be twice the input amplitudes. If J_+ and J_- are unequal we lose all information about which is larger. Although the sign of δ_{xy} is lost, we can still measure the magnitude $|\delta_{xy}|$.

These self-matched filters are interesting, but not at all useful. If J is large we can select the portion of the spectrum which contains only the parent peak. Using this as the line shape we can construct a matched filter for the satellites. This procedure permits the determination of the sign of δ_{xy} , which can be valuable for the analysis of ^{13}C spectra. If J is small, J_+ and J_- will be nearly equal, and the fact that we cannot determine which is larger with a self-filter

becomes unimportant. Unfortunately, a self-matched filter cannot resolve the satellite peaks when J is small. We therefore examine a self-resolution enhancement filter, which has the frequency response function:

$$H(\omega) = \frac{c(q) S_f^*(\omega)}{1 + q |S_f(\omega)|^2}, \quad (5.4.12)$$

where $S_f(\omega)$ is defined by Eq. (5.4.3). We cannot use a very large value of q , because:

$$\text{Limit}_{q \rightarrow \infty} F_0(\omega) = \text{Limit}_{q \rightarrow \infty} H(\omega) F_1(\omega), \quad (5.4.13)$$

or, from Eqs. (5.4.12) and (5.4.3):

$$\text{Limit}_{q \rightarrow \infty} F_0(\omega) = \frac{c(q) S_f^*(\omega) F_1(\omega)}{q |S_f(\omega)|^2} = \frac{c(q)}{q} a_k e^{-i\omega \delta_k}. \quad (5.4.14)$$

That is, for large q , $f_0(t)$ approaches a Dirac delta function of amplitude a_k , centered at $t = \delta_k$. The satellite peaks have been removed. If we use modest values of q ($< \sim 15$), the satellites will still be present, but with decreased amplitudes.

Two ^{13}C satellite peaks were added to the chloroform spectrum discussed in the previous section ($J_+ = J_- = 1.90$ Hz). The spectrum was then filtered using a self-resolution enhancement filter [Eq. (5.4.12)] in which the value of q was varied to obtain the minimum interference from the parent peak. The resulting spectrum shows

easily visible peaks in the positions of the satellites (Fig. 5.4.1). The satellites are nicely resolved and their intensity is still more than 25% of the intensity of satellite peaks filtered with a self-matched filter. Unfortunately, the "wiggles" in the tail of the parent peak also look like satellite peaks. A chloroform spectrum with no satellites added has been filtered in the same manner (Fig. 5.4.2).

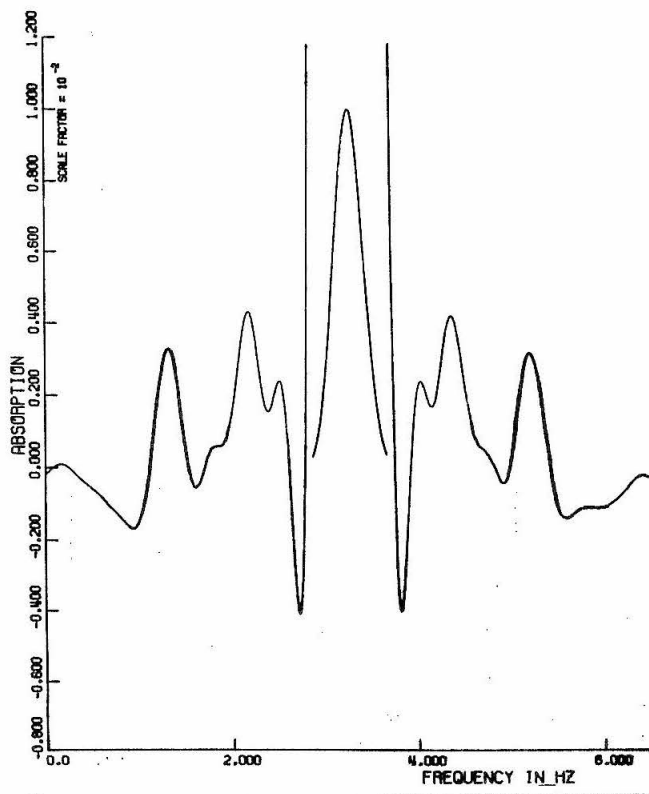


Figure 5.4.1. Self-resolution enhancement spectrum [Eq. (5.4.12)] with $q = 12$. The peaks at 1.4 Hz and 5.2 Hz are ^{13}C satellites. The amplitude of the parent peaks is reduced by a factor of 100.

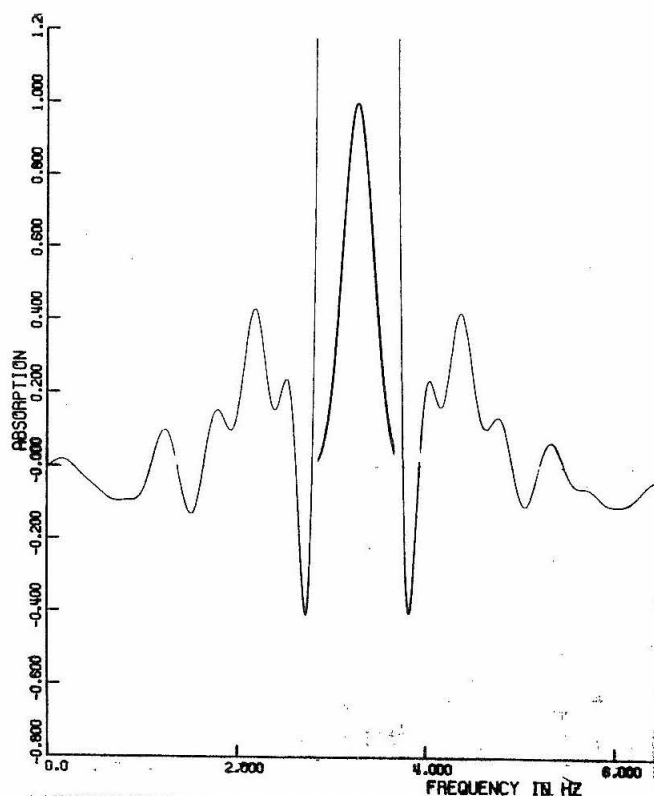


Figure 5.4.2. Self-resolution enhancement in the absence of satellites (see Fig. 5.4.1).

Comparing the two makes it clear that our interpretation of Fig. 5.4.1 was correct. In practice, we will not have Fig. 5.4.2 available for comparison and we will not know J in advance. The "wiggles" in the tail of the output line shape destroy the usefulness of these filters.

The "wiggles" in the tail of an output line shape are easily understood by considering the limiting form [Eq. (5.4.14)]. Taking the Fourier transform of this equation gives:

$$\text{Limit}_{q \rightarrow \infty} f_0(t) = a_k \text{Limit}_{q \rightarrow \infty} \left\{ \frac{\sin[(t - \delta_k)\omega]}{\pi(t - \delta_k)} \right\}, \quad (5.4.15)$$

which is the well known oscillatory form of the Dirac delta function. In order to remove the "wiggles" we must convert the output line shape to some non-oscillating form. We can convert an arbitrary input line shape to any output line shape by setting:

$$H(\omega) = c S_0(\omega)/S_1(\omega), \quad (5.4.16)$$

if $S_0(\omega)$ exists and $S_1(\omega)$ is never zero. Ernst³⁹ points out that such filters exist for the conversion of a Lorentzian line to a Gaussian line of reduced line width. This Lorentzian to Gaussian filter has the frequency response function:

$$H(\omega) = \frac{e^{-\frac{b^2}{4 \ln 2} \left(\frac{\nu_0}{\nu_1}\right)^2 \omega^2}}{e^{-b|\omega|}}, \quad (5.4.17)$$

where b describes the line width of the Lorentzian input line shape. The line shape of a typical n. m. r. signal is not Lorentzian and the filter which converts it to a Gaussian:

$$H(\omega) = \frac{e^{-\frac{b^2}{4 \ln 2} \left(\frac{\nu_0}{\nu_1}\right)^2 \omega^2}}{S_1(\omega)}, \quad (5.4.18)$$

does not necessarily exist. Even if it does exist, the self-filter:

$$H(\omega) = \frac{e^{-\frac{b^2}{4 \ln 2} \left(\frac{\nu_0}{\nu_i}\right)^2 \omega^2}}{S_f(\omega)}, \quad (5.4.19)$$

leads to a single output peak centered at $t = \delta_k$. The Gaussian modification of Eq. (5.4.12) is given by:

$$H(\omega) = \frac{c(q) e^{-\frac{b^2}{4 \ln 2} \left(\frac{\nu_0}{\nu_i}\right)^2 \omega^2} S_f^*(\omega)}{1 + q |S_f(\omega)|^2}. \quad (5.4.20)$$

This frequency response function will exist for any value of q , and if q is not too terribly large, it will not remove the satellite peaks. As q approaches infinity, the output line shape from this filter will approach a Gaussian of line width ν_0 .

The parameters ν_i , ν_0 , and b must now be determined. We can consider these Gaussian self-filters to be a sequence of two filters. The first is a matched filter and the second has the form of Eq. (5.4.18) with the denominator equal to $S_m(\omega)$. We therefore set ν_i in Eq. (5.4.20) equal to ν_m , the line width resulting from a matched filter. From Figs. 5.4.1 and 5.4.2, we see that our problem is not to narrow the output line shape, but only to remove the "wiggles". Since a reduction of the output line width would reduce the signal-to-noise ratio, we set ν_0 equal to the output line width we would have if $b = 0$. This will be a function of q . A sufficiently

accurate empirical estimate of this dependence is given by:

$$\left(\frac{\nu_q}{\nu_m} \right) \doteq \frac{1}{1 + 0.53 \ln(q+1)} \quad (5.4.21)$$

which is independent of the sweep rate (see Sec. 3.3).

We shall now estimate the proper value of b . The quantity $|S_f(\omega)|^2$ in Eq. (5.4.20) has the line shape which results from a matched filter. Since $s_m(t)$ looks very much like a Lorentzian function regardless of the sweep rate (Fig. 3.3.1), one could make the approximation:

$$|S_f(\omega)|^2 \doteq a_f e^{-b_f |\omega|}, \quad (5.4.22)$$

where a_f and b_f may be determined by a least-squares procedure.

Substituting our estimates of the parameters ν_i , ν_0 , and b in

Eq. (5.4.20) we obtain:

$$H(\omega) = \frac{c(q) e^{-\left[0.36 b_f^2 \frac{\omega^2}{1 + 0.53 \ln(q+1)}\right]} S_f^*(\omega)}{1 + q |S_f(\omega)|^2} \quad (5.4.23)$$

for the frequency response function of a Gaussian self-filter.

This Gaussian self-filter has been applied to the above chloroform spectrum with satellites. In order to check our estimates of the parameters in $H(\omega)$, we varied the output line width, ν_0 . As we predicted above, the optimum value of ν_0 is approximately ν_q

(Fig. 5.4.3). That is, ν_q is the minimum output line width which will eliminate the "wiggles". The signal-to-noise ratio of the spectrum without "wiggles" in Fig. 5.4.3 ($q = 12$) is 96% of that resulting from a self-matched filter, however, the size of the satellite peaks has been reduced by a factor of four. This difficulty is easily avoided by using the approximation given by Eq. (5.4.22) for the denominator

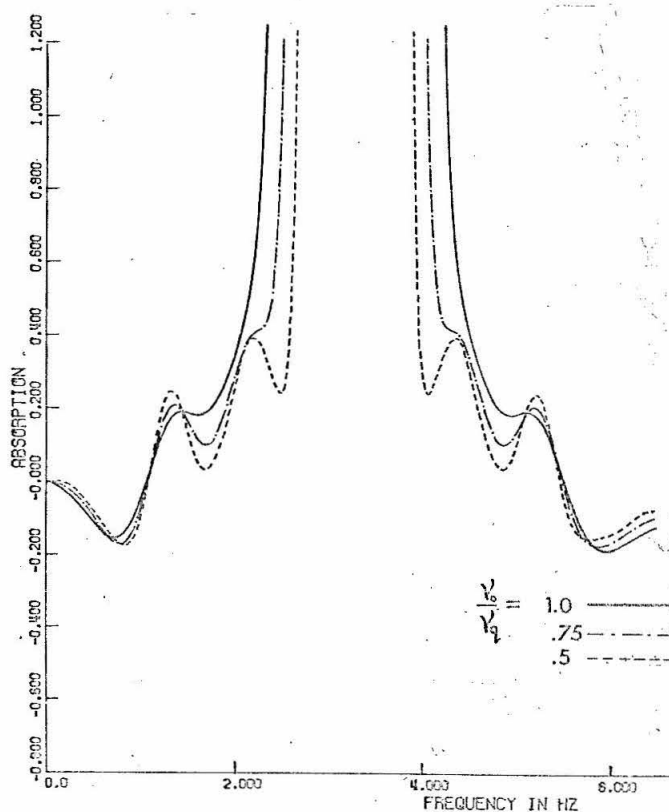


Figure 5.4.3. Resolution enhancement of the chloroform spectrum (Fig. 5.3.2) with satellites added at $J_{\pm} = \pm 1.90$ Hz. The Gaussian self-resolution enhancement filter [Eq. (5.4.20)] gives the best results when ν_0 is approximately equal to ν_q [Eq. (5.4.23)].

of Eq. (5.4.23). The frequency response function of this filter is given by:

$$H(\omega) = \frac{c(q) e^{-\left[\frac{0.36 b_f^2 \omega^2}{1 + .53 \ln(q+1)} \right]} S_f^*(\omega)}{1 + q a_f e^{-b_f |\omega|}} \quad (5.4.24)$$

where a_f and b_f are determined by a least-squares procedure (Sec. 5.2.). The above chloroform spectrum with satellites has been filtered using this frequency response function (Fig. 5.4.4).

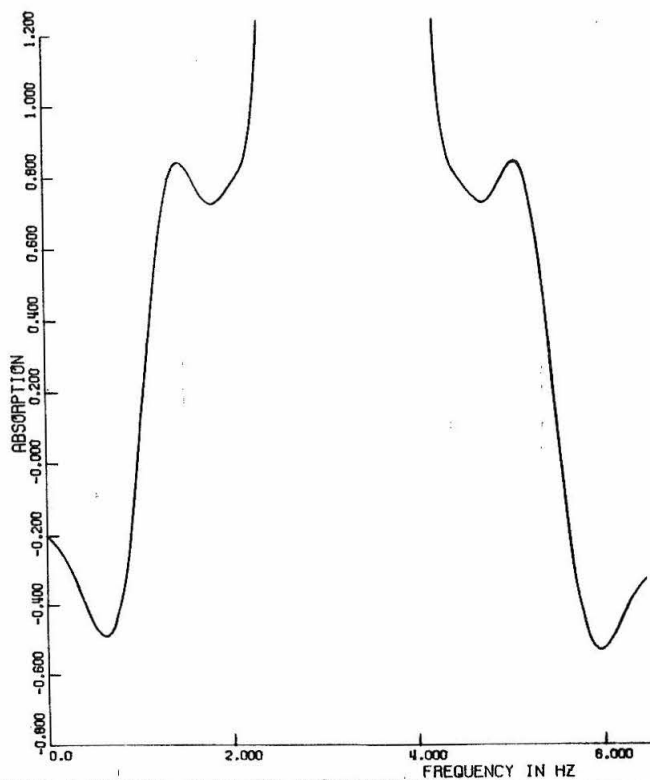


Figure 5.4.4. Resolution of the chloroform spectrum using Eq. (5.4.24).

The amplitude of the satellite peaks is independent of q . We now have a very useful pseudo-linear resolution enhancement filter for satellite peaks.

The exponential approximation [Eq. (5.4.22)] is valid for large ω only if all "wiggles" in the input line shape are included in the spectrum. Therefore, these filters should not be used with large values of q for a spectrum such as that shown in Fig. 5.3.2. If all "wiggles" are included in the spectrum, we can achieve substantial resolution enhancement (Fig. 5.4.5). In this case, large values of q simply reduce the signal-to-noise ratio. They do not introduce any fluctuations which have the appearance of a satellite.

In practice, it is difficult to obtain a spectrum of the quality of Fig. 5.4.5 when studying (^{13}C , ^{13}C) coupling constants with natural abundance samples. Several hundred scans are necessary in order to achieve an adequate signal-to-noise ratio. With presently available spectrometers, this introduces a broadening due to the drift of the field (Fig. 5.4.6). When large values of q are used in Eq. (5.4.24), these spectra tend to produce minima adjacent to the parent peak (Fig. 5.4.7). Although this limits the resolution which is possible, there is no problem of producing spurious "satellite" peaks. When the input line shape is determined primarily by field drift, the exponential approximation [Eq. (5.4.22)] breaks down for large ω . The slow drift of the field limits the resolution, however, we can still obtain very useful spectra when small values of q are used (Fig. 5.4.8).

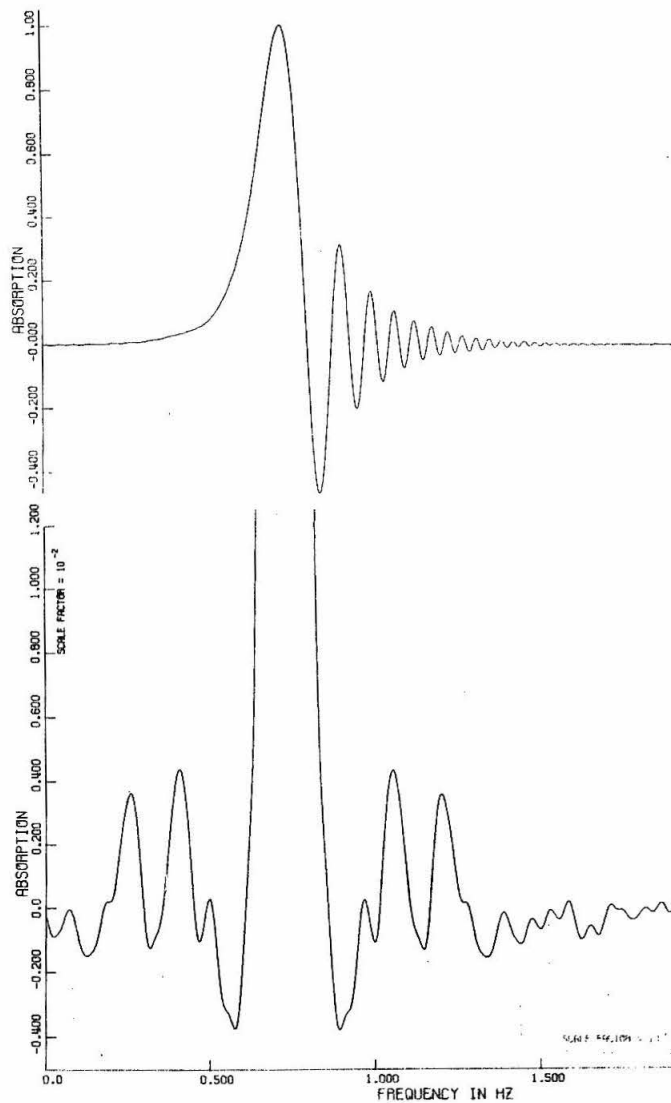


Figure 5.4.5. The proton resonance of CHCl_3 ($\alpha = 2.5$) with satellites added ($J_+ = 4.75$ Hz, $J_- = -3.29$ Hz). The frequencies are scaled by a factor of 10. Note that the upfield satellite is easily resolved even though it is completely buried in the "wiggles" before filtering.

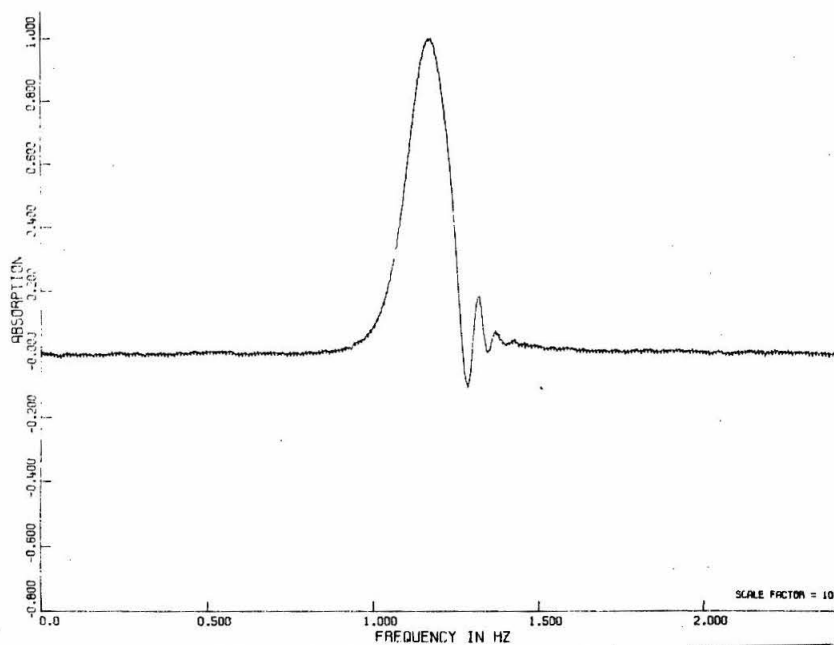


Figure 5.4.6. The natural abundance ^{13}C spectrum of carbons two and three from cyclopropyl chloride (925 scans), courtesy of F. J. Weigert.

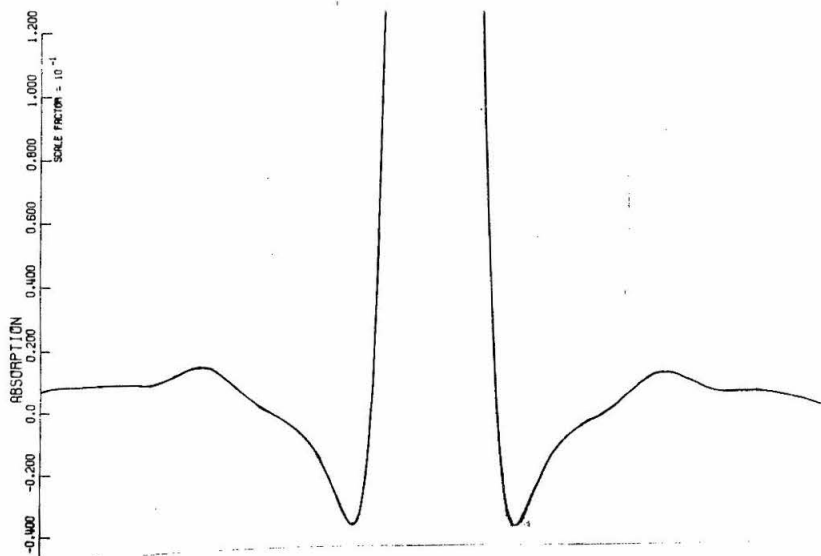


Figure 5.4.7. The resolution enhancement of the spectrum in Fig. 5.4.6. using Eq. (5.4.24) for the filter ($q = 10^{14}$).

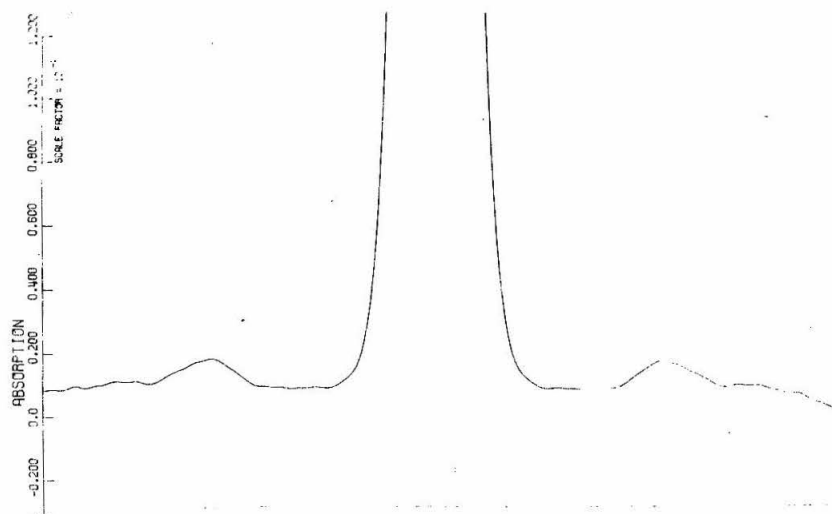


Figure 5.4.8. The resolution enhancement of the spectrum in Fig. 5.4.6 using Eq. (5.4.24) for the filter ($q = 1.4$). The observed value of J (14.0 ± 0.1 Hz) compares favorably with the value (13.9 ± 0.2 Hz) obtained after 2,600 scans without resolution enhancement.

In principle we could measure an arbitrarily small spin-spin coupling constant using the pseudo-linear filter given in Eq. (5.4.24). Unfortunately, the signal-to-noise level available to measure J falls off extremely rapidly for couplings smaller than about twice the full width at half height resulting from a matched filter (Fig. 5.4.9). This is about the limit of the region which is accessible with least-squares filters (Sec. 5.3).

The asymptotic behavior of these pseudo-linear filters can be determined by the techniques used in section 3.4 for linear filters. We find that:

$$\lim_{q \rightarrow \infty} \frac{(S/N)_o}{(S/N)_m} = \left(\frac{\pi \ln 2}{2}\right)^{1/4} \left(\frac{\nu_m}{\nu_o}\right)^{1/2} e^{-\left(\frac{\ln 2}{4}\right) \left(\frac{\nu_m}{\nu_o}\right)^2}. \quad (5.4.25)$$

The signal-to-noise level falls off much more rapidly than it does with optimum linear resolution enhancement filters [Eq. (3.5.19)].⁴⁰

The point at which the signal-to-noise level begins to fall off is roughly the same as the point at which "wiggles" begin to appear in the tail of the output line shape. These "wiggles" are not important

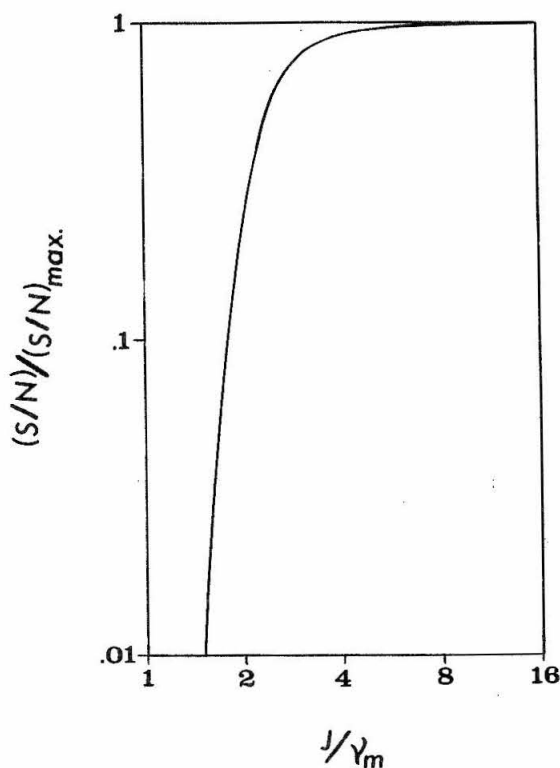


Figure 5.4.9. The signal-to-noise level available to measure the position of a ^{13}C satellite using the pseudo-linear filter given in Eq. (5.4.24).

when filtering lines of comparable magnitude since the amplitude of the largest "wiggle" is always less than 12.8% of the amplitude of the peak [Eq. (5.4.15)]. We cannot afford to sacrifice much signal-to-noise when filtering satellite spectra. The importance of removing these "wiggles" by transforming to a Gaussian output function is therefore somewhat questionable, since in practice we can achieve approximately the same resolution without this transformation.

If the spin-spin coupling of the satellite peak is greater than eight times the natural line width [$\nu_m(\alpha = 0)/2$], we can increase the signal-to-noise level by increasing the sweep rate. The maximum signal-to-noise ratio is achieved when ν_m is approximately $4J$. These filters permit the practical measurement of spin-spin coupling constants as small as 0.5 Hz for both (^{13}C , H) and (^{13}C , ^{13}C) using natural abundance samples.

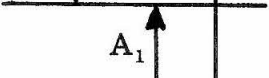
5.5 Spectral Analysis Using Satellites

Pseudo-linear and least-squares filters are complementary rather than competitive procedures. Pseudo-linear filters can be used to measure both J_+ and J_- , however they cannot distinguish between the two. Least-squares filters can be used to measure J_- (or J_+ if we sweep downfield). By using both pseudo-linear and least-squares filters one can obtain separate measurements of J_+ and J_- from a single spectrum. If J is large, this can be accomplished by using a linear filter (Sec. 5.4). The knowledge of J_+ and J_- can be valuable for the analysis of spectra.

Natural abundance ^{13}C spectra are much simpler than equivalent proton spectra. If the protons are decoupled, the ^{13}C spectrum consists of single lines centered at the resonance frequencies of the various carbons. The chemical shifts can be measured directly, however the assignments of these shifts is not necessarily trivial.⁴¹

Let us assume that the chemical shift of carbon A is known. It is then possible to assign carbon B based upon the measured values of J_+ and J_- for the (A, B) coupling. The energy levels for an AB system⁴² are shown in Table 5.5.1. Using these values we find that

TABLE 5.5.1 Energy Levels for an AB System

State	Transitions	Energy
1		$+ J/4 + (\gamma H_0/2) (2 - \sigma_A - \sigma_B)$
2		$- J/4 - (1/2) \sqrt{J^2 + \gamma^2 H_0^2 (\sigma_A - \sigma_B)^2}$
3		$- J/4 + (1/2) \sqrt{J^2 + \gamma^2 H_0^2 (\sigma_A - \sigma_B)^2}$
4		$+ J/4 - (\gamma H_0/2) (2 - \sigma_A - \sigma_B)$

the transition energies are given by:

$$\Delta E_{A_1} = -J/2 - \frac{1}{2} \sqrt{J^2 + \gamma^2 H_0^2 (\sigma_A - \sigma_B)^2} + (\gamma H_0/2) (2 - \sigma_A - \sigma_B); \quad (5.5.1)$$

$$\Delta E_{A_2} = +J/2 - \frac{1}{2} \sqrt{J^2 + \gamma H_0^2 (\sigma_A - \sigma_B)^2} + (\gamma H_0/2)(2 - \sigma_A - \sigma_B) \quad (5.5.2)$$

we now define:

$$X^2 \equiv J^2/\gamma^2 H_0^2 (\sigma_A - \sigma_B)^2, \quad (5.5.3)$$

and assume that $X^2 \ll 1$. The transition energy is then:

$$\Delta E_{A_1} = -J/2 - (\gamma H_0/2)(\sigma_A - \sigma_B) \sqrt{1 + X^2} + (\gamma H_0/2)(2 - \sigma_A - \sigma_B). \quad (5.5.4)$$

We can expand the square root in a Taylor's series:

$$\sqrt{1 + X^2} \doteq 1 + \frac{1}{2}X^2 - \frac{1}{8}X^4 + \dots \quad (5.5.5)$$

Substituting this in Eq. (5.5.4) gives:

$$\Delta E_{A_1} \doteq -J/2 + \gamma H_0 (1 - \sigma_A) - (\gamma H_0/2)(\sigma_A - \sigma_B) \left(\frac{1}{2}X^2 - \frac{1}{8}X^4 \right). \quad (5.5.6)$$

Using the definitions of J_- and δ_{AB} this becomes:

$$J_- \doteq -J/2 - \frac{1}{4} \left[(J^2/\delta_{AB}) - \frac{1}{4} (J^4/\delta_{AB}^3) \right]. \quad (5.5.7)$$

Treating Eq. (5.5.2) similarly, we find:

$$J_+ \doteq +J/2 - \frac{1}{4} \left[(J^2/\delta_{AB}) - \frac{1}{4} (J^4/\delta_{AB}^3) \right]. \quad (5.5.8)$$

Therefore:

$$J_+ + J_- \doteq \frac{1}{2} \left[(J^2/\delta_{AB}) - \frac{1}{4} (J^4/\delta_{AB}^3) \right]. \quad (5.5.9)$$

Finally, we rearrange this expression and obtain:

$$\delta_{AB} \doteq - \frac{J^2}{2(J_+ + J_-)} \left[1 - \frac{J^2}{4\delta_{AB}^2} \right] \quad (5.5.10)$$

This relationship can be quite useful in the assignment of the resonance line of a carbon which is directly bonded to another carbon whose chemical shift is known. When A and B are directly bonded, J_{AB} and $(J_+ + J_-)$ are both large and can therefore be measured with reasonable accuracy.

6 ERROR ESTIMATES

The techniques discussed in this thesis all involve the measurement of line positions. It is obviously desirable to have realistic estimates of the errors in these measurements. If we consider the derivation of a matched filter given in Section 1.1, a suitable method immediately suggests itself.

The output spectrum $f_0(t)$ is the weighted average of the values:

$$f_0(t, \tau) = f_i(t - \tau) s_i(0)/s_i(-\tau). \quad (6.1)$$

We can therefore calculate the standard deviation of $f_0(t)$. This serves several very useful purposes. The points of the "base line" should all be within about one standard deviation of a straight line. If a point rises two standard deviations above the base line, the probability is 0.954 that it is a peak (the filtered noise is Gaussian, since each filtered point is a linear combination of points with Gaussian distributions³³). If a point rises three standard deviations above the base line, the probability is 0.997 that it is a peak.

The standard deviations also provide a method of estimating the error in a measurement of a peak position. Let $f(t)$ be the "true" value of $f_0(t)$. The upper and lower ends of the error bars (which indicate one standard deviation) constitute an envelope around $f_0(t)$. We shall call the upper curve $f_0^+(t)$ and the lower curve $f_0^-(t)$. The probability that any point of $f(t)$ lies within these curves is 0.683. Therefore, 68.3% of $f(t)$ lies within this envelope. This is true

whether we consider $f(T_1)$ in Fig. 6.2 to be above $f_0(T_1)$ or to the left of $f_0(T_2)$. Therefore, the interval of t with a probability of 0.683 that $f(t)$ takes on a particular value is the horizontal distance to $f_0^+(t)$ or $f_0^-(t)$. Let t_1 and t_2 (Fig. 6.1) be chosen such that:

$$f_0^+(t_j) = f_0(t)_{\max}. \quad (6.2)$$

These points will then satisfy:

$$P(t_1 < \delta < t_2) = .683, \quad (6.3)$$

where δ is the position of the peak. We therefore estimate the error in the peak position to be $\pm(t_2 - t_1)/2$.

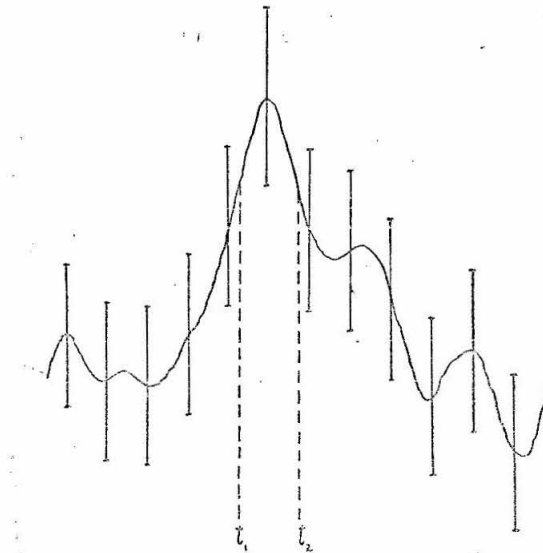


Figure 6.1. The standard deviations of $f_0(t)$.

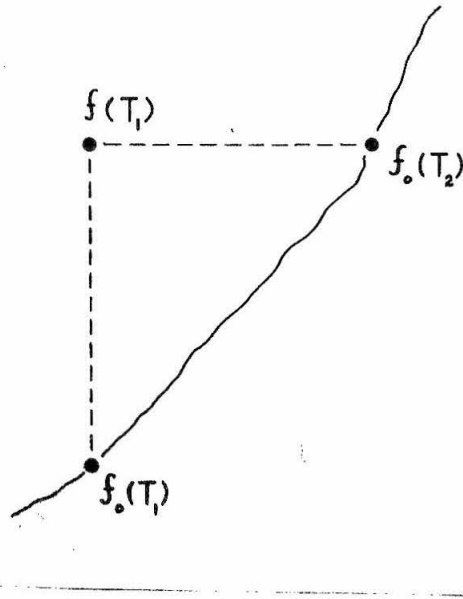


Figure 6.2. The standard deviations of t .

It can be shown that a maximum-likelihood estimate is normally distributed.⁴³ A peak position obtained with a matched filter is therefore normally distributed with standard deviation $(t_2 - t_1)/2$. Peak positions which are measured with resolution enhancement filters are not necessarily normally distributed, however the output from any linear filter will satisfy Eq. (6.3). Since an RC filter is linear, this provides a convenient error estimate for routine work.

7. APPLICATIONS

The filtering techniques discussed in this thesis are useful for improving the signal-to-noise ratio and the resolution of any spectrum where one or both present a problem. Although Fourier transform spectroscopy promises to provide additional sensitivity enhancement,⁴⁴ this new technique is not in competition with linear filtering. On the contrary, Fourier transform spectroscopy will make linear filters even easier to apply. One must simply multiply the spectrum by the frequency response function of the filter before taking the Fourier transform.

A set of instructions for the filtering program is included as Appendix A and a complete FORTRAN listing as Appendix B. We shall briefly discuss some experiments which were done with the intention of using this program, since they illustrate the kind of results one can expect.

7.1 Signal-to-Noise Enhancement

Dr. Robert L. Lichter has found the filtering program developed in this thesis useful for natural-abundance ¹⁵N studies of substituted hydrazines. Although the double section RC filter built into the spectrometer gives near optimum results, the extreme signal-to-noise problem inherent in natural-abundance ¹⁵N work justifies the use of a matched filter. The resonance from nitrogen-2 of 1,1-dimethyl hydrazine can be observed only after 1300 scans (Fig. 7.1.1).

The error bars constitute a valuable indication of the statistical significance of the peak. In general it would be desirable to obtain a better signal-to-noise ratio for the line shape than that shown in Fig. 7.1.1, however, the above spectra are quite acceptable.

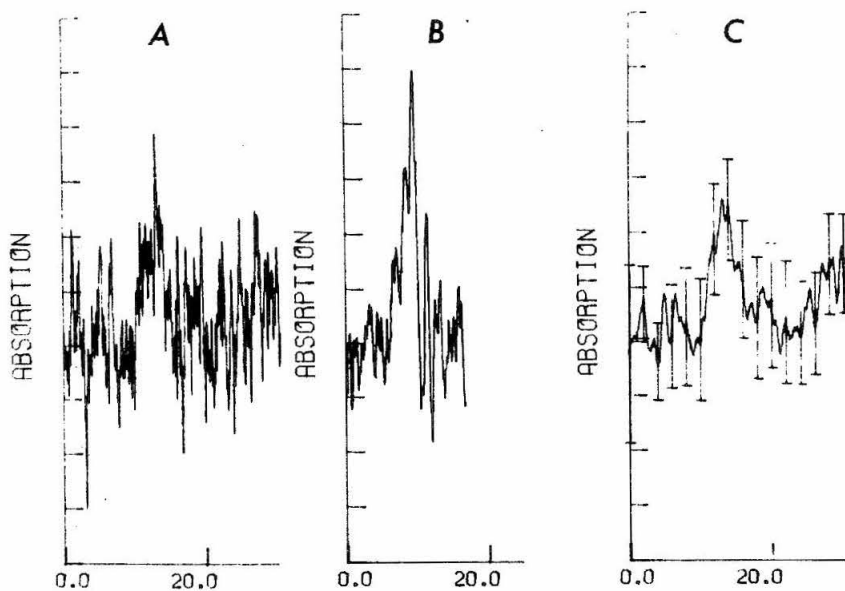


Figure 7.1.1. Natural-abundance ^{15}N spectrum showing the resonance from nitrogen-2 of 1, 1-dimethyl hydrazine, courtesy of Robert L. Lichter. Trace A is the experimental spectrum, B is the line shape (^{15}N enriched nitric acid), and C is the filtered spectrum.

7.2 Resolution Enhancement

Dr. Robert L. Lichter has measured the directly bonded (^{15}N , ^{13}C) spin-spin coupling in pyridine. Using a 98.9% ^{15}N labeled sample, he found the proton-decoupled ^{13}C spectrum of carbon-1 to be a singlet when the sweep rate was 1.0 Hz/sec (Fig. 7.2.1). Using a line shape from the cyclopentane solvent (Fig. 7.2.2), he was able to resolve this singlet into a doublet with a linear resolution enhancement filter (Fig. 7.2.3). The observed coupling was 0.45 ± 0.1 Hz. He then recorded the spectrum with a sweep rate of 0.1 Hz/sec and directly observed a coupling of 0.42 ± 0.05 Hz (Fig. 7.2.4).

In the above example we could verify the coupling measured with resolution enhancement by direct observation. If the coupling were smaller than the natural line width (or inhomogeneity in the magnetic field), direct observation would not be possible. However, it might still be possible to measure such a coupling using linear resolution enhancement filters. The spectra shown in Figs. 7.2.1 and 7.2.2 were recorded with the RC filter connected (frequency response setting = 5 Hz). This improved the signal-to-noise of the unfiltered spectra, and in this case did not interfere with the resolution enhancement. It would be a safer practice to disconnect the RC filter completely.

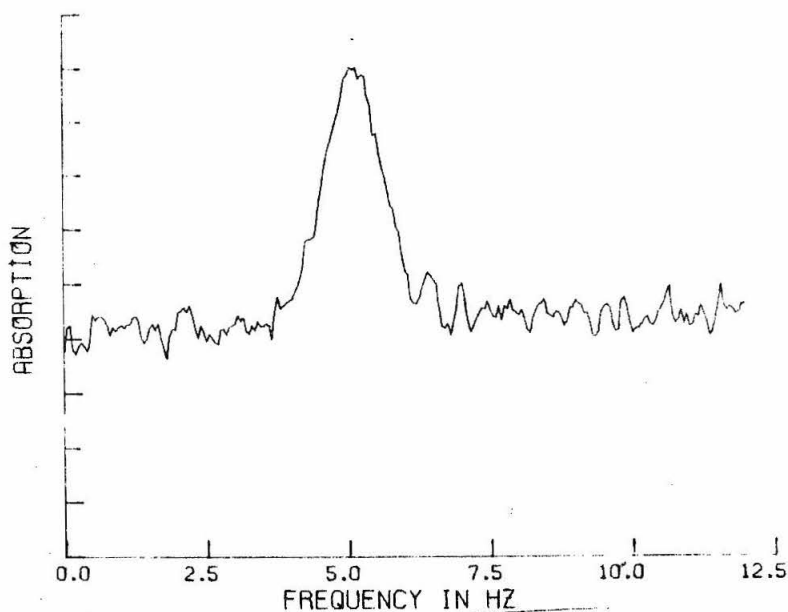


Fig. 7.2.1. The natural abundance ^{13}C spectrum from carbon-1 of ^{15}N labeled pyridine, courtesy of Robert L. Lichter ($\alpha = 1.0$ Hz/sec).

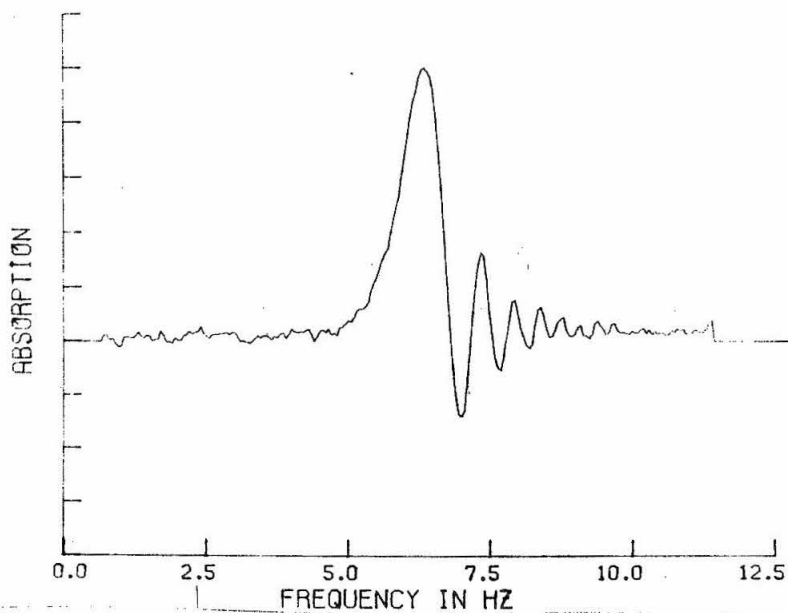


Fig. 7.2.2. The natural abundance ^{13}C spectrum of cyclopentane, courtesy of Robert L. Lichter ($\alpha = 1.0$ Hz/sec).

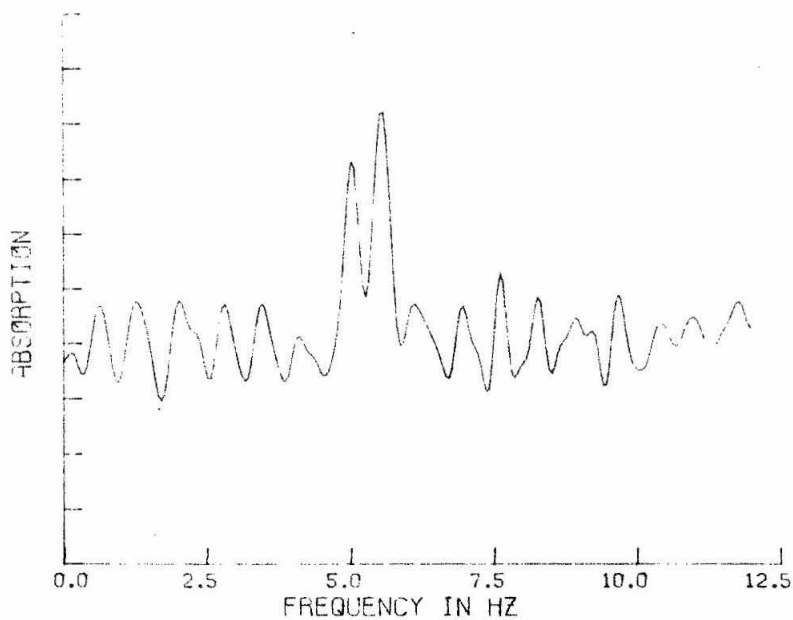


Fig. 7.2.3. The pyridine spectrum in Fig. 7.2.1 has been resolved with a linear resolution enhancement filter based upon the line shape in Fig. 7.2.2.



Fig. 7.2.4. The natural-abundance ^{13}C spectrum from carbon-1 of ^{15}N labeled pyridine, courtesy of Robert L. Lichter ($\alpha = 0.1 \text{ Hz/sec}$).

7.3 Filtering Satellite Peaks

The pseudo-linear filter given by Eq. (5.4.24) permits the observation of ^{13}C satellites which cannot be observed with conventional filters. We shall use the natural-abundance ^{13}C spectrum of 2,3-dimethyl-2-butene to illustrate this point. The proton decoupled spectrum of this molecule consists of two singlets from the vinyl and methyl carbons (Fig. 7.3.1). The methyl resonance was recorded with a reduced sweep rate (Fig. 7.3.2). This spectrum was then filtered with a double section RC filter, the time constant of which was varied in order to maximize the visibility of the ^{13}C satellites. Even with the optimum time constant the satellite peaks remain buried in the noise (Fig. 7.3.3). If, however, we use a pseudo-linear filter, the ^{13}C satellites resulting from the directly bonded coupling are clearly visible (Fig. 7.3.4). The pseudo-linear filter has taken full advantage of the symmetry in this "AX" system. For the rather modest resolution required to observe this coupling, the field drift indicated in this spectrum (Fig. 7.3.2) did not present any problems. We shall now demonstrate the kind of results which are possible in the absence of significant field drift.

The natural-abundance ^{13}C spectrum of trans-1,3-pentadiene (Fig. 7.3.5) provides examples of applications for several of the filters discussed above. Although the assignment of the methyl resonance is trivial, the assignment of the vinyl carbon resonances is quite difficult. The off-resonance decoupled ^{45}C spectrum (Fig. 7.3.6) indicates that the line at -46.9 ppm results from a carbon directly

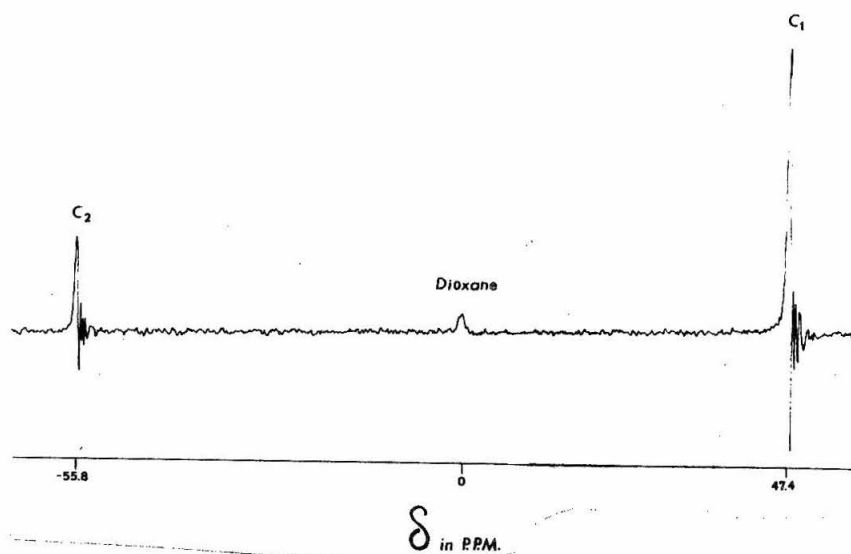


Fig. 7.3.1. The proton decoupled ^{13}C spectrum of 2,3-dimethyl-2-butene ($\alpha = 100$ Hz/sec).

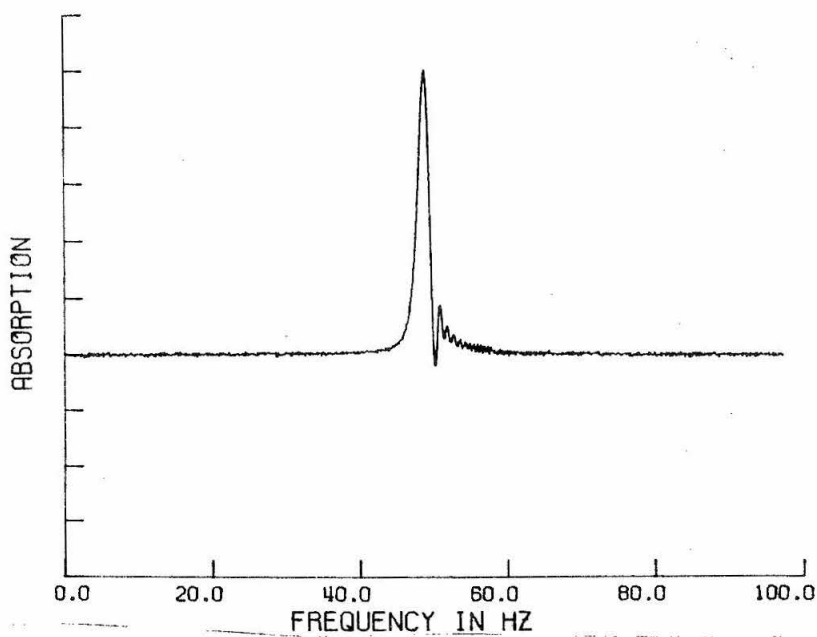


Fig. 7.3.2. The methyl ^{13}C resonance from 2,3-dimethyl-2-butene ($\alpha = 4$ Hz/sec). The spinning rate was 30 ± 2 Hz.

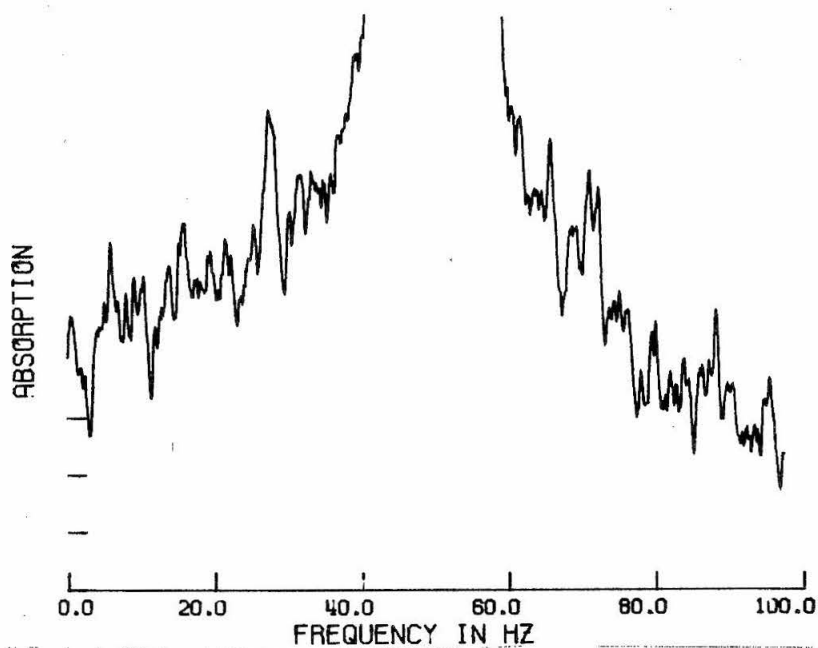


Fig. 7.3.3. The spectrum shown in Fig. 7.3.2 has been filtered with a double section RC filter and the vertical scale has been attenuated by a factor of 100.

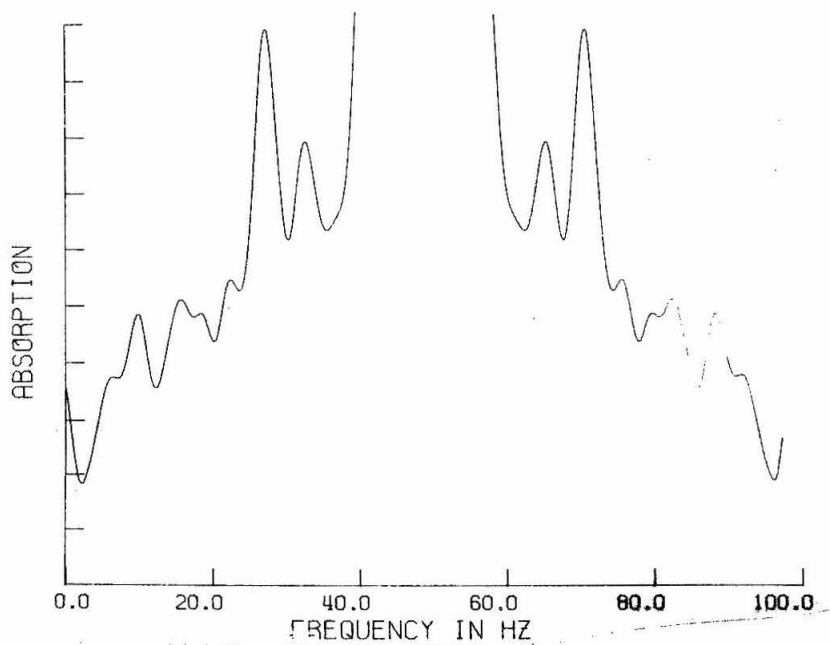


Fig. 7.3.4. The spectrum shown in Fig. 7.3.2 has been filtered with a pseudo-linear filter [Eq. (5.4.24)].
 $J = 43.9 \pm 1$ Hz.

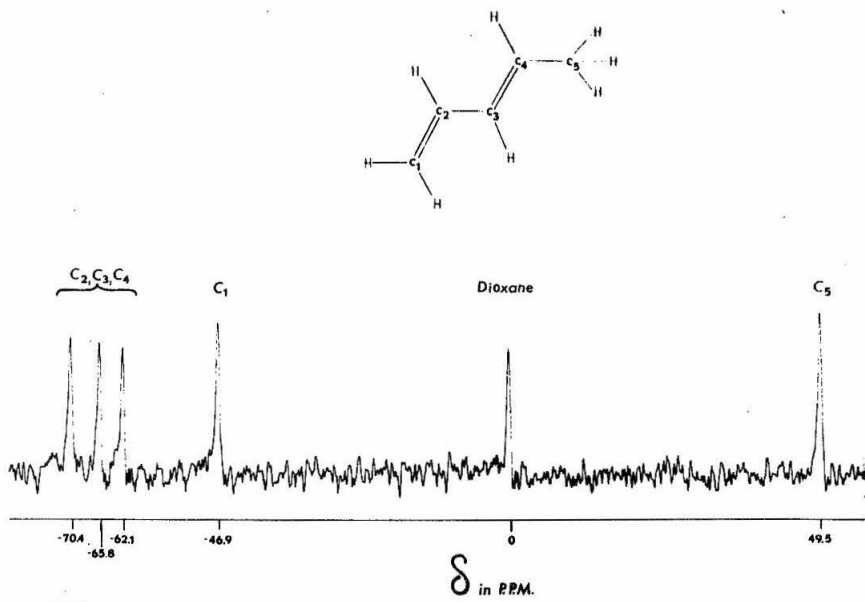


Fig. 7.3.5. The noise decoupled natural-abundance ^{13}C spectrum of *trans*-1,3-pentadiene.

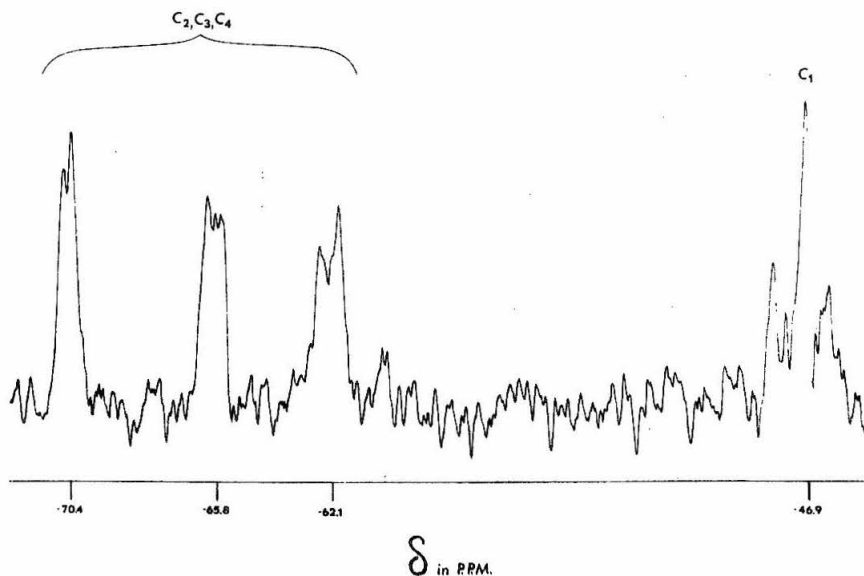


Fig. 7.3.6. The off-resonance decoupled spectrum of the vinyl carbons of *trans*-1,3-pentadiene.

bonded to two protons, hence this line results from carbon-1. The resonance from carbon-1 was then recorded at a reduced sweep rate (Fig. 7.3.7). This high resolution spectrum was used to observe the ^{13}C satellites.

A small portion of the spectrum (Fig. 7.3.8) was used to calculate the weighting function for a pseudo-linear resolution enhancement filter. This made the filter pseudo-linear only in the region immediately surrounding the parent peak and linear everywhere else. The asymmetry of the directly bonded (^{13}C , ^{13}C) spin-spin coupling satellites could therefore be measured (Fig. 7.3.9). The observed values of J_+ and J_- were 31.1 ± 1.0 Hz and -38.8 ± 0.7 Hz, respectively. Substituting these values in Eq. (5.5.10) one calculates that the chemical shift of carbon-2 relative to dioxane is -68.0 ± 3 ppm. The directly observed chemical shift of carbon-2 relative to dioxane is therefore either -70.4 ± 0.1 ppm or -65.8 ± 0.1 ppm (Fig. 7.3.6), since both of these peaks fall within the calculated interval. The analysis of this spectrum could be completed by scanning the region surrounding these peaks.

In addition to the large directly bonded coupling, Fig. 7.3.9 also indicates the presence of a smaller coupling ($J = 9.8 \pm 0.6$ Hz). In order to demonstrate that these peaks represent real and reproducible satellites, a slow sweep rate spectrum was recorded (Fig. 7.3.10). This spectrum was then filtered with a least-squares satellite filter (Sec. 5.3). The resulting filtered spectrum (Fig. 7.3.11) clearly indicates the presence of a long range spin-spin

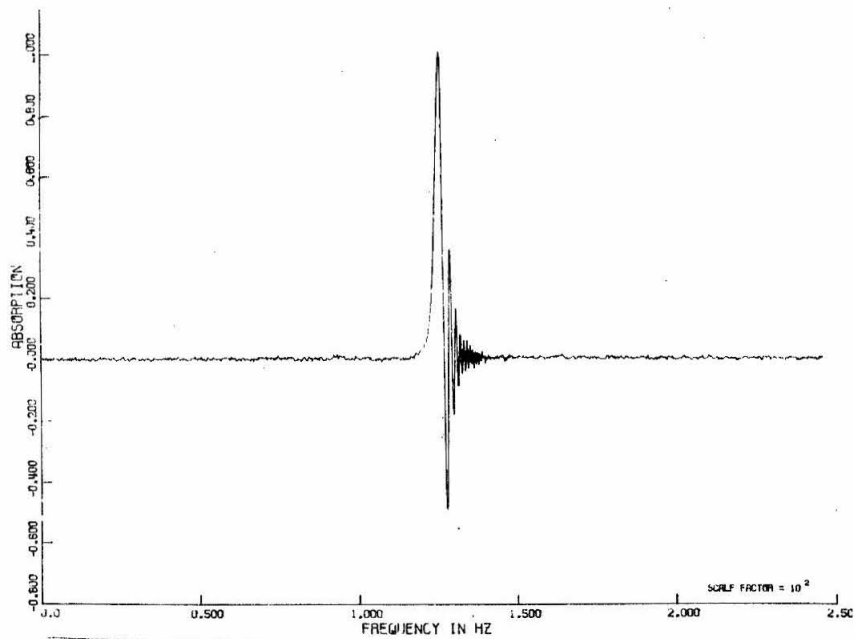


Fig. 7.3.7. The natural-abundance ^{13}C spectrum from carbon-1 of trans-1,3-pentadiene ($\alpha = 10 \text{ Hz/sec}$). The spinning rate was $15 \pm 5 \text{ Hz}$.

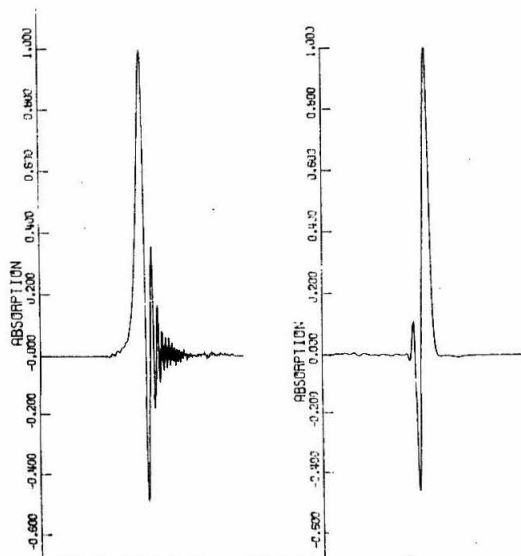


Fig. 7.3.8. The line shape (left) and weighting function (right) used to filter the spectrum in Fig. 7.3.7.

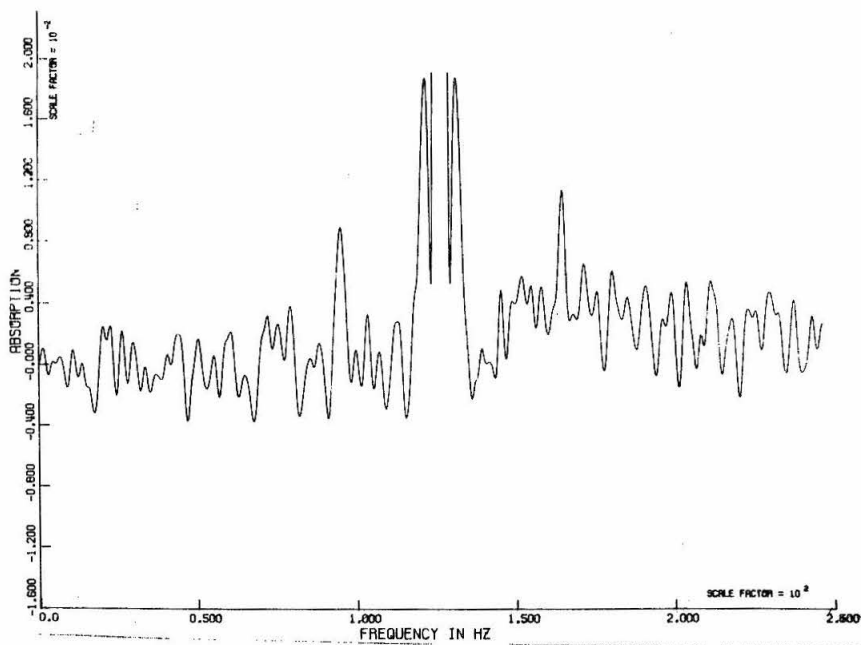


Fig. 7.3.9. The spectrum in Fig. 7.3.7 has been filtered with the weighting function shown in Fig. 7.3.8.

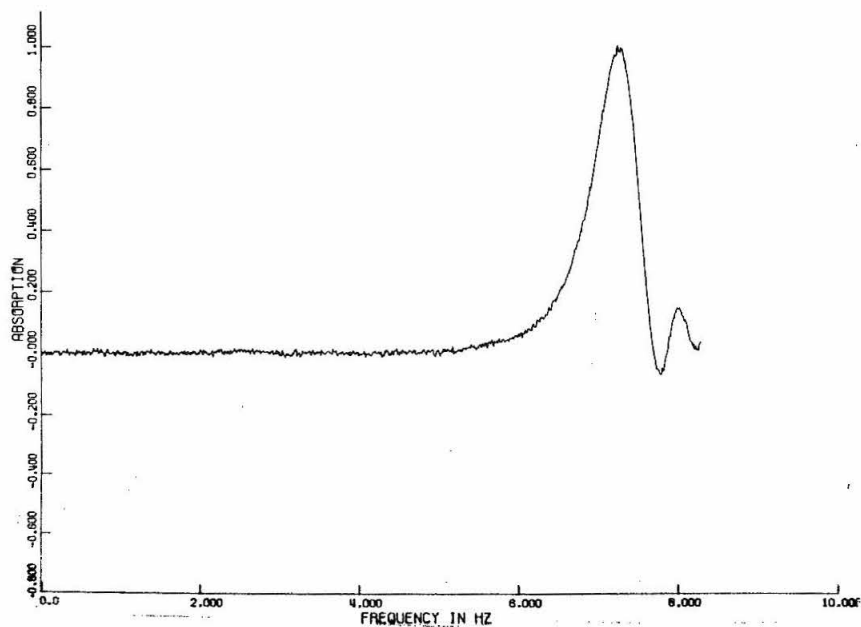


Fig. 7.3.10. The natural-abundance ^{13}C spectrum from carbon-1 of trans-1,3-pentadiene ($\alpha = 0.4$ Hz/sec). The spinning rate was 15 ± 5 Hz.

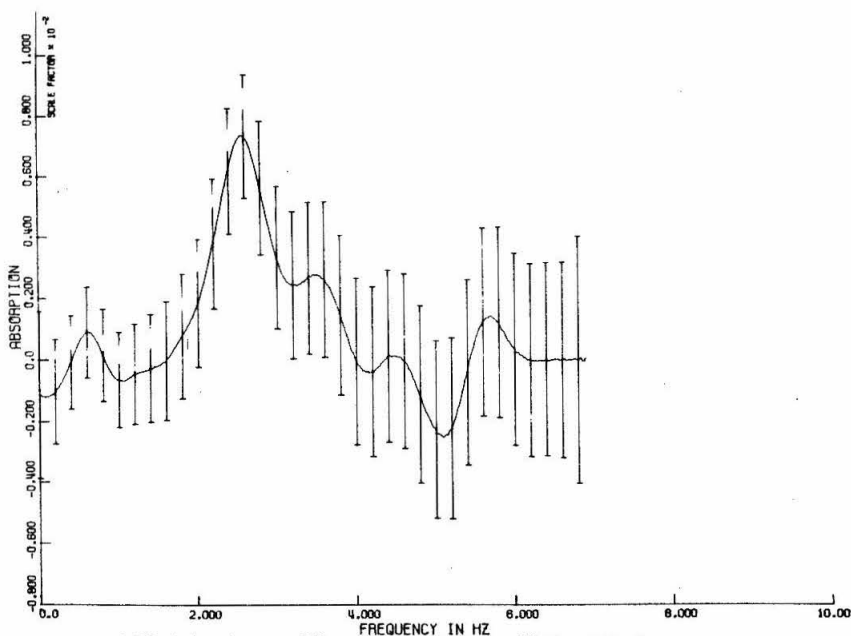


Fig. 7.3.11. The spectrum shown in Fig. 7.3.10 has been filtered with a least-squares satellite filter.

coupling of 9.5 ± 0.3 Hz. The origin of this satellite is not important for our present interests. The significant point is that the satellite is consistently observed.

The directly bonded (^{13}C , ^{13}C) spin-spin couplings we have measured are consistent with the general trend of the variation of these couplings with the percent S hybridization (Fig. 7.3.12). If we base our prediction on the observed coupling in ethylene, the measured values are smaller than the predicted ones for small percent S and larger for large percent S. This has been rationalized in terms of the contraction of the carbon S orbitals as the multiplicity of the bonding increases.⁴⁶

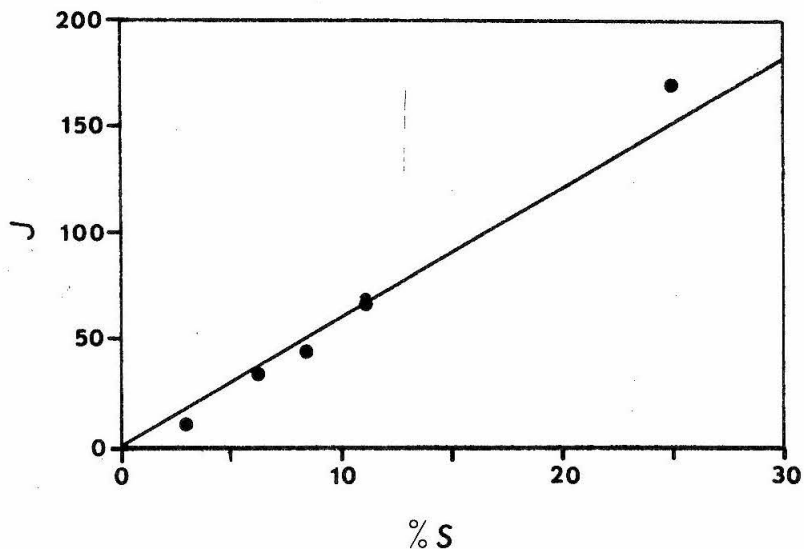


Fig. 7.3.12. Directly bonded (^{13}C , ^{13}C) spin-spin couplings as a function of the product of the S character at the two centers. In order of increasing coupling constant, the experimental values represent cyclopropane,⁴⁷ ethane,⁴⁸ tetramethyl ethylene, ethylene,⁴⁸ pentadiene, and acetylene.⁴⁸

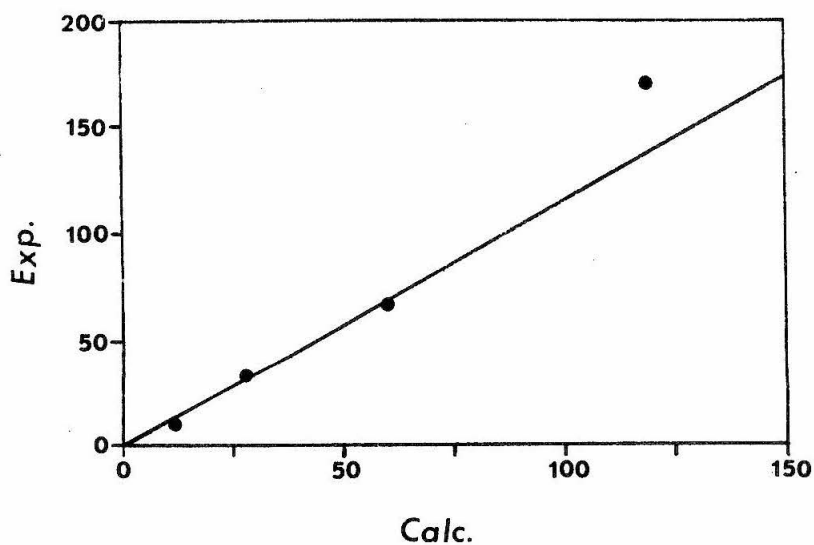


Fig. 7.3.13. Directly bonded (^{13}C , ^{13}C) spin-spin couplings as a function of the values calculated by extended Hückel theory.

If we compare the experimental spin-spin couplings with those obtained from extended Hückel theory (see Appendix C), the general behavior is unchanged (Fig. 7.3.13). It would seem reasonable to use the calculated spin-spin couplings to select more realistic exponents for the 2S orbitals of extended Hückel calculations. These calculations should then give a better description of the effects of hybridization.

8. EXPERIMENTAL

The 2, 3-dimethyl-2-butene was purchased from Aldrich Chemical Co., and the trans-1, 3-pentadiene from Matheson Coleman and Bell. These samples were then sealed in 10-mm n. m. r. tubes.

The ^{13}C and ^{15}N spectra were determined with the DFS-60 spectrometer discussed by Weigert and Roberts,⁴⁹ and the proton spectra were determined with a Varian Associates A-56/60 spectrometer. The spectra were accumulated on a Varian C-1024 computer and later transferred to cards with a Varian C-1001 coupler interface to an I. B. M. 526 printing summary punch. The data were then processed using the program SNARE on an I. B. M. 360/75 computer.

The spinning rates of the sample tubes were measured with a General Radio Co. model 631-B Strobotac which had been calibrated using the spinning side bands from the A-56/60 spectrometer.

Finally, we note that our experimental spectra were really filtered. A completely unfiltered spectrum, $f_i(t)$, would have zero signal-to-noise ratio, because the measurement at each frequency must be accomplished in zero time. All n. m. r. spectrometers involve an approximation of the form:

$$f_i(t) \doteq \int_{-T/2}^{T/2} h(\tau) f_i(t - \tau) d\tau. \quad (8.1)$$

If T is much smaller than the narrowest "wiggle" in the spectrum, this will have negligible effect on the line shape.⁵⁰ A digital sweep

spectrometer generally uses a weighting function which is constant. That is, it simply takes the average of the measured signal over a small frequency range, $\Delta\nu$, and uses this for a data point. Continuous sweep spectrometers generally use an RC filter. If we had used it, the recording device on the spectrometer would have introduced additional filtering depending upon the response time of the pen. The exact form of $h(\tau)$ is unimportant, provided that T is sufficiently small (Sec. 2.7). We are not faced with the question of whether or not a spectrum should be filtered, but rather how it should be filtered.

APPENDIX A

USING THE PROGRAM SNARE

If one knows the line shape of an n. m. r. signal, it is possible to distinguish between one or more absorption lines and random noise. Given the line shape of a nuclear magnetic resonance signal as input, the program SNARE will remove most of the random noise in a spectrum or reduce the width of the lines, depending upon the options specified. In these instructions we shall not attempt to discuss the theory of filtering n. m. r. spectra, but limit ourselves to the use of the filtering program SNARE. We strongly recommend that the user of SNARE become moderately acquainted with the theory of filtering so that he may use the program to maximum advantage and avoid incorrect interpretation of the results. We shall begin by describing the types of filtering available with SNARE.

Signal-to-Noise Enhancement

The filter which gives the maximum signal-to-noise ratio for a given spectrum is called a matched filter. SNARE provides a matched filter as one option. The signal-to-noise ratio of a multiple-scan n. m. r. experiment can be further improved by increasing the sweep rate. The maximum signal-to-noise ratio available for measuring the position of a single line is obtained by using the fastest sweep rate available (i. e., with due consideration for the relaxation times of the nuclei and instrument limitations). The dependence of the signal-to-noise ratio upon the experimental parameters is approximately:

$$S/N = k(\text{sweep rate})^{\frac{1}{4}} (\text{sweep width})^{-\frac{1}{2}}.$$

One should therefore use the fastest sweep rate and the smallest sweep width which is practical. However, one should also keep in mind that increasing the sweep rate will increase the line width, although this does not necessarily decrease the accuracy with which the position of a line can be measured.

A matched filter requires an independent measurement of the line shape.

Resolution Enhancement for Lines of Comparable Magnitude

The program SNARE includes an optimum linear resolution enhancement filter. The capabilities of this filter are indicated in Fig. 1. These filters "trade off" signal-to-noise for resolution. Decreasing the sweep rate will also trade signal-to-noise for resolution. The optimum procedure is to combine the two as

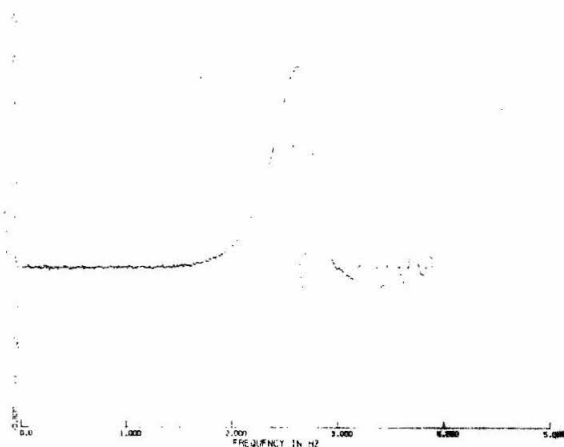


Figure 1. Resolution enhancement of an n. m. r. signal. The large peak and its "wiggles" are an unresolved doublet. The two smaller peaks are the same doublet after resolution enhancement ($q = 3000$).

indicated in Fig. 2. The curve which intersects all the points represents the result of varying the sweep rate and using a matched filter. The curves which intersect only one point represent the effect of using a linear resolution enhancement filter and the indicated sweep rate. The point labeled 0.1 should be interpreted as the minimum sweep rate for which the first downward "wiggle" goes below zero. The numerical value of the sweep rate at which this occurs will depend upon the sample used. The optimum process varies the sweep rate and uses a linear resolution enhancement filter. This gives the maximum signal-to-noise for a given line width and is represented by the envelope of the curves in Fig. 2. To use this optimum process one preselects the sweep rate and resolution enhancement filter such that one obtains the desired line width after resolution enhancement, and the signal-to-noise ratio is a maximum for this line width.

We shall illustrate the use of this optimum process with an example. Let us assume that we wish to measure the separation between two closely spaced lines (approximately 0.5 Hz separation) of a natural abundance ^{13}C spectrum. We therefore decide that ν_0 should be 0.2 Hz in order to provide adequate resolution. We find that the minimum sweep rate for which the first downward "wiggle" for a sample of CS_2 crosses zero is 0.05 Hz/sec, and that the matched filter line width for this sweep rate is 0.27 Hz. We then modify Fig. 2 as indicated in Fig. 2a and find the point on the horizontal scale corresponding to 0.2 Hz. We see from Fig. 2a that we will

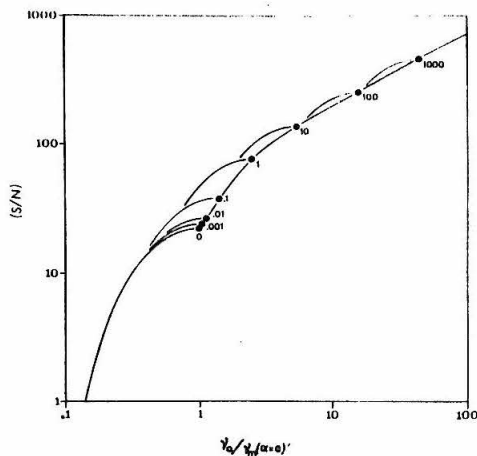


Figure 2. Resolution enhancement in which we vary both the sweep rate, α , and the filter. The output line width is ν_0 and the line width resulting from a matched filter is ν_m . The numbers at the points indicate the sweep rate in Hz. This curve was obtained from several CHCl_3 spectra with the exception of the point $\alpha = 0$, which was obtained from the asymptotic form.

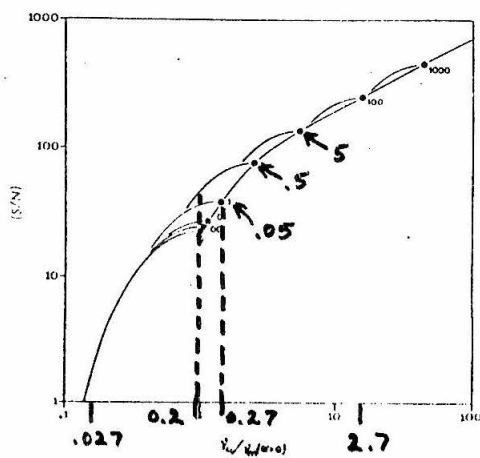


Figure 2a. The use of Fig. 2 to select the sweep rate for an n. m. r. experiment.

obtain the maximum output signal-to-noise by using the following procedure: first collect data using a sweep rate of 0.5 Hz/sec, then use a linear resolution enhancement filter to reduce the line width to 0.2 Hz.

Several filters are compared in Fig. 3. The optimum linear filter discussed above gives the highest signal-to-noise ratio for a given line width of any filter presenting known. The instrument RC filter is clearly adequate for routine work. The curve representing this filter may be somewhat optimistic, however, because it assumes that the optimum time constant was used at each sweep rate. This is not generally done in practice. If either signal-to-noise or resolution is a problem, one should use the optimum linear filter. If one wishes to resolve lines differing in amplitude by more than a factor of five, a pseudo-linear filter, which is described in the next section, should be used.

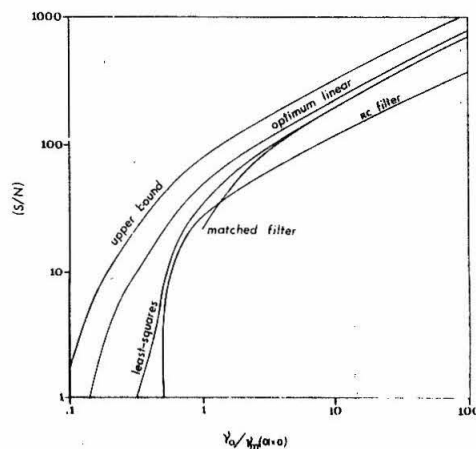


Figure 3. Resolution enhancement by various methods in which the sweep rate is varied.

A linear resolution enhancement filter requires an independent measurement of the line shape.

Pseudo-Linear Filters

These filters are similar to linear filters except the spectrum itself is used for the line shape. They produce a symmetric output spectrum regardless of the nature of the input spectrum. If a pair of satellites are not symmetric about the parent peak, the output spectrum will contain four satellites (Fig. 4). If the satellites are

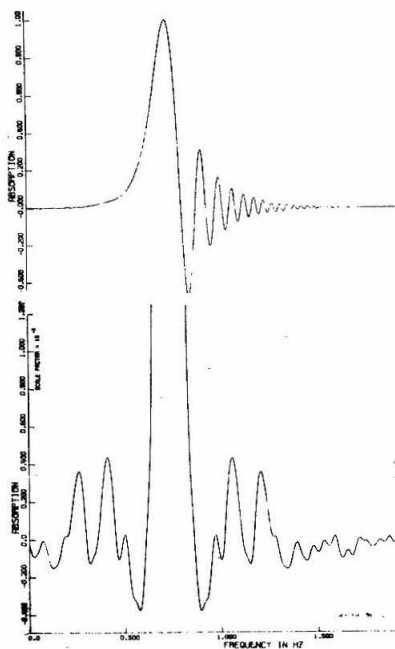


Figure 4. The proton resonance of CHCl_3 ($\alpha = 2.5$) with satellites added ($J_+ = 4.75$ Hz, $J_- = -3.29$ Hz). The frequencies are scaled by a factor of 10. Note that the upfield satellite is easily resolved even though it is completely buried in the "wiggles" before filtering.

symmetric in the input spectrum, their intensity will be doubled in the filtered spectrum.

Pseudo-linear filters are the most powerful presently known for resolving satellite peaks which are close to the parent peak. They should not be used to resolve lines which differ in amplitude by less than a factor of five.

If one wishes to determine whether the closer or farther satellite, of those on one side of the parent peak, is actually to the left of the parent peak, the least-squares satellite filter described in the next section can be used.

Filtering Satellite Peaks with Least-Squares Filters

The usefulness of these filters is described in the preceding section. This procedure approximates the parent peak by the Lorentzian asymptotic form (Fig. 5). The parameters in the Lorentzian are determined by performing a least-squares fit up to the point where the parent peak reaches "FIT" (a fraction which should be set between 0.05 and 0.5) of its maximum value. The resulting least-squares function $f(t, b)$ is then subtracted from the input spectrum $f_1(t)$, leaving the satellite spectrum $f_1(t)$ (Fig. 6).

The position of the satellite can be estimated from $f_1(t)$. This estimate is then used as data ("SEPRTE") for the second iteration. This second iteration should remove the distortion in $f_1(t)$ indicated in Fig. 6, and produce a new spectrum, $f_2(t)$ with a maximum in the correct position (Fig. 7).

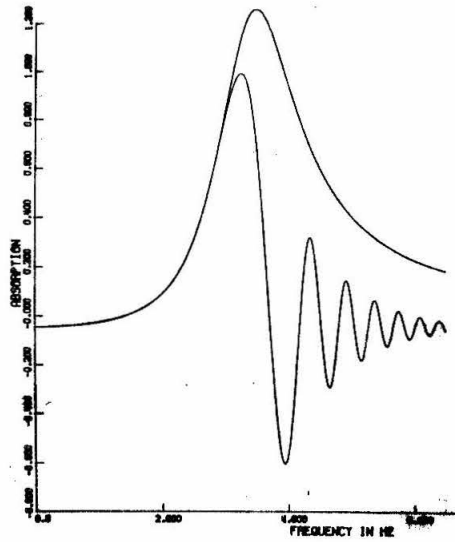


Figure 5. The least-squares fit of the proton resonance of CHCl_3 ($\alpha = 1.0$) using a Lorentzian line shape function.

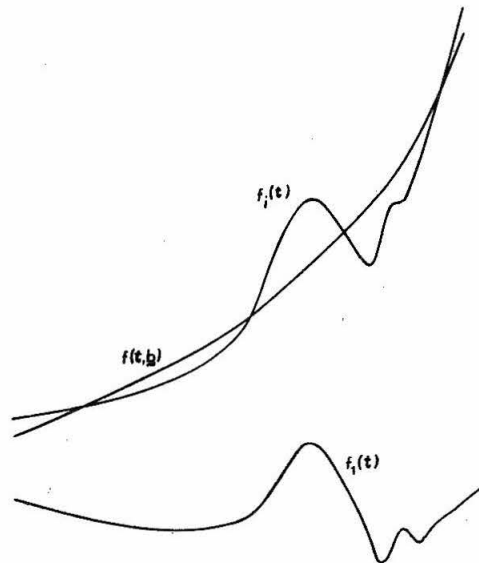


Figure 6. The line shape of the satellite peak is distorted by removing the parent peak.

The sum of the squares of the residues from the least-squares fit, ϕ , should decrease by about $0.25 E_s$ (the output parameter E_s is a convenient normalization for ϕ) during the second iteration (Fig. 7). If ϕ increases, the estimated position of the satellite was incorrect. This procedure should converge after two iterations.

The "wiggles" in the line shape must be to the right when the least-squares fit is performed. This is accomplished with the input parameter "NRFLCT".

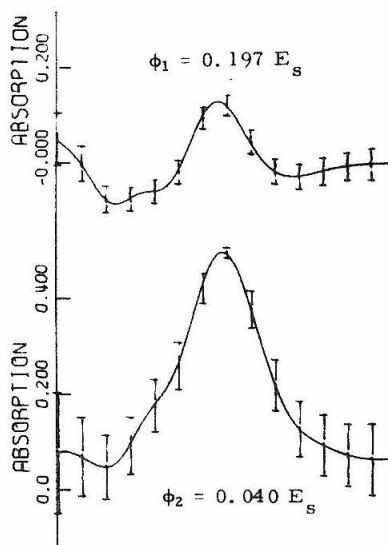


Figure 7. The functions $f_1(t)$ (top) and $f_2(t)$ (bottom) [Eqs. (5.3.1) and (5.3.3)] resulting from the above CHCl_3 spectrum. A matched filter has been used and the scale is such that $f_1(\delta) = 100$. The error bars represent one standard deviation

Data Collection

All spectra must be taken with the instrument RC filter disconnected. This can be accomplished by setting the "function" switch of the DFS-60 spectrometer to "scope" or the "filter bandwidth" of the A-60 spectrometer to "4 cps". If the instrument RC filter is not disconnected, the noise in the spectrum will not be white, and using SNARE to filter spectra will not be valid.

If the line shape is determined separately, it is critical that all experimental parameters (sweep time, sweep width, phase, rf field strength, etc.) be as nearly identical to those for the spectrum as is possible. In order to accomplish this one should alternately scan the sample and the line-shape standard.

Considerable computing time can be saved by using only the portion of the line shape which differs significantly from zero.

The number of data sets to be added to form a spectrum, "NSTITL", can be arbitrarily large. Each data set must be properly "rolled over". Any data set in which one of the peaks is truncated is useless. To add m data sets, simply set "NSTITL" equal to m , place a card giving "NPOINT" and "NALIGN" in front of each data set, and place the data sets in the input data deck. The data set with the largest peak farthest to the left must be placed first. Two data sets should not be added unless the same setting of the "gain control" was used for both.

The Program

The current version of SNARE will cost between \$1 and \$5 per spectrum depending upon the options specified.

The program can select a portion of the input spectrum, $FI(T)$, to use for the line shape, $S(T)$. This will be convenient if the standard line shape sample and the spectrum were scanned simultaneously. To use this option, set "NSIG" equal to zero and set "FIT" slightly larger than $(S/N)^{-1}$. The program will then find the largest peak in $FI(T)$ and use a segment of $FI(T)$ which includes this peak for the line shape $S(T)$. For absolute control of the segment used for the line shape-duplicate the cards representing this segment and submit them as a separate signal shape. Regardless of how the line shape is measured, the signal-to-noise ratio for the line shape must be better (by at least a factor of two) than that for the signal.

The functions $F(T)$, $H(T)$, and $FO(T)$ are the least-squares Lorentzian, the weighting function and the output spectrum, respectively. The weighting function is calculated from $S(T)$ and is of interest when considering the theory of filtering. A complete list of the input parameters is given on the next two pages.

It is assumed that the data has been punched on cards in format (8X, 12Ø6), and that there is a maximum of 1024 data points per scan.

DATA		SNAR0016
		SNAR0014
		SNAR0018
CARD 1.....NSPECT(15)	THE NUMBER OF INDEPENDENT SPECTRAL PROBLEMS TO BE CONSIDERED. THE DATA CARDS FOR EACH PROBLEM ARE PREFACED HERE BY A0,A1,....ETC.	SNAR0010
CARD A0....DSCRPT(2044)	TITLE FOR THE PRINTED OUTPUT.	SNAR
CARD A1....TITLE(46)	TITLE FOR THE PLOTS.	SNAR001F
	NSWEEP(15) NUMBER OF POINTS EQUIVALENT TO THE SWEEP WIDTH. THIS WILL GENERALLY BE 1024 FOR SPECTRA FROM THE A-60 AND 999 FOR SPECTRA FROM THE DFS-60.	SNAR001E
	NSTITL(15) NUMBER OF SPECTRA TO BE ADDED AS 'A', SEE SEPARATE INSTRUCTIONS AS TO DATA COLLECTION.	SNAR001H
	1PSDL(12) = 0 PSEUDO-LINEAR FILTER	SNAR0011
	= 1 LINEAR OR LEAST-SQUARES FILTER	SNAR002E
	NSIG(13) = -1 REMOVE PARENT PEAK	SNAR002A
	= 0 SIGNAL SHAPE IN SPECTRUM	SNAR0024
	= +1 SIGNAL SHAPE SEPARATE.	SNAR002C
	NREFLCT(15) = -1 NO REFLECTIONS-USE FOR DOWNFIELD SPECTRA FROM A-60 AND DFS-60.	SNAR002D
	= 0 TWO REFLECTIONS-USE FOR DOWNFIELD SPECTRA FROM 6-60.	SNAR002E
	= +1 ONE REFLECTION -USE FOR DOWNFIELD SPECTRA FROM DFS-60.	SNAR0024
	NSTON(15) SIGNAL TO NOISE .GT.1 OPTIMUM RESOLUTION ENHANCEMENT FILTER -SEE SNAR	SNAR003E
	NSTON EQUAL TO TEN	SNAR003A
	TIMES THE LOSS IN	SNAR003B
	SIGNAL TO NOISE THAT	SNAR003C
	YOU THINK YOU CAN	SNAR003D
	AFFORD.	SNAR003F
	1 MATCHED FILTER - NO	SNAR003F
	ERROR BARS.	SNAR003G
	0 MATCHED FILTER - ERROR	SNAR003H
	BARS.	SNAR003I
	= -1 RC FILTER	SNAR004E
	SET NSTON EQUAL TO	SNAR004A
	-100*(THE HALF WIDTH	SNAR004B
	AT HALF HEIGHT OF THE	SNAR004C
	NARROWEST LINE) FOR THE	SNAR004D
	OPTIMUM TIME CONSTANT	SNAR004E
	FOR THE DOUBLE SECTION	SNAR004F
	RC FILTER.	SNAR004G
	SWEEP(F11.5) SWEEP WIDTH IN HZ. A POSITIVE NUMBER WHICH CORRESPONDS TO NSWEEP.	SNAR004H
	FIT(F11.5) THE FRACTION OF THE INTENSITY OF THE PARENT PEAK TO WHICH FITTING IS PERFORMED IN THE REMOVAL OPERATION. -OR- THE PARAMETER WHICH DETERMINES THE SIZE OF THE SEGMENT USED FOR THE LINE SHAPE WHEN NSIG=0.	SNAR004I
	YSCALE(F11.5) A SCALING FACTOR FOR THE FILTERED SPECTRUM. YSCALE TIMES THE SCALE FOR THE ORIGINAL SPECTRUM IS THE SCALE OF THE FILTERED SPECTRUM.	SNAR005A
	IF YSCALE .LE.0, YSCALE IS	SNAR005F
	CALCULATED TO FIT THE FILTERED SPECTRUM ON THE PLOTTING PAPER AND THE SCALE IS	SNAR005G
	PRINTED.	SNAR005H
	ABNDNC(F7.5) THE FRACTIONAL NATURAL ABUNDANCE OF THE NUCLEUS RESPONSIBLE FOR THE SATELLITE.	SNAR005I
	SEPRTE(F11.9) DISTANCE IN HERTZ BETWEEN THE SATELLITE PEAK AND THE PARENT PEAK. SET TO 0. IF UNKNOWN.	SNAR
		SNAR
		SNAR
CARD A7....IFPLOT(1)(13)	= 0 DO NOT PLOT THE LEAST-SQUARES DETERMINED LORENTZIAN.	SNAR006A
	= 1 PLOT THE LEAST-SQUARES FUNCTION.	SNAR006B
	IFPLOT(2)(13) = 0 DO NOT PLOT F(I).	SNAR006C
	= 1 PLOT F(I).	SNAR006E
	= 2 PLOT AND LABEL F(I).	SNAR006G
	IFPLOT(3)(13) = 0 DO NOT PLOT S(I).	SNAR006H
	= 1 PLOT S(I).	SNAR006I
	= 2 PLOT AND LABEL S(I).	SNAR007E
	IFPLOT(4)(13) = 0 DO NOT PLOT H(I).	SNAR007A
	= 1 PLOT H(I).	SNAR007H
	= 2 PLOT AND LABEL H(I).	SNAR007C
	IFPLOT(5)(13) = 0 DO NOT PLOT F(I)-F(I).	SNAR007D
	= 1 PLOT F(I)-F(I).	SNAR007E
	= 2 PLOT AND LABEL F(I)-F(I).	SNAR007F
	IFPLOT(6)(13) = 0 DO NOT PLOT FO(I).	SNAR007G
	= 1 PLOT FO(I).	SNAR007H
	= 2 PLOT AND LABEL FO(I).	SNAR007I
	XLNGTH(F7.2) THE LENGTH OF THE X-AXIS IN INCHES.	SNAR008E
	YLNGTH(F7.2) THE LENGTH OF THE Y-AXIS IN INCHES.	SNAR008A
CARD A3K...NPOINT(15)	THE NUMBER OF DATA POINTS IN THIS SCAN. THERE ARE A TOTAL OF NSTITL SCANS TO BE PROCESSED AS 'A', EACH OF WHICH IS PRECEDED BY A CARD A3K. NPOINT WILL BE LESS THAN NSWEEP IF ANY PART OF THE SPECTRUM IS ARBITRARILY OMITTED OR OMITTED BECAUSE OF NOISE, SPIKES, ETC.	SNAR008B
	NALIGN(15) THE NUMBER OF POINTS TO THE LEFT THIS SCAN IS TO BE SHIFTED. THE SCAN WHOSE MAXIMUM IS FARTHEST TO THE LEFT MUST BE READ IN FIRST.	SNAR008C
	NALIGN = 0 NO SHIFT OR FIRST SCAN.	SNAR008D
	USE A POSITIVE VALUE FOR NALIGN WHEN THERE IS AMBIGUITY ABOUT WHICH PEAKS SHOULD BE ALIGNED.	SNAR008E
	NALIGN .LE.-1 THE MAXIMA WILL BE LINED UP.	SNAR008F
	CARDS (A4K)...A(NPOINT/12)K....DATA POINTS (IX,120)K	SNAR008H
	THE FOLLOWING CARDS ARE USED ONLY IF NSIG = +1.	SNAR008I
	CARD A3K'...NSPOINT(15) THE NUMBER OF DATA POINTS IN THE SIGNAL SHAPE.	SNAR009E
	CARDS (A4K')...A(NSPOINT/12)K'....SIGNAL SHAPE DATA POINTS (IX,120)K.	SNAR009A
		SNAR009K
		SNAR009C
		SNAR009D
		SNAR009E
		SNAR009F
		SNAR009G

SNARE is currently on a disc library as JDR.NMRFLTR.

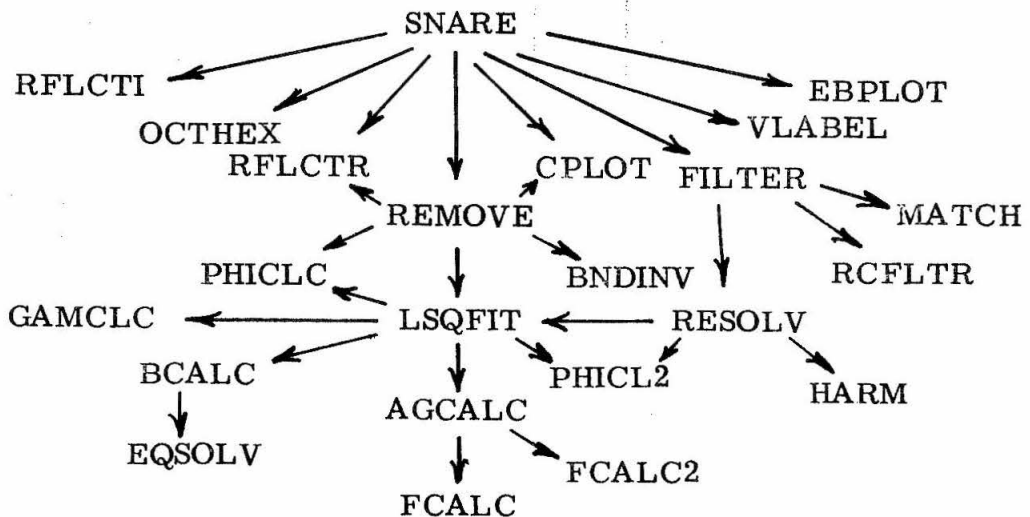
The necessary Job Control Language cards and sample data cards are shown below:

```
//      JOB (98532,GAP,CH),'GEORGE A. PETERSSON',MSGLEVEL=1
//      EXEC PGM=SNARE,REGION=150K,TIME=1
//STEPLIB DD DSN=JDR.NMRFLTR,VOL=SER=CITSC2,UNIT=SYSDA,DISP=SHR
//FT06F001 DD SYSOUT=A,DCB=(RECFM=FBSA,LRECL=133,BLKSIZE=1596)
//SYSPLTDM DD SYSOUT=N,UNIT=(,SEP=FT06F001)
//FT05F001 DD *
1
TRANS-1,3-PENTADIENE   CARBON-1   3710 SCANS
6A-F 999   6 0 0   -1   8 250.0   0.05   0.02   0.01
1 2 2 2 2 2 12.50 10.00
998 0
```

Data from C. A. T.

These are the only cards necessary to use SNARE.

The subroutine structure of SNARE is as follows:



APPENDIX B

A LISTING OF THE PROGRAM SNARE

```

-----SNARE-----SNAR000A
C-----SNARE-----SNAR
C-----SNARE-----SNAR000A
C THIS PROGRAM PERFORMS A VARIETY OF FILTERING OPERATIONS ON SNAR000H
C NMR SPECTRA. THE DETAILS ARE DESCRIBED IN THE PHD THESIS OF SNAR000C
C G.A.PETERSSON, CALIFORNIA INSTITUTE OF TECHNOLOGY (1970). SNAR000D
C THE PROGRAM CALLS THE FOLLOWING PLOTTING SUBROUTINES: SNAR000F
C CPLLOT: X,Y PLOTTING ROUTINE SNAR000F
C EBLOT: PLOTS ERROR BARS SNAR000F
C VLABEL: LABELS THE AXES OF PLOTS. SNAR000H
C THESE SUBROUTINES ARE NOT INCLUDED IN THIS PROGRAM. SNAR000I
C-----SNARE-----SNAR000I
C DATA SNAR001A
C SNAR001A
C SNAR001A
C CARD 1.....NSPECT(15) THE NUMBER OF INDEPENDENT SPECTRAL PROBLEMS SNAR001C
C TO BE CONSIDERED. THE DATA CARDS FOR EACH SNAR
C PROBLEM ARE PREFACED HERE BY A0,A1,....,ETC. SNAR
C CARD A0.....OSCRPT(20A4) TITLE FOR THE PRINTED OUTPUT. SNAR001F
C CARD A1.....TITLE(A4) TITLE FOR THE PLOTS. SNAR001F
C NSWEEP(15) NUMBER OF POINTS EQUIVALENT TO THE SWEEP SNAR
C WIDTH. THIS WILL GENERALLY BE 1024 FOR SNAR
C SPECTRA FROM THE A-60 AND 999 FOR SPECTRA SNAR
C FROM THE DFS-60. SNAR
C NSTITL(15) NUMBER OF SPECTRA TO BE ADDED AS 'A'. SEE SNAR001H
C SEPARATE INSTRUCTIONS AS TO DATA COLLECTION. SNAR
C IPSDL(I2) = 0 PSEUDO-LINEAR FILTER SNAR001I
C .NE.0 LINEAR OR LEAST-SQUARES FILTER SNAR002E
C NSIG(I3) =-1 REMOVE PARENT PEAK SNAR002A
C 0 SIGNAL SHAPE IN SPECTRUM SNAR002B
C +1 SIGNAL SHAPE SEPARATE. SNAR002C
C NRFLCT(I5) =-1 NO REFLECTIONS-USE FOR UPFIELD SPECTRA SNAR002D
C FROM A-60 AND DFS-60. SNAR002E
C 0 TWO REFLECTIONS-USE FOR DOWNFIELD SNAR002F
C SPECTRA FROM A-60. SNAR002G
C +1 ONE REFLECTION -USE FOR DOWNFIELD SNAR002H
C SPECTRA FROM DFS-60. SNAR002I
C NSTON(I5) SIGNAL TO NOISE .GT.1 OPTIMUM RESOLUTION SNAR003E
C ENHANCEMENT FILTER -SET SNAR
C NSTON EQUAL TO TEN SNAR003A
C TIMES THE LOSS IN SNAR003B
C SIGNAL TO NOISE THAT SNAR003C
C YOU THINK YOU CAN SNAR003D
C AFFORD. SNAR003E
C 1 MATCHED FILTER - NO. SNAR003F
C ERROR BARS. SNAR003G
C 0 MATCHED FILTER - ERROR SNAR003H
C BARS. SNAR003I
C .LE.-1 RC FILTER SNAR004E
C SET NSTON EQUAL TO SNAR004A
C -100*(THE HALF WIDTH SNAR004B
C AT HALF HEIGHT OF THE SNAR004C
C NARROWEST LINE) FOR THE SNAR004D
C OPTIMUM TIME CONSTANT SNAR004E
C FOR THE DOUBLE SECTION SNAR004F
C RC FILTER. SNAR004G
C SWEEP(F11.5) SWEEP WIDTH IN HZ, A POSITIVE NUMBER WHICH SNAR004H
C CORRESPONDS TO NSWEEP. SNAR
C FIT(F11.5) THE FRACTION OF THE INTENSITY OF THE PARENT SNAR004I
C PEAK TO WHICH FITTING IS PERFORMED IN THE SNAR
C REMOVAL OPERATION. -OR- THE PARAMETER SNAR
C WHICH DETERMINES THE SIZE OF THE SEGMENT SNAR005A
C USED FOR THE LINE SHAPE WHEN NSIG=0. SNAR005B
C YSCALE(F11.5) A SCALING FACTOR FOR THE FILTERED SNAR005C
C SPECTRUM. YSCALE TIMES THE SCALE FOR THE SNAR
C ORIGINAL SPECTRUM IS THE SCALE OF THE SNAR
C FILTERED SPECTRUM. SNAR
C IF YSCALE .LE.0. YSCALE IS SNAR005E
C CALCULATED TO FIT THE FILTERED SPECTRUM SNAR005F
C ON THE PLOTTING PAPER AND THE SCALE IS SNAR005G
C PRINTED. SNAR005H
C ABNDNC(F7.5) THE FRACTIONAL NATURAL ABUNDANCE OF THE SNAR005I
C NUCLEUS RESPONSIBLE FOR THE SATELLITE. SNAR006E
C SEPRTE(F11.5) DISTANCE IN HERTZ BETWEEN THE SATELLITE SNAR
C PEAK AND THE PARENT PEAK. SET TO 0. IF SNAR
C UNKNOWN. SNAR
C CARD A2....IFPLOT(1)(I3) = 0 DO NOT PLOT THE LEAST-SQUARES SNAR006A
C DETERMINED LORENTZIAN. SNAR006C
C 1 PLOT THE LEAST-SQUARES FUNCTION. SNAR006D
C IFPLOT(2)(I3) = 0 DO NOT PLOT FI(T). SNAR006E
C 1 PLOT FI(T). SNAR006F
C 2 PLOT AND LABEL FI(T). SNAR006G
C IFPLOT(3)(I3) = 0 DO NOT PLOT S(T). SNAR006H
C 1 PLOT S(T). SNAR006I
C 2 PLOT AND LABEL S(T). SNAR006J
C IFPLOT(4)(I3) = 0 DO NOT PLOT H(T). SNAR007A
C 1 PLOT H(T). SNAR007B
C 2 PLOT AND LABEL H(T). SNAR007C
C IFPLOT(5)(I3) = 0 DO NOT PLOT FI(T)-F(T). SNAR007D
C 1 PLOT FI(T)-F(T). SNAR007E
C 2 PLOT AND LABEL FI(T)-F(T). SNAR007F
C IFPLOT(6)(I3) = 0 DO NOT PLOT FO(T). SNAR007G
C 1 PLOT FO(T). SNAR007H
C 2 PLOT AND LABEL FO(T). SNAR007I

```



```

80 LO = LO+L(I) SNAR016D
   LO = LO/LOMAX SNAR016E
----- SNAR016F
C ADD THE SCANS. SNAR016G
----- SNAR016H
C DO 11 I = 1, IMAX SNAR016I
   K = I + NALIGN SNAR017A
   YL = L(K)-LO SNAR017A
11 Y(I) = Y(I) + YL SNAR017B
   NPT = MINO(NPT,IMAX) SNAR017C
----- SNAR017D
C IF THIS IS THE FIRST SCAN FIND THE MAXIMUM. SNAR017E
----- SNAR017F
C IF(NREAD) 15,15,18 SNAR017G
15 YBIG = 0. SNAR017H
   DO 17 I = 1,NPOINT SNAR017I
   IF (YBIG - Y(I)) 16,17,17 SNAR017J
16 NBIG = I SNAR017K
   YBIG = Y(I) SNAR018B
17 CONTINUE SNAR018C
18 NREAD = NREAD + 1 SNAR018D
   IF (NSTITL - NREAD) 19,19,4 SNAR018E
----- SNAR018F
C ALL SCANS HAVE BEEN READ IN, ALIGNED, AND ADDED. WE NOW FIND SNAR018G
C THE MAXIMUM OF THE COMBINED SPECTRUM. SNAR018H
----- SNAR018I
C 19 YBIG = 0. SNAR019E
   DO 117 I=1,NPT SNAR019A
   IF(YBIG-Y(I)) 116,117,117 SNAR019B
116 NBIG = I SNAR019C
   YBIG = Y(I) SNAR019D
117 CONTINUE SNAR019E
   IF(NSIG) 20,200,22 SNAR019F
----- SNAR019G
C USE THE ENTIRE SPECTRUM FOR THE LINE SHAPE. SNAR019H
----- SNAR019I
C 20 DO 21 I = 1, NPT SNAR020E
21 S(I) = Y(I) SNAR020A
   NSPT = NPT SNAR020B
   NSMAX = NBIG SNAR020C
   SMAX = Y(NBIG) SNAR020D
   GO TO 27 SNAR020E
----- SNAR020F
C SELECT PART OF THE SPECTRUM FOR THE LINE SHAPE. SNAR020G
----- SNAR020H
C 200 YFIT = FIT*Y(NBIG) SNAR020I
   DO 201 I=1,NBIG SNAR021E
   IF(YFIT-Y(I)) 202,201,201 SNAR021A
201 CONTINUE SNAR021B
202 NFIT = I SNAR021C
   NM = NBIG-NFIT SNAR021D
   NSFIT = NFIT-NM SNAR021E
   NSFIT = MAXO(1,NSFIT)
   NSPT = 7*NM SNAR021F
   NTEMP = NPT-NSFIT
   NSPT = MINO(NSPT,NTEMP)
   NSMAX = NBIG-NSFIT
   SMAX = Y(NBIG) SNAR021H
   DO 203 I=1,NSPT SNAR021I
   K = I+NSFIT SNAR022E
203 S(I) = Y(K) SNAR022A
   GO TO 27 SNAR022B
----- SNAR022C
C READ IN THE LINE SHAPE. SNAR022D
----- SNAR022E
C 22 READ (5,1) NSPT SNAR022F
   CALL OCTHEX(L,NSPT) SNAR022G
   SMAX = 0. SNAR022H
   DO 24 I = 1, NSPT SNAR022I
   S(I) = L(I) - L(1) SNAR023E
   IF ( SMAX - S(I) ) 23,24,24 SNAR023A
23 NSMAX = I SNAR023B
   SMAX = S(I) SNAR023C
24 CONTINUE SNAR023D
   IF(NRFLCT.EQ.0) CALL RFLCTR(S,NSPT) SNAR023E
----- SNAR023F
C FILTER THE SPECTRUM. SNAR023G
----- SNAR023H
C 27 IF (NSIG) 28,29,29 SNAR023I
28 CALL REMOVE(NBIG,X,Y,FIT,FI,B,NPT,NFIT,ABNDNC,NSWEEP,SWEEP,SEPRTE, SNAR024E
   INWDTH,NRFLCT,A,PHI,IFPLOT(1)) SNAR024A
   CALL FILTER(INSTON,S,NSPT,NFIT,NSMAX,SMAX,FI,FO,H,SDM,SWEEP,NSWEEP, SNAR024B
   IHELP,IPSDL) SNAR024C
   NFPT = NFIT SNAR024D
   GO TO 30 SNAR024E
29 CALL FILTER (INSTON,S,NSPT,NPT,NSMAX,SMAX,Y,FO,H,SDM,SWEEP,NSWEEP, SNAR024F
   IHELP,IPSDL) SNAR024G
----- SNAR024H
C SET THE PARAMETERS FOR PLOTTING FI(T). SNAR024I
----- SNAR025E
C NFPT = NPT SNAR025A
30 TITLE(3) = 1. SNAR025B
   TITLE(1) = LABEL(1) SNAR025C

```

```

YMIN = -0.8*(NBIG)
YMAX = 1.2*(NBIG)
NOUT = NFIPT
NXO = NBIG
IF(INSTON.LT.0) GO TO 300
-----
C          CALCULATE THE AVERAGE ENHANCEMENT OF THE SIGNAL-TO-NOISE
C          RATIO WHICH WOULD RESULT FROM A MATCHED FILTER.
C-----
SIGMA = 0.
SSQ (1) = (S(1))**2
DO 46 I=2,NSPT
46 SSQ(I) = SSQ (I-1) + (S(I))**2
DO 44 J=1,NFIPT
K = NSMAX - J
IMAX = NSPT - K
IMAX = MINO(NFIPT,IMAX)
IMIN = 1-K
IMIN = MAXO(1,IMIN)
IXK = IMAX+K
INK = IMIN+K
44 SIGMA = SIGMA+SQRT(SSQ(IXK)-SSQ(INK))
FINPT = NFIPT
ENHMT = SIGMA/(SMAX*FINPT)
300 IF(NRFLCT) 51,47,47
-----
C          REFLECT AND SHIFT THE SPECTRUM.
C-----
47 NBIG = NPT-NBIG+1
CALL RFLCTR(Y,NPT)
CALL RFLCTR(S,NSPT)
CALL RFLCTR(FO,NFIPT)
IF(NPT.EQ.NFIPT) GO TO 51
DO 501 I=1,NFIPT
501 FO(NPT-I+1) = FO(NFIPT-I+1)
K = NPT-NFIPT
BIG = 10.*Y(NBIG)
DO 502 I=1,K
502 FO(I) = BIG
NFIPT = NPT
-----
C          PLOT F(I).
C-----
51 IF(IFPLOT(2).EQ.2)
ICALL VLABEL(0.,0.,-8,1.2,YLNG,10,YAXIS,10,1,FMTV,8)
IF(IFPLOT(2).EQ.2)
ICALL VLABEL(0.,0.,0.,SWEEP,XLNG,5,XAXIS,15,0,FMT,8)
IF(IFPLOT(2).GE.1)
ICALL CPLLOT(Y,NPT,NWDTH,TITLE,YMAX,YMIN,1)
IF(INSTON.LT.0) GO TO 500
-----
C          PLOT S(I).
C-----
TITLE(1) = LABEL(2)
TMIN = -0.8*SMAX
TMAX = 1.2*SMAX
IF(IFPLOT(3).EQ.2)
ICALL VLABEL(0.,0.,-8,1.2,YLNG,10,YAXIS,10,1,FMTV,8)
IF(IFPLOT(3).EQ.2)
ICALL VLABEL(0.,0.,0.,SWEEP,XLNG,5,XAXIS,15,0,FMT,8)
IF(IFPLOT(3).GE.1)
ICALL CPLLOT(S,NSPT,NWDTH,TITLE,TMAX,TMIN,1)
IF(INSTON.LE.0) GO TO 500
-----
C          PLOT H(I).
C-----
IF(NRFLCT.GE.0) CALL RFLCTR(H,NSPT)
305 TITLE(1) = LABEL(5)
HMAX = 0.
DO 707 I=1,NSPT
ABSOL = ABS(H(I))
707 HMAX = AMAXI(HMAX,ABSOL)
HMIN = -HMAX
IF(IFPLOT(4).EQ.2)
ICALL VLABEL(0.,0.,-1.,1.0,YLNG,10,YAXIS,10,1,FMTV,8)
IF(IFPLOT(4).EQ.2)
ICALL VLABEL(0.,0.,0.,SWEEP,XLNG,5,XAXIS,15,0,FMT,8)
IF(IFPLOT(4).GE.1)
ICALL CPLLOT(H,NSPT,NWDTH,TITLE,HMAX,HMIN,1)
500 CONTINUE
IF(YSCALE) 31,31,33
-----
C          DETERMINE THE SCALE FOR THE INPUT AND OUTPUT SPECTRA.
C-----
31 FOMIN = 0.
FOMAX = 0.
MINI = 1
IF(NRFLCT.GE.0) MINI = NFIPT-NOUT+1
DO 32 I=MINI,NFIPT
FOMIN = AMINI(FOMIN,FO(I))
32 FOMAX = AMAXI(FOMAX,FO(I))
GO TO 34
33 FOMIN = YSCALE*YMIN
FOMAX = YSCALE*YMAX

```

```

34 IF(NSIG) 35,36,36
-----
C          PLOT FI(T) - F(IT)
C          SNAR034H
C          SNAR034I
C          SNAR035E
C          SNAR035A
35 TITLE(1) = LABEL(3)
   FIMIN = 10.*FOMIN
   FIMAX = 10.*FOMAX
   (FIMRFLCT,GE,0) CALL RFLCTA(FI,NPT)
54 XMN = FIMIN/(NBIG)
   XMN = FIMIN/(NBIG)
   IF(IFPLOT(5),EQ,2)
   ICALL VLABEL(0.,0.,XMN,XX,VLNG,10,YAXIS,10,1,FMTV,8)
   IF(IFPLOT(5),EQ,2)
   ICALL VLABEL(0.,0.,0.,SWEEP,XLNG,5,XAXIS,15,0,FMTH,8)
   IF(IFPLOT(5),GE,1)
   ICALL CPLOT(FI,NPT,NWIDTH,TITLE,FIMAX,FIMIN,1)
-----
C          SNAR036D
C          SNAR036E
C          PLOT FO(T) WITH OR WITHOUT ERROR BARS.
C          SNAR036F
C          SNAR036G
C          SNAR036H
36 TITLE(1) = LABEL(4)
   IF(NSTON) 38,37,38
-----
C          SNAR036I
C          SNAR037E
C          SNAR037A
37 WDTN = NWIDTH
   DO 45 J=1,NOUT,20
   IF(NRFLCT) 56,55,55
55 K = NFIPT-J+1
   GO TO 75
56 K = J
75 T = K
   WIDE = WDTN*(15./XLNGTH)
   HIGHT = (FOMAX-FOMIN)*(10./VLNGTH)+FOMIN
45 CALL EBPLT (T,FO(K),SDM(J),0.,WIDE,FOMIN,HIGHT,0,13)
38 XMN = FOMIN/(NBIG)
   XMN = FOMAX/(NBIG)
   IF(IFPLOT(6),EQ,2)
   ICALL VLABEL(0.,0.,XMN,XX,VLNG,10,YAXIS,10,1,FMTV,8)
   IF(IFPLOT(6),EQ,2)
   ICALL VLABEL(0.,0.,0.,SWEEP,XLNG,5,XAXIS,15,0,FMTH,8)
   IF(IFPLOT(6),GE,1)
   ICALL CPLOT(FO,NFIPT,NWIDTH,TITLE,FOMAX,FOMIN,1)
-----
C          SNAR039E
C          SNAR039A
C          SNAR039B
   WRITE (6,101) (DSCRIPT(I),I=1,20)
   WRITE (6,42) TITLE(2),NSWEEP,NSTITL,NSIG,NRFLCT,NSTON,SWEEP,FIT,
1YSCALE,ENHCMT,ABNDNC,SEPRTE,IPSDL
   WRITE (6,302) HELP
   IF(NSIG) 39,40,40
39 AA = R(1)/(NBIG)
   D = B(2)/SQRT(B(3))
   WDTN = NSWEEP
   YO = (WDTN/SWEEP)
   BB = B(3)*(YO**2)
   XO = NXO
   XO = (XO-B(4))/YO
   YO = B(5)/(NBIG)
   WRITE(6,43) AA,D,BB,XO,YO
   PHI = PHI*(SMAX**2)/(SSO(NSPT)*((Y(NBIG)*.5*ABNDNC)**2))
   WRITE (6,998) PHI
   WRITE (6,999) ((A(I,J),I=1,5),J=1,5)
40 CONTINUE
   WRITE (6,77)
77 FORMAT(1H1)
101 FORMAT (1H1,1X,20A4)
42 FORMAT(1X,A4,/,/,1X,9HNSWEEP = ,15,/,1X,9HNSTITL = ,15,/,3X,7HNSIGSNAR041D
1 = ,15,/,1X,9HNRFLCT = ,15,/,2X,8HNSTON = ,15,/,2X,8HSWEEP = ,F11,SNAR041E
25,/,4X,6HFIT = ,F11.5,/,1X,9HYSCALE = ,F11.5,/,/,1X,9HENHCMT = ,F55SNAR041F
3,1,/,/,1X,9HABNDNC = ,F7.5,/,1X,9HSEPRTE = ,F11.5,/,2X,8HIPSDDL = ,SNAR041G
415)
43 FORMAT (/,24X,3H1/2,/,15X,20H( 1 - D*B * (X-XO) ),/,1X, 34H(1X) SNAR041I
1 = YO + A*
2,/,/,2X,4HA = ,E16.8,/,2X,4HD = ,E16.8,4X,1H2,/,2X,4HB = ,E16.8,4HNSAR042A
3 /HZ,/,1X,5HXO = ,E16.8,3H HZ,/,1X,5HYO = ,E16.8)
302 FORMAT(1X,32HTHE IMPROVEMENT IN NOISE LEVEL =,F7.3,/,1H+,31X,1H:/,
1)
998 FORMAT(/,5X,6PHI = ,E16.8,6H F(FI),/)
999 FORMAT(40X,18HCORRELATION MATRIX,5(/,1X,5F19.6))
100 CONTINUE
   STOP
   END
   SUBROUTINE REMOVE (NBIG,X,Y,FIT,FI,B,NPT,NFIT,ABNDNC,NSWEEP,SWEEP,PREM,IOO0A
1,SEPRTE,NWIDTH,NRFLCT,A,PHI,IFPLOT)
-----
C          REM0000B
C          REM0000C
C          THIS SUBROUTINE REMOVES THE PARENT PEAK.
C          REM0000D
C          REM0000E
   DIMENSION XI(1024),Y(1024),FI(1024),FPRIME(5),XFIT(5),YFIT(5),B(5)
   DIMENSION DD(3),A(5,5),SORTC(5),DELTA(5),BTEST(5),ATEST(5,5)
   COMMON/COMCPL/ITEST,XLNGTH,VLNGTH
   DOUBLE PRECISION CMTX
   DIMENSION CMTX(5,5)
   REAL LAMDAZ,LAMBDA
   DD(1) = 0.
   REM0000F
   REM0000G
   REM0000H
   REM0000I
   REM0001A
   REM0001B

```

```

DD(3) = 1. REM0001C
FITT = FIT*Y(NBIG) REM0001D
DD 1 I = 1, NBIG REM0001E
IF (Y(I) - FITT) 1,1,2 REM0001F
1 CONTINUE REM0001G
2 NFIT = 1 REM0001H
----- REM0001I
C SUBTRACT THE SATELLITE PEAK FROM THE PARENT PEAK FOR THE REM0002E
C LEAST-SQUARES FIT. REM0002A
----- REM0002B
C SWEEPN = NSWEEP REM0002C
JHALF = SEPRTE*(SWEEP/NSWEEP) REM0002D
IF (JHALF.LE.0) GO TO 23 REM0002E
ADD = 0.5*ABNDNC REM0002F
IMAX = NPT-JHALF REM0002G
MAX = MINO(NFIT,IMAX) REM0002H
DO 21 I=1,MAX REM0002I
21 Y(I) = Y(I)-ADD*Y(I+JHALF) REM0003E
----- REM0003A
C OBTAIN AN APPROXIMATE FIT USING ONLY FIVE DATA POINTS. REM0003B
----- REM0003C
C 23 XFIT (1) = 1. REM0003D
YFIT (1) = Y(1) REM0003E
DD 3 I = 2,5 REM0003F
J = (1-I)*(NFIT/4) REM0003G
XFIT (I) = J REM0003H
3 YFIT (I) = Y(J) REM0003I
----- REM0004E
C SET THE INITIAL VALUES OF THE PARAMETERS, B. REM0004A
----- REM0004B
C B(1) = Y(NBIG) REM0004C
B(2) = 0. REM0004D
B(4) = NBIG REM0004E
B(5) = 0. REM0004F
B(3) = (B(1)/(YFIT(5)) - 1.)/(XFIT(5) - B(4))**2 REM0004G
PHIO = 5.*B(1)**2 REM0004H
TEST = ((.05*ABNDNC)**2)*PHIO REM0004I
LAMDZ = .01 REM0005E
CALL PHICLC(PHIZ,5,XFIT,YFIT,FI,B,5) REM0005A
CALL LSQFIT(5,5,XFIT,YFIT,FI,B,1,PHI,FPRIME,LAMDZ,PHIZ,LAMBDA, REM0005B
IA,SQRTC,1,ATEST,DELTA,BTEST) REM0005C
PHIO = PHI REM0005D
DO 4 I=1,5 REM0005E
LAMDZ = LAMBDA REM0005F
PHIZ = PHI REM0005G
CALL LSQFIT(5,5,XFIT,YFIT,FI,B,3,PHI,FPRIME,LAMDZ,PHIZ,LAMBDA, REM0005H
IA,SQRTC,1,ATEST,DELTA,BTEST) REM0005I
DELPHI = PHIO - PHI REM0006E
IF (TEST - DELPHI) 4,4,5 REM0006A
4 PHIO = PHI REM0006B
----- REM0006C
C FIND THE LEAST-SQUARES LORENTZIAN USING ALL DATA POINTS. REM0006D
----- REM0006E
C 5 T = NFIT REM0006F
PHIO = T*(Y(NBIG) )**2 REM0006G
TEST = ((.05*ABNDNC)**2)*PHIO REM0006H
LAMDZ = .01 REM0006I
CALL PHICLC(PHIZ,NFIT,X,Y,FI,B,5) REM0007E
CALL LSQFIT(NFIT,5,X,Y,FI,B,1,PHI,FPRIME,LAMDZ,PHIZ,LAMBDA, REM0007A
IA,SQRTC,1,ATEST,DELTA,BTEST) REM0007B
PHIO = PHI REM0007C
DO 6 I = 1,10 REM0007D
LAMDZ = LAMBDA REM0007E
PHIZ = PHI REM0007F
CALL LSQFIT(NFIT,5,X,Y,FI,B,3,PHI,FPRIME,LAMDZ,PHIZ,LAMBDA, REM0007G
IA,SQRTC,1,ATEST,DELTA,BTEST) REM0007H
DELPHI = PHIO - PHI REM0007I
IF (TEST - DELPHI) 6,6,7 REM0008E
6 PHIO = PHI REM0008A
7 IF (I.EQ.10) WRITE(6,9) REM0008B
----- REM0008C
C CALCULATE THE CORRELATION MATRIX REM0008D
----- REM0008E
C DD 40 I=1,5 REM0008F
DD 40 J=1,5 REM0008G
40 CMTX(I,J) = A(I,J) REM0008H
CALL RNDINV(CMTX,5,DETERM,0.,ITFSD) REM0008I
IF (ITFSD.NE.0) WRITE(6,45) ITFSD REM0009E
IF (ITFSD.NE.0) GO TO 44 REM0009A
DD 41 I=1,5 REM0009B
CMT = CMTX(I,1) REM0009C
41 SQRTC(I) = SQRT(CMT) REM0009D
DD 42 I=1,5 REM0009E
DD 42 J=1,1 REM0009F
42 A(I,J) = CMTX(I,J)/(SQRTC(I)*SQRTC(J)) REM0009G
DD 43 I=1,4 REM0009H
IP1 = I+1 REM0009I
DD 43 J=IP1,5 REM0010E
43 A(I,J) = A(J,I) REM0010A
44 CONTINUE REM0010B
----- REM0010C
C ADD THE SATELLITE PEAK BACK TO THE PARENT PEAK AFTER THE REM0010D
C LEAST-SQUARES FIT. REM0010E
----- REM0010F

```

```

IF(JHALF.LE.0) GO TO 24
MAXP1 = MAX+1
DO 22 I=1,MAX
K = MAXP1-I
22 Y(K) = Y(K)+ADD*Y(K+JHALF)
24 CONTINUE
-----
C      COMPLETE THE LORENTZIAN IN THE PART OF THE SPECTRUM NOT USED
C      FOR THE LEAST-SQUARES FIT.
-----
DO 10 I=NFIT,NPT
X1 = X(I)-B(4)
10 FI(I) = B(5)+B(1)*(1.-R(2)*X1)/(1.+B(3)*X1**2)
-----
C      SHIFT THE BASELINE OF THE SPECTRUM AND THE LEAST-SQUARES
C      LORENTZIAN.
-----
DO 8 I=1,NPT
8 Y(I) = Y(I)-B(5)
YMIN = -.8*Y(NBIG)
YMAX = 1.2*Y(NBIG)
DO 12 I=1,NPT
12 FI(I) = FI(I)-B(5)
IF(NRFLCT.GE.0) CALL RFLCTR(FI,NPT)
-----
C      PLOT THE LORENTZIAN DETERMINED BY LEAST-SQUARES.
-----
15 IF(IFPLOT.EQ.1)
1CALL CPLOT(FI,NPT,NWIDTH,DD,YMAX,YMIN,0)
IF(NRFLCT.GE.0) CALL RFLCTR(FI,NPT)
35 CONTINUE
-----
C      REMOVE THE PARENT PEAK (I.E. SUBTRACT THE LEAST-SQUARES
C      DETERMINED LORENTZIAN FROM THE INPUT SPECTRUM).
-----
DO 11 I=1,NPT
11 FI(I) = Y(I)-FI(I)
9 FORMAT (1X,38HTHE LEAST-SQUARES FIT DID NOT CONVERGE,/,1X,24HMORE
1SCANS ARE NECESSARY)
45 FORMAT(1X,30HCORRELATION MATRIX IS SINGULAR,/,1X,8HTEST = ,15)
RETURN
END
SUBROUTINE RFLCTR(S,NSPT)
-----
C      THIS SUBROUTINE REFLECTS A REAL VECTOR ABOUT THE CENTER.
-----
DIMENSION S(NSPT)
25 J = NSPT/2
DO 26 I=1,J
K = NSPT + 1 - I
SI = S(I)
S(I) = S(K)
26 S(K) = SI
RETURN
END
SUBROUTINE OCTHEX(L,NPOINT)
-----
C      THIS SUBROUTINE CONVERTS 8X,1206 INPUT TO THE PROPER VALUES
C      WHEN READ IN AS 8X,7221,
-----
DIMENSION L(1024)
INTEGER LREAD*(72)
1 FORMAT (8X,7221)
NCARD = NPOINT/12
IPOINT = 0
DO 2 ICARD=1,NCARD
READ (5,1) (LREAD(I),I=1,72)
IDIGIT = -6
DO 2 I=1,12
IDIGIT = IDIGIT+6
IPOINT = IPOINT+1
L(IPOINT) = LREAD(IDIGIT+1)
DO 2 J=2,6
2 L(IPOINT) = 8*L(IPOINT)+LREAD(IDIGIT+J)
NLEFT = NPOINT-12*NCARD
IF(NLEFT) 5,5,3
3 NREAD = 6*NLEFT
READ (5,1) (LREAD(I),I=1,NREAD)
IDIGIT = -6
DO 4 I=1,NLEFT
IDIGIT = IDIGIT+6
IPOINT = IPOINT+1
L(IPOINT) = LREAD(IDIGIT+1)
DO 4 J=2,6
4 L(IPOINT) = 8*L(IPOINT)+LREAD(IDIGIT+J)
5 RETURN
END
SUBROUTINE LSQFIT(NOBS,NPARAM,X,Y,F,B,NITER,PHI,FPRIME,LAMDAZ,PHI7
L,LAMBDA,A,SQRTA,ICALC,ATEST,DELTA,BTEST)
-----
C      THIS SUBROUTINE PERFORMS A LEAST-SQUARES FIT OF THE NON-
C      LINEAR PARAMETERS,B, TO THE OBSERVED QUANTITIES Y(I) AT THE POINTS
C      X(I), USING THE METHOD OF MARQUARDT. J.SOC.INDUST.APPL.MATH.,11,
C      431 (1963).
-----

```

```

REMO010G
REMO010H
REMO010I
REMO011G
REMO011A
REMO011B
REMO011C
REMO011D
REMO011E
REMO011F
REMO011G
REMO011H
REMO011I
REMO012G
REMO012A
REMO012B
REMO012C
REMO012D
REMO012E
REMO012F
REMO012G
REMO012H
REMO012I
REMO013G
REMO013A
REMO013B
REMO013C
REMO013D
REMO013E
REMO013F
REMO013G
REMO013H
REMO013I
REMO014G
REMO014A
REMO014B
REMO014C
REMO014D
REMO014E
REMO014F
REMO014G
REMO014H
RFLR000A
RFLR000B
RFLR000C
RFLR000D
RFLR000E
RFLR000F
RFLR000G
RFLR000H
RFLR000I
RFLR001E
RFLR001A
RFLR001B
RFLR001C
OCTH000A
OCTH000B
OCTH000C
OCTH000D
OCTH000E
OCTH000F
OCTH000G
OCTH000H
OCTH000I
OCTH001E
OCTH001A
OCTH001B
OCTH001C
OCTH001D
OCTH001E
OCTH001F
OCTH001G
OCTH001H
OCTH001I
OCTH002E
OCTH002A
OCTH002B
OCTH002C
OCTH002D
OCTH002E
OCTH002F
OCTH002G
OCTH002H
OCTH002I
OCTH003E
OCTH003A
OCTH003B
LSQF000A
LSQF000B
LSQF000C
LSQF000D
LSQF000E
LSQF000F
LSQF000G

```

```

C
C
C      NOBS = THE NUMBER OF OBSERVATIONS OF Y(X).
C      NPARM = THE NUMBER OF PARAMETERS IN F, WHERE Y=F(X).
C      X = THE INDEPENDENT VARIABLE - DIMENSION X(NOBS).
C      Y = THE MEASURED VALUES OF THE DEPENDENT VARIABLE - DIM Y(NOBS).
C      F = THE CALCULATED VALUES OF THE DEPENDENT VARIABLE - DIM F(NOBS).
C      B = THE PARAMETERS - DIMENSION B(NPARM).
C      NITER = THE NUMBER OF ITERATIONS REQUESTED.
C      PHI = THE SUM OF THE SQUARES OF THE RESIDUES.
C      FPRIME(J) = THE PARTIAL OF F WITH RESPECT TO B(J).
C      LAMDAZ = THE INITIAL VALUE OF LAMBDA.
C      PHIZ = THE INITIAL VALUE OF PHI.
C      LAMBDA = THE FINAL VALUE OF LAMBDA.
C      ICALC = 1, PHICLC AND FCALC ARE USED.
C      F = 2, PHICL2 AND FCALC2 ARE USED.
C      A = SCRATCH
C      ATEST = SCRATCH
C
C-----
C      THE SUBROUTINES PHICLC AND FCALC MUST BE PROVIDED!
C-----
C      DIMENSION A(NPARM,NPARM),G( 5),FPRIME(NPARM),SORTA(NPARM),
C      1 DELTA(NPARM),BTST(NPARM),ATEST(NPARM,NPARM)
C      DIMENSION X(NOBS),Y(NOBS),F(NOBS),B(NPARM)
C      REAL LAMBDA,LAMTST,LAMDAZ
C      MAX = 5
C      V = 10.0
C      LAMTST = LAMDAZ
C      PHITST = PHIZ
C      DO 5 ITER=1,NITER
C      LAMBDA = LAMTST
C      PHI = PHITST
C      CALL AGCALC(A,G,NPARM,NOBS,X,B,F,Y,SORTA,FPRIME,ICALC)
C      IF(LAMBDA.LE.0.0001) GO TO 1
C      LAMTST = LAMBDA/V
C      C = 1.
C      1 CALL BCALC(NPARM,A,LAMTST,G,DELTA,MAX,IT,B,SORTA,C,BTST,ATEST)
C      IF(IT.EQ.MAX) GO TO 2
C      IF(ICALC.EQ.1) CALL PHICLC(PHITST,NOBS,X,Y,F,BTST,NPARM)
C      IF(ICALC.EQ.2) CALL PHICL2(PHITST,NOBS,X,Y,F,BTST,NPARM)
C      IF(PHITST.LE.PHI) GO TO 4
C      CALL GAMCLC(NPARM,DELTA,G,GAMMA)
C      IF(GAMMA.GE.0.7854) GO TO 3
C      C = 0.5*C
C      GO TO 1
C      2 WRITE(4,6) NPARM,LAMTST
C      3 LAMTST = LAMTST*V
C      GO TO 1
C      4 CONTINUE
C      DO 5 I=1,NPARM
C      5 B(I) = BTST(I)
C      PHI = PHITST
C      LAMBDA = LAMTST
C      6 FORMAT(1X,14HWARNING IT=MAX,/,1X,6HNPARM=,I6,/,1X,7HLAMBDA=,F15.7)
C      RETURN
C      END
C      SUBROUTINE PHICLC(PHI,NOBS,X,Y,F,B,NPARM)
C
C      THIS SUBROUTINE CALCULATES THE SUM OF THE SQUARES OF THE
C      RESIDUES WHEN A LORENTZIAN IS USED.
C
C-----
C      DIMENSION X(NOBS),Y(NOBS),F(NOBS),B(NPARM)
C      PHI = 0.
C      DO 1 I=1,NOBS
C      X1 = X(I)-B(4)
C      F(I) = B(5)+B(1)*(1.-B(2)*X1)/(1.+B(3)*X1**2)
C      1 PHI = PHI+(Y(I)-F(I))**2
C      RETURN
C      END
C      SUBROUTINE FCALC(X,B,F,P,I,NOBS)
C
C-----
C      THIS SUBROUTINE CALCULATES THE VALUES OF THE LORENTZIAN AND
C      ITS DERIVATIVES FOR THE LEAST SQUARES FIT.
C-----
C      DIMENSION X(NOBS),F(NOBS),B(5),P(5)
C      X1 = X(I)-B(4)
C      BX2 = 1./(1.+B(3)*X1**2)
C      P(1) = (1.-B(2)*X1)*BX2
C      P(2) = -B(1)*X1*BX2
C      PT = P(1)*P(2)
C      P(3) = X1*PT
C      P(4) = B(1)*B(2)*BX2-2.*B(3)*PT
C      P(5) = 1.
C      F(I) = B(1)*P(1)+B(5)
C      RETURN
C      END
C      SUBROUTINE PHICL2(PHI,NOBS,X,Y,F,B,NPARM)
C
C      THIS SUBROUTINE CALCULATES THE SUM OF THE SQUARES OF THE
C      RESIDUES WHEN AN EXPONENTIAL IS USED.
C

```



```

EN = N                                RCFL002E
H(N) = RC12*EN*EXH                    RCFL002A
3 FXH = FX*FXH                        RCFL002B
RETURN                                 RCFL002C
END                                    RCFL002D
SUBROUTINE RESOLV (INSTN,S,NSPT,NEIPT,JSMAX,SMAX,FI,FO,H,IPSDL) RSLV000A
----- RSLV000B
C THIS SUBROUTINE PERFORMS LINEAR AND PSEUDO-LINEAR FILTERING RSLV000C
C IN FREQUENCY SPACE. RSLV000D
----- RSLV000E
DIMENSION S(1024),F1(1024),F0(1024),H(1024),INV(256),M(3),DELTA(3) RSLV000F
1,BPT(1,3),F(512),B(4),FPRIME(3),A(3,3),SORIA(3),ZJ(512),ATEST(3,3) RSLV000G
REAL LAMDAZ,LAMBDA RSLV000H
COMPLEX FORIER(1024),COMJ RSLV000I
----- RSLV001G
C CENTER SMAX RSLV001A
----- RSLV001B
IF(JSMAX.LE.511) GO TO 25 RSLV001C
ISHIFT = JSMAX-511 RSLV001D
JSMAX = 511 RSLV001E
NSPT = NSPT-ISHIFT RSLV001F
DO 27 I=1,NSPT RSLV001G
27 S(I) = S(I+ISHIFT) RSLV001H
25 IT = NSPT-JSMAX RSLV001I
IF(IT.LE.511) GO TO 26 RSLV002E
NSPT = NSPT-IT+511 RSLV002A
26 NCENTR = 2*JSMAX-NSPT RSLV002F
IF(NCENTR) 3,6,1 RSLV002C
1 MIN = NSPT+1 RSLV002D
NSPT = NSPT+NCENTR RSLV002E
DO 2 I=MIN,NSPT RSLV002F
2 S(I) = 0. RSLV002G
GO TO 6 RSLV002H
3 MAX = NSPT-NCENTR RSLV002I
DO 4 I=1,NSPT RSLV003B
4 S(MAX-I+1) = S(NSPT-I+1) RSLV003A
NSPT = MAX RSLV003B
JSMAX = JSMAX-NCENTR RSLV003C
MAX = -NCENTR RSLV003D
DO 5 I=1,MAX RSLV003E
5 S(I) = 0. RSLV003F
6 CONTINUE RSLV003G
----- RSLV003H
C NSPT MUST EQUAL 2*M FOR HARM RSLV003I
----- RSLV004E
M(2) = 0 RSLV004A
M(3) = 0 RSLV004B
NSPTT = NSPT RSLV004C
M(1) = 1 RSLV004D
M2 = 2 RSLV004E
7 NSPTT = NSPTT/2 RSLV004F
IF(NSPTT.LT.1) GO TO 8 RSLV004G
M(1) = M(1)+1 RSLV004H
M2 = 2*M2 RSLV004I
GO TO 7 RSLV005E
8 NSDIFF = M2-NSPT RSLV005A
MAX = M2-NSDIFF/2 RSLV005B
DO 9 I=1,NSPT RSLV005C
9 S(MAX-I+1) = S(NSPT-I+1) RSLV005D
IMIN = MAX+1 RSLV005F
DO 10 I=IMIN,M2 RSLV005E
10 S(I) = 0. RSLV005G
MAX = MAX-NSPT RSLV005H
DO 11 I=1,MAX RSLV005I
11 S(I) = 0. RSLV006E
JSMAX = JSMAX+MAX RSLV006A
NSPT = M2 RSLV006B
----- RSLV006C
C CALCULATE SI(OMEGA) RSLV006D
----- RSLV006E
DO 12 I=1,NSPT RSLV006F
12 FORIER(I) = S(I) RSLV006G
CALL HARM(FORIER,M,INV,FO,1,IFERR) RSLV006H
NSPT2 = NSPT/2 RSLV006I
IF(IPSDL.NE.0) GO TO 21 RSLV007E
----- RSLV007A
C DETERMINE THE EXPONENTIAL DECAY OF SI(OMEGA) BY LEAST-SQUARES RSLV007B
FITTING. RSLV007C
----- RSLV007D
DO 117 J=1,NSPT2 RSLV007E
ZJ(J) = J RSLV007F
H(J) = CABS(FORIER(J)) RSLV007G
117 H(J) = H(J)*H(J) RSLV007H
B(1) = 0. RSLV007I
B(2) = H(1) RSLV008E
B(3) = (ALOG(H(2)/H(10)))/ZJ(10) RSLV008A
LAMDAZ = 0.01 RSLV008B
CALL PHICL2(PHI2,NSPT2,ZJ,H,F,B,3) RSLV008C
CALL USOFIT(NSPT2,3,ZJ,H,F,B,5,PHI,FPRIME,LAMDAZ,PHI2,LAMBDA,A, RSLV008D
ISORIA,2,ATEST,DELTA,BTES) RSLV008E
----- RSLV008F
C ELIMINATE THE HIGH FREQUENCY NOISE IN SI(OMEGA). RSLV008G
----- RSLV008H
21 CUTOFF = 0. RSLV008I

```

```

I START = NSPT2-9
DO 103 I=1,NSPT2
103 CUTOFF = CUTOFF+CABS(FORIER(I))
CUTOFF = CUTOFF/5.
DO 17 I=1,NSPT2
FORI = CABS(FORIER(I))
IF (FORI.LE.CUTOFF) GO TO 18
17 CONTINUE
GO TO 20
18 JMAX = NSPT-I+1
DO 19 J=1,JMAX
19 FORIER(J) = (0.,0.)
20 CONTINUE
-----RSLV009E
C CALCULATE H(Omega) RSLV009A
C-----RSLV009B
STON = NSTON RSLV009C
STON = 0.1*STON RSLV009D
IF (IPSDL.FO.0) STON=EXP(STON)-1. RSLV009E
U = 137.*(STON-.1)**2/((CABS(FORIER(1)))**2) RSLV009F
C = 0. RSLV009G
IF (IPSDL.NE.0) GO TO 22 RSLV009H
B1 = 0+1. RSLV009I
H1 = B(3)/(1.+0.5275*ALOG(B1)) RSLV010E
B1 = -0.36*(B1**2) RSLV010A
U = 0*B(2) RSLV010B
DO 13 J=1,NSPT RSLV010C
CONJ = CONJG(FORIER(J)) RSLV010D
X2 = FORIER(J)*CONJ RSLV010F
CJ = J RSLV010G
IF (J.GT.NSPT2) CJ = NSPT-J+1 RSLV010H
D = 0*(EXP(-B(3)*CJ))+1. RSLV010I
CJ = CJ-1. RSLV011E
EJ = H1*(CJ**2) RSLV011A
EJ = EXP(EJ) RSLV011B
C = C+(X2/D)*EJ RSLV011C
13 FORIER(J) = (CONJ/D)*EJ RSLV011D
GO TO 24 RSLV011F
22 CONTINUE RSLV011G
DO 23 J=1,NSPT RSLV011H
CONJ = CONJG(FORIER(J)) RSLV011I
X2 = FORIER(J)*CONJ RSLV011J
D = 1.+0*X2 RSLV012E
C = C+X2/D RSLV012A
23 FORIER(J) = CONJ/D RSLV012B
24 RNSPT = NSPT RSLV012C
C = RNSPT*SMAX/C RSLV012D
DO 14 J=1,NSPT RSLV012F
14 FORIER(J) = C*FORIER(J) RSLV012G
-----RSLV012H
C CALCULATE H(T) RSLV012I
C-----RSLV012J
CALL HARM(FORIER,M,INV,FO,-2,IFERR) RSLV012K
DO 15 I=1,NSPT RSLV013E
15 H(I) = FORIER(I) RSLV013A
-----RSLV013B
C CALCULATE FO(T) RSLV013C
C-----RSLV013D
DO 16 N=1,NFIPT RSLV013D
FO(N) = 0. RSLV014I
MAX = N-1+JSMAX RSLV015E
MAX = MINO(MAX,NSPT) RSLV015A
MIN = N-NFIPT+JSMAX RSLV015B
MIN = MAXO(MIN,1) RSLV015C
DO 16 I=MIN,MAX RSLV015D
16 FO(N) = FO(N)+H(I)*FI(N-1+JSMAX) RSLV015F
RETURN RSLV015G
END RSLV015G

```

APPENDIX C

A SEMIEMPIRICAL CALCULATION OF
SPIN-SPIN COUPLING CONSTANTS

We have used the extended Hückel theory type orbitals of R. Hoffmann and W. N. Lipscomb⁵¹ to compute coupling constants for e. p. r. and n. m. r. spectra. Only the e. p. r. first-order Fermi-contact⁵² coupling, and the n. m. r. second-order Fermi-contact coupling are considered. The e. p. r. coupling constants of nuclei which lie at a node of the odd electron's orbital in a π -electron radical could not be calculated. The results for e. p. r. are similar to those obtained by the hyperconjugation approach. The computer programs used make the method easy to apply, and the results show substantial agreement with experiment. A description of the calculation of the e. p. r. coupling constants has been published.⁵³

The semiempirical method used attempts to guess the results which would be obtained from a single-determinant minimum basis set Hartree-Fock calculation. The inner-shell electrons are not explicitly taken into account in these calculations. All overlap integrals are computed. This is quite simple, because they have been evaluated analytically.⁵⁴ Extended Hückel theory approximates the diagonal elements of the Hamiltonian matrix by valence-state ionization potentials, and uses the Wolfsberg-Helmholz⁵⁵ approximation, Eq. (C1), for the off-diagonal elements.

$$H_{ij} = \frac{1}{2}K(H_{ii} + H_{jj})S_{ij}. \quad (C1)$$

The constant K, Eq. (C1), is set equal to 1.75. Slater⁵⁶ 1s orbitals are used for the hydrogens and Slater 2s and 2p orbitals are

used for the first row elements.

These approximations give Hamiltonian matrix elements quite different from the calculated elements for small molecules. The resulting occupied orbitals and the associated eigenvalues are, however, an excellent approximation to those obtained by ab initio calculations on small molecules. The unoccupied orbitals and associated eigenvalues bear no obvious relation to the Hartree-Fock quantities.

Computation of the contact coupling of the first-row elements requires a 2s function which does not have a node at the nucleus. Since the Slater 2s function has such a node, a function of the form

$$2s' = (1 - S^2)^{-\frac{1}{2}}(2s - S \cdot 1s), \quad (C2)$$

where S is the $\psi_{1s} - \psi_{2s}$ overlap integral, was used. In the computation of overlap integrals the 2s overlap was substituted for the $2s'$ overlap. This did not cause any serious error in the overlap integrals.⁵⁴ The value of these orbitals at the nucleus is similar to that obtained by S. C. F. calculations for the atoms.⁵⁷

The Fermi-contact operator for electron-spin resonance is

$$\mathcal{H}'' = \frac{16\pi}{3} \beta \sum_N g_N \beta_N \delta(\underline{r}_N - \underline{r}_e) \underline{S} \cdot \underline{I}_N \quad (C3)$$

where δ is the Dirac delta operator, S and I_N are electron and nuclear spin operators, and β , β_N , and g_N have their usual meanings. This is a perturbation on the electronic Hamiltonian. By evaluating this

perturbation to first order in terms of the above orbitals, the coupling constant may be expressed as

$$A_N = -\frac{16\pi}{3} g_N \beta_N \beta \phi_N^2 \quad (C4)$$

where ϕ_N is the value of the orbital of the unpaired electron at nucleus N.

Although Hoffmann and Lipscomb⁵¹ used a Slater exponent of 1.0 for hydrogen, S. C. F. calculations indicate that an exponent of about 1.2 would be preferable. This contraction of hydrogen 1s functions would increase ϕ_N^2 in Eq. (C4) by a factor of 1.728. The relative sizes of the splittings are not affected, since the H_{ij} and S_{ij} in Eq. (C1) are insensitive to the exponent. The S. C. F. calculations included first-row 1s basis functions, so we varied the exponent to obtain agreement with experiment. A value of 1.15 reproduces the experimental results for the vinyl and 1-methylvinyl radicals reasonably well.

Table I gives the results of this treatment of several radicals. The values obtained by Dixon⁵⁸ are listed for comparison. Dixon used a hydrogen exponent of 1.20 and slightly different geometries. We used the experimental geometry of the parent compound for the present set of calculations except in those cases for which special notes appear in the Table.

Since the bond angles and bond lengths of most radicals are not known, a useful semiempirical scheme for correlating coupling

TABLE I. Comparison of experimental and calculated coupling constants.

Radical	A (G)			Ref.
	Experimental	Calculated		
		Extended Hückel	Hyperconjugation	
Formyl ^a	136	74.3		59
Vinyl ^b (<i>gem</i>) (<i>cis</i>) (<i>trans</i>)	13.4, 15.7	13.6	17.3 ^b	60
	34.2	32.9	49.7 ^b	
	68.5	66.8	81.6 ^b	
1-Methylvinyl ^c (CH ₃) (<i>cis</i>) (<i>trans</i>)	19.48	18.2		60
	32.92	28.4		
	57.89	59.8		
Phenyl (<i>ortho</i>) (<i>meta</i>) (<i>para</i>)	18.1	12.5	23.3	61
	6.4	5.3	4.2	
	0.0	11.0	17.9	
Cyclopropyl ^d (α) (β)	6.51	6.5		60
	23.42	16.8	24.1	
Ethyl ^e (β)	26.87	21.4	27.1	
2-Propyl ^{f,g} (β)	24.68	18.8	22.8	
<i>tert</i> -Butyl ^f	22.72	16.8	20.3	
Cyclobutyl ^{f,g} (β) (γ)	36.66	29.6	38.2	
	1.12	1.46	2.9	
Cyclopentyl ^{f,g} (β) (γ)	35.16	30.4	37.2	
	0.53	0.42	0.57	
Cyclohexadienyl ^{f,h} (CH ₂)	47.71	42.0	54	
Ethynyl	16.1	74		62
Nitrogen dioxide	107	74		63

^a \angle (H-C=O) = 120 deg.⁶⁴

^b \angle (H-C=C) = 146 deg.

^c \angle (C-C=C) = 146 deg.

^d The α hydrogen is 28.6° out of the carbon plane.

^e The C-CH₃ group is planar.

^f The carbon skeleton is planar.

^g The α hydrogen is in the carbon plane.

^h The single and conjugated bond lengths are 1.51 and 1.34 Å, respectively.

TABLE II. Variation of parameters.

Parameter	Values	Radical	A (G)	
			Value (1)	Value (2)
Hydrogen exponent	(1) 1.15 (2) 1.20	Vinyl (<i>gem</i>)	13.6	14.5
		(<i>cis</i>)	32.9	35.0
		(<i>trans</i>)	66.8	74.6
		Ethyl (β)	21.4	23.6
		2-Propyl (β)	18.8	21.1
		<i>tert</i> -Butyl (β)	16.8	19.0
C-C bond length	(1) 1.54 (2) 1.44	Ethyl (β)	21.4	29.0
		2-Propyl (β)	18.8	24.9
		<i>tert</i> -Butyl (β)	16.8	21.8
C _o out of the plane of the ring	(1) 0° (2) 10°	Cyclopentyl (β)	30.4	29.7
		(γ)	0.42	0.40

constants cannot be very sensitive to small changes in geometry and hydrogen exponent. Our results in Table II show that the coupling constants computed from extended Hückel wave functions generally satisfy these requirements. The coupling constants of the vinyl radical have a strong dependence on the bond angle. However, Adrian and Karplus,⁶⁵ and Cochran, Adrian, and Bowers⁶² have also obtained optimum agreement with experiment for an angle of 140° to 150° using a valence-bond approach.

The low value for nitrogen coupling is to be expected, since no 1s first-row orbitals were used. Ethynyl radical may be a π radical, in which case these calculations would not apply. The complete disagreement for the para coupling in phenyl radical is not understood at this time.

The results obtained by computing e. p. r. spin-spin coupling constants from extended Hückel theory molecular orbitals show general agreement with experiment. The theory predicts changes within a given group of radicals very well. For example, the computed coupling constants of aliphatic radicals are all 5.7 ± 0.2 gauss lower than the experimental values.

The contact operator for n. m. r. is

$$\mathcal{H}'' = \frac{16\pi\beta\hbar}{3} \sum_k \sum_N \gamma_N \delta(\underline{r}_{kN}) \underline{S}_k \cdot \underline{I}_N \quad (C5)$$

where γ_N is the nuclear gyromagnetic ratio. The first-order perturbation term vanishes, and the second-order term

$$- \sum_{n \neq 0} \frac{|(0|\mathcal{K}''|n)|^2}{E_n - E_0} \quad (\text{C6})$$

when applied to wave functions of the type used gives

$$J_{\text{KL}} = -h \left[\frac{8\beta}{3} \right]^2 \gamma_{\text{K}} \gamma_{\text{L}} \sum_i^{\text{occ.}} \sum_j^{\text{unocc.}} \frac{\phi_{\text{ik}} \phi_{\text{iL}} \phi_{\text{jk}} \phi_{\text{jL}}}{E_j - E_i} \quad (\text{C7})$$

where ϕ_{jk} is the value of M.O. j at nucleus K . Because the energies could not be evaluated by the extended Hückel method, the molecular orbital eigenvalues were used instead.

The coupling constants obtained by this procedure are given in Table III. Fahey, Graham, and Piccioni⁶⁶ have obtained essentially the same results using hydrogenic 2s orbitals instead of orthogonalized Slater 2s orbitals. The approximations involved in computing the coupling constants were evaluated by making the same approximation for the energies, but using the Hartree-Fock orbitals and eigenvalues for formaldehyde which were obtained by Foster and Boys.⁷² This gave a coupling constant for formaldehyde of 40.7 Hz compared to an experimental value⁷¹ of between 40.2 and 42.4, and a Hückel value of -12.7. A set of ethane orbitals and eigenvalues similar to those of R. M. Pitzer also gave coupling constants in agreement with experiment. On this basis, it appears that the major error in these calculations is that the extended Hückel method does not reproduce the Hartree-Fock results with sufficient accuracy.

TABLE III

Molecule	J in Hz		Ref.
	Exp.	Calc.	
1. $H^1 - H^1$			
A. Saturated molecules			
Hydrogen	280	316	67
Methane	-12.4	-11.3	68
Ethane (vic)	8.0	3.3	48
Methanol (gem)	-10.8	-14.4	69, 70
B. Unsaturated molecules			
Ethylene (gem)	2.3	-10.1	48
(cis)	11.5	4.4	48
(trans)	19.1	10.7	48
Acetylene	9.8	5.1	48
Formaldehyde	40.2-42.4*	-12.7(40.7) ⁺	71
2. $C^{13} - H^1$			
Ethane (short)	125.0	74.8	48
(long)	-4.8	-3.2	48
Ethylene (short)	156.2	98.5	48
(long)	-2.4	-6.7	48
Acetylene (short)	248.7	160.4	48
(long)	49.7	-3.6	48
3. $C^{13} - C^{13}$			
Ethane	34.6	27.7	48
Ethylene	67.2	60.0	48
Acetylene	170.6	119.1	48

* Solvent dependent.

⁺ Hartree-Fock orbitals were used.

The extended Hückel approach reproduces the general trends for both vicinal and directly bonded couplings reasonably well. This is hardly a triumph, because these trends are easily predicted within the framework of an average excitation energy approximation.⁷³ The calculated values for geminal spin-spin couplings bear little resemblance to the experimental values. Because the basic purpose of this approach was to remove the average excitation energy approximation, we must consider it a failure.

The results of these calculations for e. p. r. coupling constants are in excellent agreement with experiment, but the agreement for n. m. r. is poor. In hindsight, we recall the remarks about the accuracy of occupied and unoccupied orbitals that we made previously, and note that we could have expected the relative accuracy of the computed e. p. r. and n. m. r. coupling constants. We would expect extended Hückel theory to accurately predict n. m. r. couplings only when the contributions from the various excited states do not involve small differences between large numbers, and precise information about the excited states is unimportant. Comparison with successful applications of the average excitation energy approximation indicates that this is the case. It appears that a method, such as Lipscomb's N. E. M. O. calculations, which gives results similar to those from a rigorous Hartree-Fock calculation, in those cases for which the rigorous calculations have been done, would be successful in predicting n. m. r. spin-spin couplings.

REFERENCES

1. J. A. Pople, W. G. Schneider, and H. J. Bernstein, "High Resolution Nuclear Magnetic Resonance", p. 27, McGraw-Hill New York (1959).
2. R. Ernst, Advances in Magnetic Resonance, 2, 1, Academic Press, New York (1966).
3. Hugh D. Young, "Statistical Treatment of Experimental Data", P. 108, McGraw-Hill, New York (1962).
4. D. O. North, "Analysis of the Factors which Determine Signal/ Noise Discrimination in Radar", R. C. A. Tech. Rep. PTR-6-C, June 1953; reprinted in Proc. IRE, 51, 1016 (1963).
5. Reference 2, page 53.
6. J. Todd, "Survey of Numerical Analysis", p. 74, McGraw-Hill, New York (1962).
7. D. Middleton, "An Introduction to Statistical Communication Theory", p. 684, McGraw-Hill, New York (1960).
8. R. Bracewell, "The Fourier Transform and Its Applications", p. 24, McGraw-Hill, New York (1965).
9. Reference 7, p. 92.
10. L. S. Schwartz, "Principles of Coding, Filtering, and Information Theory", p. 137, Spartan Books, Inc., Baltimore (1963).
11. George Buchman, "Elements of Abstract Harmonic Analysis", p. 24, Academic Press, New York (1964).
12. N. Wiener, "The Extrapolation, Interpolation, and Smoothing of Stationary Time Series with Engineering Applications", John Wiley & Sons, Inc., New York (1949).
13. H. Margenau and G. Murphy, "The Mathematics of Physics and Chemistry", p. 210, D. Van Nostrand, Inc., New York (1956).

14. A. Messiah, "Quantum Mechanics", Vol. 1, p. 183, John Wiley & Sons, Inc., New York (1964).
15. J. W. Cooley and J. W. Tukey, Mathematics of Computations, 19, 297 (1965).
16. H. V. Malmstadt, C. G. Enke, and E. C. Toren, Jr., "Electronics for Scientists", p. 406, W. A. Benjamin, Inc., New York (1963).
17. L. R. Ford, "Differential Equations", p. 33, McGraw-Hill, New York (1955).
18. Publication Number 87-101-002, p. 4-34, Varian Associates, Palo Alto, California.
19. Reference 3, page 96.
20. F. Bloch, Phys. Rev., 70, 460 (1946).
21. Varian Instruments offers the SpectroSystem 100 which uses a Lorentzian line shape for resolution enhancement of n. m. r. spectra.
22. Reference 2, p. 24.
23. Ibid., p. 23.
24. Ibid., p. 59.
25. R. Ernst and W. A. Anderson, Rev. Sci. Instr., 36, 1696 (1965).
26. Reference 6, p. 316.
27. Andrew D. McLachlan and A. Carrington, "Introduction to Magnetic Resonance", p. 192, Harper and Row, New York (1967).
28. Reference 2, p. 74.
29. Reference 27, p. 184.
30. Reference 3, p. 104.
31. Z. W. Birnbaum, "Introduction to Probability and Mathematical Statistics", p. 18, Harper and Brothers, New York (1962).

32. Kenneth S. Miller, "Multidimensional Gaussian Distributions", p. 20, John Wiley & Sons, Inc., New York (1962).
33. Ibid., p. 103.
34. Ibid., p. 97.
35. B. A. Jacobsohn and R. K. Wangsness, Phys. Rev., 73, 942 (1948).
36. F. Brusentsev and V. Dvoryankin, Zhurnal Strukturnoi Khimii, 4, 465 (1963).
37. Reference 6, pp. 223-243.
38. D. Marquardt, J. Soc. Indust. Appl. Math., 11, 431 (1963).
39. Reference 2, p. 60.
40. The asymptotic form we obtain agrees very well with our numerical results and those of Ernst (reference 2, page 58). The asymptotic form given by Ernst (Ibid., page 60) appears to contain a misprint.
41. D. Dorman and J. D. Roberts, J. Amer. Chem. Soc., in press.
42. J. D. Roberts, "An Introduction to the Analysis of Spin-Spin Splitting in High-Resolution Nuclear Magnetic Resonance Spectra", p. 54, W. A. Benjamin, Inc., New York (1962).
43. Walter Clark Hamilton, "Statistics in Physical Science", p. 39, The Ronald Press Company, New York (1964).
44. R. R. Ernst and W. A. Anderson, Rev. Sci. Instr., 37, 93 (1966).
45. Hans J. Reich, M. Jautelat, Mark T. Messe, F. J. Weigert, and J. D. Roberts, J. Amer. Chem. Soc., in press.
46. D. M. Grant and W. M. Lichtman, J. Amer. Chem. Soc., 87, 3994 (1965).
47. F. J. Weigert, Ph.D. Thesis, California Institute of Technology, 1968.
48. D. M. Graham and C. E. Holloway, Can. J. Chem., 41, 2114 (1963).

49. F. J. Weigert and J. D. Roberts, *J. Amer. Chem. Soc.*, 89, 2967 (1967).
50. Reference 2, p. 67.
51. (a) R. Hoffmann and W. N. Lipscomb, *J. Chem. Phys.*, 36, 3489 (1962); (b) R. Hoffmann, *J. Chem. Phys.*, 39, 1397 (1963).
52. E. Fermi, *Z. Phys.*, 60, 320 (1930).
53. G. A. Petersson and A. D. McLachlan, *J. Chem. Phys.*, 45, 628 (1966).
54. R. S. Mulliken, C. A. Rieke, D. Orloff, and H. Orloff, *J. Chem. Phys.*, 17, 1248 (1949).
55. M. Wolfsberg and L. Helmholz, *J. Chem. Phys.*, 20, 837 (1952).
56. J. C. Slater, *Phys. Rev.*, 36, 57 (1930).
57. For example, compare the value for nitrogen obtained by this method with that obtained by D. R. Hartree and W. Hartree, *Proc. Roy. Soc. (London)*, A193, 299 (1948).
58. W. T. Dixon, *Mol. Phys.*, 9, 201 (1965).
59. F. J. Adrian, E. L. Cochran, and V. A. Bowers, *J. Chem. Phys.*, 36, 1661 (1962).
60. R. W. Fessenden and R. H. Schuler, *J. Chem. Phys.*, 39, 2147 (1963).
61. J. E. Bennett, B. Mile, and A. Thomas, *Chem. Commun.*, 265 (1965).
62. E. L. Cochran, F. J. Adrian, and V. A. Bowers, *J. Chem. Phys.*, 40, 213 (1964).
63. G. R. Bird, J. C. Baird, and R. B. Williams, *J. Chem. Phys.*, 28, 738 (1958).
64. G. Herzberg and D. A. Ramsay, *Proc. Roy. Soc. (London)*, A233, 34 (1955).
65. F. J. Adrian and M. Karplus, *J. Chem. Phys.*, 41, 56 (1964).
66. R. C. Fahey, G. C. Graham, and R. L. Piccioni, *J. Amer. Chem. Soc.*, 88, 193 (1966).

67. H. Y. Carr, and E. M. Purcell, *Phys. Rev.*, 88, 415 (1952).
68. M. Karplus, D. H. Anderson, T. C. Farrar, and H. S. Gutowsky, *J. Chem. Phys.*, 27, 597 (1957).
69. H. J. Bernstein and N. Sheppard, *J. Chem. Phys.*, 37, 3012 (1962).
70. F. A. L. Anet, *J. Amer. Chem. Soc.*, 84, 3767 (1962).
71. B. L. Shapiro, R. M. Kopchik, and S. J. Ebersole, *J. Chem. Phys.*, 39, 3145 (1963).
72. J. M. Foster and S. F. Boys, *Rev. Mod. Phys.*, 32, 303 (1960).
73. (a) H. M. McConnell, *J. Chem. Phys.*, 24, 460 (1956);
(b) M. Karplus, *J. Amer. Chem. Soc.*, 85, 2870 (1963);
(c) M. Karplus, *J. Chem. Phys.*, 30, 11 (1959); *J. Phys. Chem.*, 64, 1793 (1960); (d) G. J. Karabatsos, J. D. Graham, and F. M. Vane, *J. Amer. Chem. Soc.*, 84, 37 (1962);
(e) This thesis, Section 8.